Exploiting PHY for improving LoRa based communication and localisation system

Author:
Liu, Jun

Publication Date:
2021

DOI:
https://doi.org/10.26190/unsworks/22796

Exploiting PHY for Improving LoRa Based Communication and Localisation System

A Dissertation Presented

by

Jun Liu

submitted in partial fulfillment of

the requirement for the degree of

Doctor of Philosophy

in School of Computer Science and Engineering
Faculty of Engineering

August 2021

Supervised

by

Associate Professor Wen Hu

Thesis Title

Exploiting PHY for Improving LoRa Based Communication and Localisation System

Thesis Abstract

LoRa is an emerging technology of low-power wide-area networks (LPWANs) operating on industrial, scientific and medical (ISM) bands to provide connectivity for Internet of Thing (IoT) devices. As the number of devices increases, the network suffers from scalability issues. Therefore, we design a cloud radio access network (C-RAN or Cloud-RAN) with multiple LoRa gateways to solve this problem. Furthermore, we develop novel algorithms to provide accurate localisation for LoRa devices.

This thesis makes three new contributions to LoRa based communication and localisation system as follows. The first contribution is a compressive sensing-based algorithm to reduce the uplink bit rate between the gateways and the cloud server.
The proposed novel compression algorithm can reduce the bandwidth usage for the fronthaul without decreasing LoRa packet delivery rates. Our evaluation shows that with four gateways up to 87.5% PHY samples can be compressed and 1.7x battery life for end devices can be achieved.

The second contribution is a novel algorithm to improve the resolution of the radio signals for localisation. The proposed algorithm synchronises multiple non-overlapped communication channels by exploiting the unique features of the LoRa radio to increase the overall bandwidth. We evaluate its performance in an outdoor area of 100 m × 60 m, which shows a median error of 4.4 m, and a 36.2% error reduction compared to the baseline.

The above approach improves the accuracy of outdoor localisation; however, it does not work for indoor localisation due to the increase of multiple radio propagation paths. Therefore, our third contribution is an improved super-resolution algorithm for indoor localisation. By exploiting both the original and the conjugate of the physical layer, the algorithm can resolve the multiple paths from multiple reflectors in clustered indoor environments. We evaluate its performance in an indoor area of 25 m × 15 m, which shows that a median error of 2.4 m can be achieved, which is 47.8% and 38.5% less than the baseline approach and the approach without using the conjugate information, respectively. Our evaluation also shows that, different to previous studies in Wi-Fi localisation systems that have significantly wider bandwidth, time-of-fight (ToF) estimation is less effective to LoRa localisation systems with narrowband radio signals.

Thesis Title and Abstract | Declarations | Inclusion of Publications Statement | Corrected Thesis and Responses

ORIGINALITY STATEMENT

☑ I hereby declare that this submission is my own work and to the best of my knowledge it contains no materials previously published or written by another person, or substantial proportions of material which have been accepted for the award of any other degree or diploma at UNSW or any other educational institution, except where due acknowledgement is made in the thesis. Any contribution made to the research by others, with whom I have worked at UNSW or elsewhere, is explicitly acknowledged in the thesis. I also declare that the intellectual content of this thesis is the product of my own work, except to the extent that assistance from others in the project's design and conception or in style, presentation and linguistic expression is acknowledged.

COPYRIGHT STATEMENT

AUTHENTICITY STATEMENT

☑ I certify that the Library deposit digital copy is a direct equivalent of the final officially approved version of my thesis.

Thesis Title and Abstract | Declarations | Inclusion of Publications Statement | Corrected Thesis and Responses

UNSW is supportive of candidates publishing their research results during their candidature as detailed in the UNSW Thesis Examination Procedure.

Publications can be used in the candidate's thesis in lieu of a Chapter provided:

- The candidate contributed **greater than 50%** of the content in the publication and are the "primary author", i.e. they were responsible primarily for the planning, execution and preparation of the work for publication.
- The candidate has obtained approval to include the publication in their thesis in lieu of a Chapter from their Supervisor and Postgraduate Coordinator.
- The publication is not subject to any obligations or contractual agreements with a third party that would constrain its inclusion in the thesis.

☑ The candidate has declared that **some of the work described in their thesis has been published and has been documented in the relevant Chapters with acknowledgement**.

A short statement on where this work appears in the thesis and how this work is acknowledged within chapter/s:

> My conference paper "Nephalai: towards LPWAN C-RAN with physical layer compression" incorporated as the basis for Chapter 3. My conference paper "Seirios: Leveraging Multiple Channels for LoRaWAN Indoor and Outdoor Localization" incorporated as the basis for Chapter 4 and 5.

Candidate's Declaration

I declare that I have complied with the Thesis Examination Procedure.

Abstract

LoRa is an emerging technology of low-power wide-area networks (LPWANs) operating on industrial, scientific and medical (ISM) bands to provide connectivity for Internet of Thing (IoT) devices. As the number of devices increases, the network suffers from scalability issues. Therefore, we design a cloud radio access network (C-RAN or Cloud-RAN) with multiple LoRa gateways to solve this problem. Furthermore, we develop novel algorithms to provide accurate localisation for LoRa devices.

This thesis makes three new contributions to LoRa based communication and localisation system as follows. The first contribution is a compressive sensing-based algorithm to reduce the uplink bit rate between the gateways and the cloud server. The proposed novel compression algorithm can reduce the bandwidth usage for the fronthaul without decreasing LoRa packet delivery rates. Our evaluation shows that with four gateways up to 87.5% PHY samples can be compressed and 1.7x battery life for end devices can be achieved.

The second contribution is a novel algorithm to improve the resolution of the radio signals for localisation. The proposed algorithm synchronises multiple non-overlapped communication channels by exploiting the unique features of the LoRa radio to increase the overall bandwidth. We evaluate its performance in an outdoor area of 100 m $\times$ 60 m, which shows a median error of 4.4 m, and a 36.2% error reduction compared to the baseline.

The above approach improves the accuracy of outdoor localisation; however, it does not work for indoor localisation due to the increase of multiple radio propagation paths. Therefore, our third contribution is an improved super-resolution algorithm for indoor localisation. By exploiting both the original and the conjugate of the physical layer, the algorithm can resolve the multiple paths from multiple reflectors in clustered indoor environments. We evaluate its performance in an indoor area of 25 m $\times$ 15 m, which shows that a median error of 2.4 m can be achieved, which is 47.8% and 38.5% less than the baseline approach and the approach without using the conjugate information, respectively. Our evaluation also shows that, different to previous studies in Wi-Fi localisation systems that have significantly wider bandwidth, time-of-fight (ToF) estimation is less effective to LoRa localisation systems with narrowband radio signals.

Acknowledgements

My PhD research is supported by an Australian Government Research Training Program (RTP) Scholarship. Capstone Editing provided copyediting and proofreading services, according to the guidelines laid out in the university-endorsed national 'Guidelines for Editing Research Theses'.

"*Life is like a box of chocolates, and you never know what you are going to get.*" Looking back on my PhD life, this is the proverb that first emerges in my head.

Like many new PhD candidates, I started out with confusion regarding what areas to focus on, where to publish papers and how to graduate. In the later years, I am facing even greater uncertainty: COVID-19 and frequent lock-downs have made researches much tougher. Even if we computer science students are quite adapted to working from home, the closed labs and the lack of face-to-face communication have made it difficult to carry out experiments. But there is still an upside: I am more proud of myself when I managed to finish my work and achieve satisfactory publications.

My research focuses on a greener and friendlier Internet-of-Things network. Global warming is no more a concept of the future but of today. We are witnessing more extreme weather events right now, like bushfires, floods and droughts. Our research should not only focus on how to slow down the warming, but also on how to deal with it. With those in mind, I am working towards wireless communication networks with higher flexibility and availability, and hope they are robust to the rapid change of the environment. It would be no more rejoicing if my humble one step could help push the research forward, and attract more talents to work on this together.

My success of PhD relies on a lot of people, among whom there are the essential workers that supports the infrastructure. They are especially worth my respect in that they still work onsite during this pandemic, and take on all the risk. I would like to thank them for keeping the society running.

I would like to thank my supervisor, Dr. Wen Hu, for his guidance and support throughout my PhD. He has taught me not only the skills, but also the altitude towards research, from which I will benefit through my whole life.

I also thank my lab colleagues. They are Yuezhong, Jiayao, Hong, Dong, Qi, Wanli, Weitao. Although we have not had the chance for a gather-up with lobster feast due to the COVID, we will have it some day.

I thank my parents and my parents-in-law for their support and care.

I would like to give my most special acknowledgement to my wife. Her support is essential to my PhD study. Since our reunion in Sydney, we have shared laughs and tears, enjoyed sunshine and beaches as well as thunders and showers. She is a great patisserie maker, app coder, and amateur artist, adding a lot of enjoyable moments to my tough PhD life. We explored Australia together, and I will never forget our campervan trip around New South Wales or the rainfall in desserts we saw. We both pay love to animals, and we have met a wide range of Australian local wildlifes: the cockatoo and galah crowds in the trees, the kookaburras shouting against the magpies, the sick koalas, the Tasmanian devils, kangaroos, emus, ibises and pelicans, as well as the snakes and spiders. Since 2020, life changed completely due to the COVID-19. We take care of each other, and live through the hard time hand in hand. I owe

her our honeymoon trip to Tasmania due to the recent COVID-19 outbreak, but I will fulfill my promise one day.

List of Publications

Conference Proceedings

1. **J Liu**, W Xu, S Jha, W Hu. Nephalai: Towards LPWAN C-RAN with Physical Layer Compression. *The 26th Annual International Conference on Mobile Computing and Networking.* 2020. (**MOBICOM**)

2. **J Liu**, J Gao, S Jha, W Hu. Seirios: Leveraging Multiple Channels for LoRaWAN Indoor and Outdoor Localization. *The 27th Annual International Conference on Mobile Computing and Networking.* 2021. (**MOBICOM**).

3. H Jia, **J Liu**, Y Wu, et al. Condor: Mobile Swing Tracking via Sensor Fusion using Conditional Generative Adversarial Network. *The International Conference on Embedded Wireless Systems and Networks.* 2021. (**EWSN**)

4. Q Lin, W Xu, **J Liu**, et al. H2B: heartbeat-based secret key generation using piezo vibration sensors. *The 18th ACM International Conference on Information Processing in Sensor Networks.* 2019. (**IPSN**)

5. Q Lin, S Peng, Y Wu, **J Liu**, et al. E-Jacket: posture detection with loose-fitting garment using a novel strain sensor. *The 19th ACM International Conference on Information Processing in Sensor Networks.* 2020.

(**IPSN**)

Poster & Demo

1. **J Liu**, W Xu, W Hu. Energy efficient LPWAN decoding via joint sparse approximation. *The 16th ACM Conference on Embedded Networked Sensor Systems*. 2018. (**SENSYS**)

2. Q Lin, Y Wu, **J Liu**, et al. Demo Abstract: human activity detection with loose-fitting smart jacket. *The 19th ACM International Conference on Information Processing in Sensor Networks*. 2020. (**IPSN**)

3. H Jia, Y Wu, **J Liu**, et al. Mobile golf swing tracking using deep learning with data fusion. *The 17th Conference on Embedded Networked Sensor Systems*. 2019. (**SENSYS**)

List of Publications Contributing to the Thesis

1. **J Liu**, W Xu, S Jha, W Hu. Nephalai: towards LPWAN C-RAN with physical layer compression. *The 26th Annual International Conference on Mobile Computing and Networking.* 2020. (**MOBICOM**) **This work incorporated as the basis for Chapter 3. The Candidate's contribution to the work:**

    - System Design and Implementation (90%)
    - Evaluation and Results Analysis (90%)
    - Paper Writing (80%)

2. **J Liu**, J Gao, S Jha, W Hu. Seirios: Leveraging Multiple Channels for LoRaWAN Indoor and Outdoor Localization. *The 27th Annual International Conference on Mobile Computing and Networking.* 2021. (**MOBICOM**). **This work incorporated as the basis for Chapter 4 and 5. The Candidate's contribution to the work:**

    - System Design and Implementation (90%)
    - Evaluation and Results Analysis (90%)
    - Paper Writing (80%)

Contents

List of Figures

List of Tables

Acronyms

AoA Angle of Arrival. xviii, 6, 21, 23, 24, 65, 70, 72, 73, 74, 85, 86, 87, 88, 89, 90, 91, 92, 94, 97, 98, 99, 101, 104, 107, 108, 109, 110, 111, 112, 113, 114, 115, 119, 120

AP Access Point. xix, 6, 21, 67, 111, 112, 115, 116, 117

CAPEX Capital Expenditure. 4

Cloud-RAN Cloud Radio Access Network. 3, 4, 6, 7, 9, 25, 26, 28, 29, 30, 50, 51, 53, 57, 59, 120, 121

COTS Commercial Off-the-shelf. 4, 114

CRC Cyclic Redundancy Check. 11, 13, 14, 15

CS Compressive Sensing. 5, 7, 9, 31, 62, 120

CSI Channel State Information. 6, 8, 9, 15, 20, 66, 67, 78, 84, 103

CSS Chirp Spread Spectrum. 5, 10, 11, 12, 14

DCT Discrete Cosine Transform. 8, 31

DFT Discrete Fourier Transform. 8, 31

DSP Digital Signal Processing. 15, 16

ESPRIT Estimation of Signal Parameters via Rational Invariance Techniques. 71, 72, 84, 86, 87, 111, 112, 113, 114, 115, 117, 118

FFT Fast Fourier Transform. 16

FPGA Field Programmable Gate Arrays. 60

GPS Global Positioning System. 2, 5, 18, 20, 33, 64, 65

GPU Graphics Processing Unit. 60

IoT Internet of Things. 1, 64, 65, 121

ISM Industrial, Scientific and Medical. 1, 11, 21, 27, 28

LPWAN Low-Power Wide-Area Network. 1, 7, 10, 18, 19, 20, 21, 22, 25, 26, 27, 28, 30, 31, 50, 51, 57, 64, 65, 66, 67, 68

MP Matching Pursuit. 18

MUSIC Multiple Signal Classification. 71, 72, 84, 85, 86, 87

OMP Orthogonal Matching Pursuit. 18

PHY Physical Layer. 3, 4, 5, 7, 8, 9, 10, 15, 17, 25, 26, 27, 28, 29, 30, 50, 52, 55, 58, 59, 101, 120

PRR Packet Reception Rate. 27, 31, 46, 51, 52, 53, 55, 56, 57, 58, 59, 62, 120

RIP Restricted Isometry Property. 35

RSS Received Signal Strength. 3, 19, 20, 65, 66, 115

RTT Round-trip Time. 21

SDR Software-defined Radio. 4, 8, 28, 31, 33, 48, 63, 67

SER Symbol Error Rate. 41, 42, 51, 53, 54, 55

SF Spreading Factor. 27, 52, 53, 54, 58, 61, 62

SNR Signal-to-noise Ratio. 17, 26, 27, 29, 30, 41, 42, 46, 51, 53, 54, 58, 59, 62, 73, 120

TDoA Time Difference of Arrival. 3, 5, 20, 65, 66, 115

ToF Time of Flight. 9, 21, 23, 24, 65, 68, 69, 70, 72, 85, 86, 88, 89, 90, 92, 98, 104, 107, 108, 109, 111, 112, 113, 114

ULA Uniform Linear Array. 24

Chapter 1

Introduction

1.1 Research Background

Low-Power Wide-Area Network (LPWAN) is an emerging wireless technology providing long range signal coverage for low-power Internet of Things (IoT) devices. LPWAN has long communication range, low communication bandwidth, small packet sizes and a long battery lifetime [1]. LoRa is one of the major LPWAN technologies operating on unlicensed Industrial Scientific and Medical (ISM) bands. LoRaWAN is a media access control (MAC)-layer protocol based on LoRa to provide reliable and secure wireless communications [2]. Since LoRaWAN is a major LPWAN standard,[1] this thesis will focus on LoRaWAN as a representative of LPWANs to study the Cloud Radio Access Network (Cloud-RAN) architecture.

LoRaWAN is generally deployed with 125 kHz or 500 kHz narrowband channels (this bandwidth may vary in different regions). Such narrowbands limit the bit rate down to several kilo-bits or hundred-bits per second, but they benefit the demodulator's sensitivity, making it possible to detect and decode

[1] LoRa Alliance 2020 Annual Report. https://lora-alliance.org/about-lora-alliance/

LoRa signals significantly lower than the noise floor and have high signal penetration in an urban environment. Further, LoRaWAN devices can have up to 10 years of battery life. Therefore, LoRaWAN is widely used in commercial and industrial applications, such as smart agriculture and intelligent building [3].

Although LoRaWAN has had many successes, concerns about its scalability [4] and localisation accuracy [5] have been raised.

A commercial LoRaWAN network typically engages one gateway with many end devices. The gateway processes and demodulates wireless packets locally and cooperates with cloud servers for message delivery and device control. LoRaWAN follows ALOHA [6] or slotted ALOHA [7] protocols for packet transmissions, with the maximum channel utilisation rates of 18.6% and 37.2%, respectively, since the probability of collision increases with the increase in wireless packet transmissions, limiting the network capacity [8,9]. For example, a LoRaWAN gateway with a single channel can support from 200 to 1,000 nodes only, depending on applications [8, 10] and, will struggle with network congestion when there are thousands of devices. Commercial gateways can support up to eight channels, and, thus, they can increase the capacity by eight times compared to a single channel. To further increase the capacity, a naïve approach is to use several gateways simultaneously in one spot. However, such an approach is expensive (one commercial gateway may cost 1,000 USD) and difficult to maintain. To this end, an economical radio access network with more than eight LoRaWAN channels is proposed to address this challenge.

Another challenge for LoRaWAN is localisation. As millions of IoT devices are deployed with valuable assets, localisation becomes an important service to enable a wide range of location-based applications [10–12]. GPS can provide location information outdoors, but it requires extra, specialised hardware (i.e., GPS receiver) and does not work indoors. Alternatively, the existing infrastructure (i.e., LoRaWAN gateways) can be utilised to provide localisation service [13, 14]. However, the localisation performance of the state-of-the-art LoRaWAN localisation approach is poor. According to the LoRaWAN geolocation whitepaper,[2] received signal strength (RSS) based localisation can only produce 1,000-2,000 m accuracy, and time difference of arrival (TDoA) based localisation algorithms claim to produce 20-200 m accuracy. Such poor accuracy cannot meet the requirement of asset localisation applications, and further research is required to exploit the existing LoRaWAN infrastructure for better localisation accuracy.

Recent research shows that processing radio PHY samples jointly in the cloud can improve the battery life for LoRaWAN end devices [15], and such a system is easy to implement and cost-efficient to deploy [16]. Further, multiple gateways can facilitate device localisation by utilising radio path triangulation. Inspired by the recent research, this study proposes a Cloud-RAN architecture for LoRaWAN as a feasible solution to achieve high network capacity and accurate indoor and outdoor localisation.

However, Cloud-RAN brings new challenges. First, the high bandwidth of (PHY) samples from gateways to the cloud via internet infrastructures may result in back-haul network congestion and a high cost of data usage, limiting the deployment of such gateways. Second, even with multiple gateways for triangulation, localisation accuracy is still poor because a narrowband signal has poor raw resolution [17].

---

[2]LoRaWAN geolocation whitepaper. https://lora-alliance.org/sites/default/files/2018-04/geolocation_whitepaper.pdf

1.2 Research Objectives

This study aims to achieve high network capacity and high localisation accuracy for LoRaWAN, focusing on Cloud-RAN architecture with novel algorithms. Cloud-RAN architecture was originally proposed for cellular networks to improve network flexibility and reduce capital expenditure (CAPEX) [18, 19]. Cloud-RAN for LoRaWAN can also improve signal strength and provide a localisation service. However, new algorithms must be developed for LoRaWAN Cloud-RAN to overcome new challenges. The details of objectives for the proposed systems are listed as follows.

The first aim is to achieve high network capacity. With Cloud-RAN, the processing of radio signals is moved from the (gateway) site to the remote cloud. Gateways are replaced with commercial off-the-shelf (COTS) radio heads such as software-defined radios (SDRs). Since the cloud server has significantly more computing power than a single gateway, the number of channels supported by Cloud-RAN can reach well beyond that of a gateway. Further, the bandwidth of a radio front-end in Cloud-RAN is typically tens of megahertz (the details of bandwidth can be found in the datasheets of typical SDRs such as USRP,[3] bladeRF[4] and hackRF[5]), which can cover all narrowband channels that are assigned for LoRaWAN (e.g., 64 × 125 kHz channels in many regions). Nevertheless, to achieve the goal of supporting all LoRaWAN channels with Cloud-RAN, the following two tasks needs to be accomplished:

- the reduction of the network data usage during offloading PHY samples to the cloud from the gateways, and

[3]USRP N210. https://www.ettus.com/all-products/un210-kit/
[4]BladeRF 2.0. https://www.nuand.com/bladerf-2-0-micro/
[5]HackRF One. https://greatscottgadgets.com/hackrf/one/

- the accurate recovery of the information (i.e., the decoding of the LoRaWAN packets) from the offloaded PHY samples in the cloud.

The first task is to reduce the data usage between the gateways and the cloud with PHY sample compression. Cellular Cloud-RAN gateways are normally connected with optical fibres; however, the cost of optical fibres may be unaffordable for many low-cost or ad hoc IoT applications. Another solution is to detect channel activity and upload active PHY samples only. However, for large-scale deployments (i.e., tens of thousands of nodes), the probability of simultaneous multi-channel transmission is high. Therefore, PHY compression is a feasible solution.

The second task is to extract useful information (i.e., decoding of the LoRaWAN packets) from the offloaded PHY samples, whose performance depends on the selection of compression algorithms. Compression can be either lossless or lossy. Our study found that common lossless compression algorithms [20] (e.g., LZ77) have a poor compression ratio for LoRa PHY samples, which indicates that the radio signal is not *sparse* in the time domain. Conversely, the original signal is modulated with chirp spread spectrum (CSS), which is *sparse* in the frequency domain. Therefore, we can apply a compressive-sensing (CS) technique to exploit signals' *sparsity* in the frequency domain to achieve high compression efficiency while maintaining the information in the original PHY samples. In summary, this thesis will introduce *Nephelai*, a CS-based technique for LoRaWAN PHY sample compression, to address the aforementioned two tasks for the first aim.

The second aim is to reduce LoRaWAN localisation errors from tens of metres to less than 10 metres without additional hardware requirements (e.g., GPS). As discussed in Section 1.1, TDoA-based localisation techniques cannot produce metre-level accuracy because of the bandwidth limitation of LoRaWAN. With Cloud-RAN architecture, the radio signals received by different gateways (access points or APs) can be processed in the cloud jointly to improve the localisation accuracy. LoRaWAN gateways are typically equipped with two or more synchronised antennas [21], and we can exploit the phase difference between two antennas to estimate the angle of arrival (AoA) of the radio signal transmitted from a LoRaWAN end device that needs to be localised. However, there are two major challenges for AoA-based localisation for LoRaWAN.

The first challenge is the poor resolution of narrowband radio signals due to the bandwidth limitation. Unlike wide band signals, providing rich channel state information (CSI) for localisation, LoRaWAN narrowband signals have poor raw resolution and typically produce localisation errors of hundreds of metres. In practice, LoRaWAN gateways can support eight narrowband channels with an overall bandwidth of 1.6 MHz. Combining all eight narrowbands can increase the bandwidth by eight times, which can help improve the localisation accuracy. However, these channels must be synchronised, which is a challenge.

The second challenge is the radio multipath effect, especially in indoor environments, and the localisation result is highly unreliable due to multipaths. Super-resolution algorithms that are widely used with wide band Wi-Fi signals can be introduced to LoRaWAN localisation to resolve the direct path. However, the localisation performance with the measurements from eight LoRaWAN channels is still poor if we apply super-resolution algorithms directly because of the bandwidth limitation (e.g., 1.6 MHz in LoRaWAN channels v. more than 20 MHz in Wi-Fi).

To reduce the localisation errors, we need to investigate new algorithms that exploits the unique features of LoRaWAN. This thesis will first discuss the method to synchronise multiple narrowband channels for a wider bandwidth to increase the raw resolution, and then proposes a novel super-resolution algorithm to resolve multipaths for indoor and outdoor LoRaWAN localisation.

To summarise, the research aims for this thesis are to achieve high network capacity with CS for Cloud-RAN architecture and to reduce LoRaWAN localisation errors.

1.3 Research Contributions

This thesis demonstrates Cloud-RAN systems for LoRaWAN with PHY sample compression and device localisation. PHY sample compression is an essential enabling technique for Cloud-RAN. Localisation is an important feature to provide location-based services for LoRaWAN at a low cost. Both show that Cloud-RAN is beneficial for LoRaWAN compared to the conventional LoRaWAN architecture. Finally, note that the algorithms proposed in this thesis are not limited to LoRaWAN, but can also be applied to other LPWAN technologies.

1.3.1 *Nephelai*

The first work proposes a novel CS-based compression technique for cloud-assisted LoRaWAN that significantly reduces the bandwidth between the gateways and the cloud. The system is named *Nephelai*[6], and new dictionary for CS was designed to achieve high compression ratios without performance degradation. The proposed dictionary exploits the structure of LoRa radio

[6]In ancient Greek mythology, *Nephelai* is the nymph of the clouds.

signals and achieves improved sparse representation that is more than two orders of magnitude better than standard discrete Fourier transform (DFT) and discrete cosine transform (DCT) domains. A prototype of *Nephelai* is implemented with SDRs, and the empirical evaluation demonstrates its superior performance on embedded LoRaWAN end devices.

1.3.2 *Seirios* (Outdoor)

The second work develops a localisation system called *Seirios*[7] for LoRaWAN. The system achieves significantly higher accuracy than state-of-the-art approaches outdoors and does not require special hardware in the embedded LoRaWAN end devices. This thesis proposes a novel interchannel synchronisation algorithm to obtain the synchronised CSI of non-overlapped multiple channels by exploiting the unique structure of the LoRaWAN PHY. Compared to prior work [22], this approach does not require two-way communications and CSI measurements, making it more applicable to LoRaWAN architecture. A prototype of *Seirios* is designed and implemented with SDRs and off-the-shelf embedded LoRaWAN end devices, and evaluation in a 100 m $\times$ 60 m outdoor area shows that *Seirios* can reduce localisation errors by 36.2% compared to the baseline and achieves a median localisation error of 4.4 m.

1.3.3 *Seirios+* (Indoor)

The third work improves the *Seirios* localisation system for indoor localisation. The original system had poor performance indoors. Therefore, the study proposes to double the amount of channel information in *Seirios+* by utilising

[7] *Seirios* (*Sirius*) is the ancient Greek god or goddess of the Dog-Star, which is the brightest star in the night sky and an important reference for celestial navigation around the pacific ocean.

both the original and the conjugate of the CSI to increase the number of multipaths that the super-resolution algorithms can resolve (up to six reflectors for the prototype AP implementation with two antennas), thus, improving the accuracy of localisation. Our evaluation in 25 m $\times$ 15 m indoor area shows that the *Seirios+* achieves a median localisation error of 2.4 m, approximately two-fold smaller than the error from baseline approaches. Compared with observations in previous studies with Wi-Fi localisation systems, these results show that time of flight (ToF) estimation is less effective for narrowband LoRaWAN localisation due to bandwidth limitation.

1.4 Thesis Organisation

The rest of this thesis is organised as follows:

Chapter 2 is the literature review. Focusing on Cloud-RAN, the relevant literature is reviewed on LoRaWAN and PHY compression. For localisation, the conventional localisation approaches, channel combination techniques and super-resolution algorithms are reviewed.

Chapter 3 presents *Nephelai*, a CS-based technique for PHY sample compression.

Chapter 4 presents *Seirios* (outdoor)—a localisation system with a channel combination technique for narrow-band LoRaWAN end devices.

Chapter 5 presents *Seirios+* (indoor), which improvs the localisation accuracy of *Seirios* for indoor localisation.

Chapter 6 concludes the thesis.

Chapter 2

Literature Review

This chapter reviews the relevant literature on the foundation of LoRaWAN, compression techniques and localisation algorithms.

2.1 LPWAN, LoRa, LoRaWAN

LPWAN [1,3,23] has attracted much attention from academia and industry in recent years. LoRaWAN [3,9,24] is standardised by the LoRa Alliance as one of the LPWAN technologies on an unlicensed spectrum. LoRa [25–30] is the PHY foundation of LoRaWAN and defines modulation and radio communication.

Although LoRa is proprietary, recent research has discovered some LoRa decoding and demodulation procedures [26, 31]. Specifically, LoRa leverages CSS modulation for long-range wireless communications. CSS was initially developed for radar applications in the 1940s and has been adopted increasingly in data communication applications over the past 20 years because of its relatively low transmission power and robustness to channel noise and radio multipath effects. The CSS signal is modulated by frequency shift chirp pulses (frequency varying sinusoidal signals), hence improving its resilience and robustness against interference, Doppler effect, and multi-path issues [9].

2.1.1 LoRa Parameters

LoRa CSS modulation can be configured by spreading factor (SF), bandWidth (BW), and code rate (CR). SF is defined as an integer from 6 to 12, representing the number of encoded bits per chirp symbol, and BW is the spectrum constraint of a channel, typically 125, 250 or 500 kHz. CR is an integer from 1 to 4, indicating the scheme for introducing coding redundancy [2]. An up-chirp has its linearly increasing frequency, whereas a down-chirp has a decreasing frequency. A chirp is the minimum unit of a LoRa radio signal, and a LoRa packet is modulated as the concatenation of different chirps. The structure of a LoRa packet is composed of a preamble, a sync word, the start frame delimiter (SFD), payload and cyclic redundancy check (CRC). LoRa utilises up-chirps for the preamble, sync word, payload and CRC, and down-chirps for the SFD.

The duration of a chirp symbol T is given by,

$$T = \frac{2^{SF}}{BW} \tag{2.1}$$

and the bit rate (R_b) is therefore derived as [32],

$$R_b = \frac{BW \cdot SF}{2^{SF}} \cdot \frac{4}{4 + CR} \tag{2.2}$$

2.1.2 LoRaWAN Parameters

LoRaWAN defines regional parameters such as frequency, channel, SF, BW, data rate (DR). Possible DR indicated by DR0 to DR4 are shown in Table 2.1. In the USA, the 902-928 MHz ISM band has 64 × 125 kHz upstream channels with DR selected from DR0 to DR3, 8 × 500 kHz upstream channels with DR selected from DR4, and 8 × 500 kHz downstream channels with DR selected from DR8 to DR13 [2]. In this thesis, similar to Charm [15], *Nephelai* focuses on LoRa upstream traffic only (i.e., only DR0 to DR4 will be discussed).

Table 2.1: US902-928 upstream DR

DR	SF	BW (kHz)	Time (ms)	Indicative Physical Bit Rate (bit/s)
DR0	10	125	8.192	980
DR1	9	125	4.096	1,760
DR2	8	125	2.048	3,125
DR3	7	125	1.024	5,470
DR4	8	500	0.512	12,500
DR5 - DR7	-	-	-	-
DR8	12	500	8.192	980
DR9	11	500	4.096	1,760
DR10	10	500	2.048	3,125
DR11	9	500	1.024	5,470
DR12	8	500	0.512	12,500
DR13	7	500	0.256	21,900

Note. Adapted from [33]
Abbreviations: bandwidth (BW), data rate (DR), spreading factor (SF)

2.1.3 LoRa Primer

LoRa is modulated with chirp spreading spectrum (CSS). It is configured by Spreading Factor (SF) and Bandwidth (BW). SF is defined as an integer from 7 to 12, representing the number of encoded bits per chirp symbol, and BW is the bandwidth of a channel, typically 125 kHz or 500 kHz [2]. An up-chirp has its frequency increasing linearly, while an down-chirp is the opposite. A chirp is the minimum unit of LoRa radio signal, and a LoRa packet is modulated as the concatenation of different chirps. The structure of a LoRa packet is composed of a preamble, a sync word, the Start Frame Delimiter payload and Cyclic Redundancy Check. LoRa utilises up-chirps for the preamble, sync word, payload and CRC, and down-chirps for SFD. An illustration of an example LoRa packet is shown in Figure 2.1.

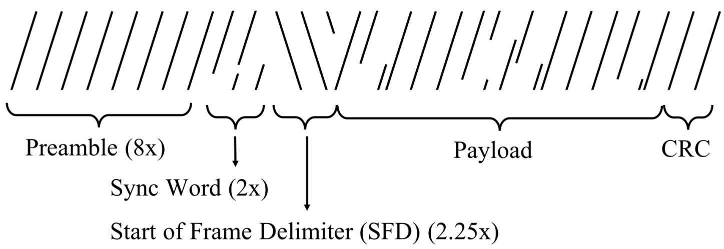

Fig. 2.1: An example physical-layer CSS of LoRa packet in time-frequency domain. (X-axis is time, and y-axis is frequency)

Although the payloads of LoRa packet varies, the preambles are identical to facilitate the packet detection. Preambles consist of predefined number (e.g., eight for LoRaWAN) of up-chirps, and the frequency of an up-chirp is defined as,

$$f(t) = \lambda t - \frac{BW}{2}, \quad t \in [0, T), \tag{2.3}$$

where $\lambda = \frac{BW^2}{2^{SF}}$ is the chirp rate, and $T = \frac{2^{SF}}{BW}$ is the duration of the chirp. The phase of up-chirp $\varphi(t)$ can be obtained by integrating $f(t)$ as,

$$\varphi(t) = 2\pi \int_0^t f(\tau) d\tau = 2\pi(\frac{\lambda}{2}t^2 - \frac{BW}{2}t), \quad t \in [0, T) \tag{2.4}$$

Then, an up-chirp with magnitude of 1 can be represented as,

$$u(t) = e^{j\,\varphi(t)}, \quad t \in [0, T). \tag{2.5}$$

Eq. (2.3) shows that LoRa CSS modulation utilises the entire bandwidth, **making it possible to measure the channel state of the whole band with high resolution by comparing the received chirps with the up-chirp reference, which can facilitate the inter-channel synchronisation** (Section 4.4.3).

2.1.4 Modulation and Demodulation

LoRa modulates payload and CRC data into different chirp symbols [26]. In the frequency domain, a modulated chirp symbol starts at a specific frequency, from one of 2^{SF} equally divided steps of the bandwidth BW, indicating the value $\lambda \in \{0, 1...2^{SF} - 1\}$ that it represents. The chirp then increases linearly through the whole channel, wrapping at the upper bandwidth bound ($BW/2$) to the lower bound ($-BW/2$). In the time domain, the derivative of phase $\varphi^{\lambda}(t)$ of a sinusoidal wave with an instantaneous frequency $f(t)$ represents the linear increment of a chirp symbol λ. Defined on $[0, T)$ for the modulation of symbol λ, the instantaneous frequency $f^{(\lambda)}(t)$ is represented as

$$f^{(\lambda)}(t) = \begin{cases} \mu t + f_0^{(\lambda)} & 0 \leq t < t_p \\ \mu t + f_0^{(\lambda)} - BW & t_p \leq t < T \end{cases} \tag{2.6}$$

where $\mu = BW/T$ is the chirp rate, $f_0^{(\lambda)}$ is the initial frequency for modulating λ, and t_p is the time when frequency wraps at the upper bound. We have,

$$f_0^{(\lambda)} = \frac{BW}{2^{SF}}\lambda - \frac{BW}{2} \tag{2.7}$$

$$t_p = T(1 - \frac{\lambda}{2^{SF}}) \tag{2.8}$$

The phase $\varphi^{(\lambda)}(t)$ can be derived by integrating $2\pi f^{(\lambda)}(t)$ as

$$\begin{aligned}\varphi^{(\lambda)}(t) &= \int_0^t 2\pi f^{(\lambda)}(\tau)d\tau \\ &= \begin{cases} 2\pi(\frac{\mu}{2}t^2 + f_0^{(\lambda)}t) & 0 \leq t < t_p \\ 2\pi(\frac{\mu}{2}t^2 + f_0^{(\lambda)}t) - 2\pi \cdot BW(t - t_p) & t_p \leq t < T \end{cases}\end{aligned} \tag{2.9}$$

Note that the second equation in Equation (2.9) above is empty when $t_p = T$ and $\lambda = 0$ (see Equation (2.8)). Namely, LoRa symbol $\lambda = 0$ has one line (linear chirp) only, while the other symbols ($\{1, 2, ...\ 2^{SF} - 1\}$) have two lines.

Thus, the in-phase component I ($z_I(\varphi^{(\lambda(t))})$) and the quadrature component Q ($z_Q(\varphi^{(\lambda(t))})$) of the modulated band-pass waveform are represented as

$$z_I(\varphi^{(\lambda(t))}) = cos(\varphi^{(\lambda)}(t) + \Gamma) \tag{2.10}$$

$$z_Q(\varphi^{(\lambda(t))}) = sin(\varphi^{(\lambda)}(t) + \Gamma) \tag{2.11}$$

where $\Gamma \in [-pi, pi)$ is an unknown phase offset caused by the radio multipath. $z_I(\varphi^{\lambda}(t))$ and $z_Q(\varphi^{\lambda}(t))$ will be used in the CS dictionary design for *Nephelai*, and CSI estimation for *Seirios*.

To modulate a packet, LoRa concatenates consecutive chirp symbols as a complete LoRa payload. By adding the preamble with a pre-defined number (e.g., eight preambles for LoRaWAN) of identical up-chirps, the SFD of 2.25 down-chirps and the CRC, a complete LoRa PHY packet is constructed.

To decode a LoRa packet on the receiver, a procedure of digital signal processing (DSP), including filtering, detection, frequency calibration, and symbol segmentation must be performed to obtain a chirp symbol from a noisy radio channel.

After DSP, a chirp symbol is ready for demodulation. One commonly used method for demodulation is fast Fourier transform (FFT) [26]. The chirp symbol is first multiplied by a down-chirp in the time domain, and then transformed into the frequency domain with FFT. The demodulation result is indicated by the maximal component in the frequency domain. A series of demodulated results will be used to recover the LoRa packet sent by a transmitter. Open-source software such as gr-lora [26] provides a packet recovery process for demodulated LoRa symbols, and *Nephelai* focuses on LoRa symbol demodulation only.

2.1.5 Synchronised Symbols

Inspired by LoRaWAN class B [2] and slotted ALOHA [34], we can synchronise end nodes and gateways so gateways can receive with non-overlapped windows as shown in Figure 2.2.

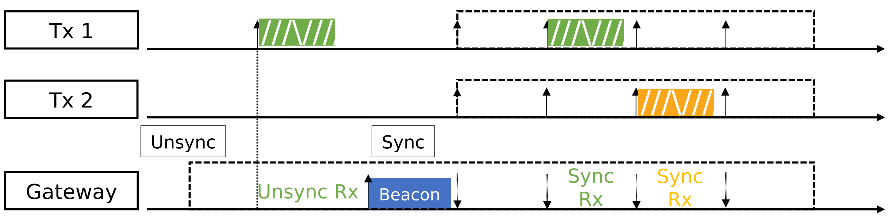

Fig. 2.2: Synchronised receiving for chirp symbols

However, perfect synchronisation is neither possible nor necessary. Here, we use synchronised reception to improve the compression performance only, and further digital signal processing is performed in the cloud for fine-grain symbol segmentation. Thus, the synchronisation error tolerance is high. This will be discussed further in Section 3.3.4.

2.2 PHY

2.2.1 Spatial Diversity

The diversity scheme, referring to improving the reliability of message signals by using more communication channels, has long been used in communication systems [35]. A recent system called Charm has exploited the diversity scheme to improve LoRa decoding by coherently combining signals captured by various LoRaWAN gateways in different locations [15]. As a result, Charm can improve the signal-to-noise ratio (SNR) of the combined signal, which enables faster transmission rates for the end devices and, in turn, improves the battery lifetime of the devices.

One contribution of Charm has been the technique of coherently decoding PHYs in the cloud. Similar concepts were studied in Wi-Fi [36], [37] and cellular networks [19], [38], but Charm was the first to introduce this approach into LoRaWAN, showing that signals with 30 dB below noise floor could be decoded [15]. Dongare et al. also discussed the challenges of implementation. One is that commercial LoRa gateways often have no synchronisation, which may introduce mismatch or failure in signal combination. To overcome this challenge, a new hardware platform was proposed by Dongare et al. with a LoRa RF front-end SX1257, a low-power FPGA IGLOO and a Raspberry Pi 3. After pre-processing with the FPGA and the Raspberry Pi, the I and Q component streams of the radio signal were encapsulated in ethernet packets and sent to the cloud for joint decoding. The modification of gateways was transparent to transmitters, and there was no requirement for other changes in the original LoRaWAN system. Therefore, Charm was backward compatible with the conventional LoRaWAN end devices.

A major challenge for Charm has been the high bandwidth requirement in sending the I/Q streams to the cloud. The minimum requirement for two streams is 9 Mbps [15], limiting the scalability of such a system when there are more gateways.

Overall, Charm represents one of the main research trends in LPWANs, and the general idea can be introduced to other LPWAN technologies (e.g., LoRaWAN and SigFox) for embedded LPWAN end device battery life improvement.

2.2.2 Compressive Sensing

Misra et al. demonstrated an energy-efficient computing framework for GPS acquisition via sparse approximation [20]. The motivation was to move GPS computation from low-power end devices to a powerful central processor to make the end devices more power efficient. Here, the GPS radio signal measurements have a large size, but are sparse in the information that indicates the ranging information between the GPS device and a satellite. Therefore, a compressive sensing method was applied [20] to reduce the size of the radio signal measurements. Specifically, for an oversampled GPS signal, a random measurement matrix was applied for compression to reduce storage in the end devices. After the compressed measurements (i.e., projections) were transferred to the central processor, a sparse approximation algorithm was applied for GPS ranging information reconstruction. Typical sparse approximation algorithms included matching pursuit (MP), orthogonal matching pursuit (OMP), and $\ell1$-minimisation. The design of dictionaries (i.e., domains) for compressive sensing was to maximise the sparsity of the original signal and the incoherence between the dictionaries and the measurement (compression) metrics, which may be learned from historical measurements.

2.3 Localisation

2.3.1 Localisation Algorithms

With the rapidly increasing popularity of LPWANs and the importance of geolocation applications, recent research has attempted to address the challenges and error sources for localisation methods based onLPWAN gateway infrastructure [39] to improve their accuracy. Table 2.2 reviews related work and then groups localisation approaches into categories as follows.

Table 2.2: Comparison of related work

Research	Technology	Low Power	Range	Accuracy
[17, 22, 40, 41]	Wi-Fi	-	12-25 m	<0.9 m
[42–44]	Bluetooth	✓	10 m	≈ 1 m
[45, 46]	Cellular	✗	35-60 m	≈ 0.85 m
[47–49]	Backscatter	✓	<10 m	<0.5m
[50, 51]	LPWAN	✓	500 m+	>100 m
OwLL [52]	LPWAN	✓	500 m+	≈ 9 m
Seirios (outdoor)	LPWAN	✓	100 m	≈ 5 m
WideSee [53]	LPWAN	✓	40 m	4.6 m
Seirios+ (indoor)	LPWAN	✓	25 m	2.4 m

2.3.1.1 RSS or CSI-Based Algorithms

RSS is measured at each LoRa packet reception. It indicates the signal strength and can be used for distance estimation with the path loss model of different environments or as the fingerprints of different locations [54–57]. However, RSS has large variations due to environmental multipath factors and wireless signal interference, resulting in hundreds of metres' in distance estimation. Further, the need for frequent and labour-intensive labelling and training is the major drawback of RSS fingerprinting via machine-learning approaches.

CSI provides finer-level channel information than RSS, and CSI-based localisation has been well studied in Wi-Fi [22, 40, 41, 58–60]. It achieves a higher localisation accuracy than RSS by providing abundant information to mitigate radio signal multipath effects; however, it suffers from similar drawbacks as RSS because of the bandwidth limitation of LPWANs, which results in poor localisation accuracy, and the requirement of labeling and training for machine learning-based approaches.

2.3.1.2 TDoA

TDoA is measured by comparing the radio arrival time differences among multiple gateways. An accurate time source such as a GPS module must be equipped with each gateway to synchronise the radio measurements. The transmitter's location can then be estimated with the hyperbolic localisation method [51, 61]. However, according to the LoRaWAN geolocation whitepaper [1], multipath radio propagation and the limited radio bandwidth of LoRaWANs fundamentally limit the accuracy of such systems. An empirical evaluation using GPS-synchronised gateways demonstrated a poor localisation performance of TDoA approaches in LPWANs [51]. Recent research presented OwLL [52], a LoRa localisation system that proposed to utilise TV whitespace band to improve the bandwidth for TDoA-based localisation. It utilised a method in Chime [62] to employ an extra transmitter to synchronise multiple base stations. It achieved approximately nine metres accuracy with a range of 500 m. This thesis will discuss OwLL further in Section 2.3.2.

[1] LoRaWAN geolocation whitepaper. https://lora-alliance.org/sites/default/files/2018-04/geolocation_whitepaper.pdf

2.3.1.3 RTT

Recent research has investigated round-trip time (RTT)-based ranging methods for LPWAN [63, 64]. For example, a new LoRa chip (SX1280) operating at 2.4GHz ISM band supported RTT-based ranging with 1.6 MHz bandwidth in hardware. However, it required hardware upgrading and is not compatible with legacy embedded LoRaWAN end devices. To this end, *Seirios* requires a hardware update in LoRaWAN gateways only, which is significantly more cost-effective. Further, the transmission performance of low power radio transceivers at 2.4 GHz is inferior to their sub-GHz (e.g., 900 MHz) counterparts, which does not meet the requirements of many LPWAN applications.

2.3.1.4 AoA

AoA localisation with triangulation has been well studied in wider band radio standards such as Wi-Fi [65–67]. The AoA localisation system can be combined with other techniques such as ToF to produce fine-grained localisation accuracy (i.e., decimetre or centimetre) [17, 68–72]. However, because of bandwidth limitations, to the best of our knowledge, such an approach has not been investigated in LPWAN yet. *Seirios* is inspired by these approaches that utilise AoA-based triangulation for localisation with multiple APs, and it addresses the bottleneck bandwidth limitation by exploiting multiple communication channels enabled by a novel channel synchronisation algorithm. The super-resolution algorithms in *Seirios* can then distinguish multipaths and achieve accurate localisation. We hope this humble step can inspire further research in the area of AoA-based localisation in narrowband LPWAN.

2.3.1.5 Amplitude-based Algorithms

Karanam et. al. propose a localisation mechanism with Wi-Fi magnitude measurements [67, 73]. Chen et. al. propose an amplitude-based anti-multipath method using LoRa signal to achieve 4.6m accuracy in a 42m $\times$ 48m outdoor area [53], a size approximately one-third of our evaluation (see Chapter 4 for more details). Further, this approach required specially designed antennas instead of the common omnidirectional antennas used by *Seirios* and mounting a LoRa receiver in a flying drone to collect the radio signal from a transmitter at multiple locations, which is not suitable for conventional, stationary LPWAN gateways deployments.

2.3.2 Channel Combination

Increasing the bandwidth is an effective approach to increasing the localisation accuracy. Xiong et al. proposed ToneTrack to utilise a channel-combining algorithm to increase the bandwidth for finer radio multipath resolution [17]. However, this approach is for overlapped wideband (Wi-Fi) signals only. Nevertheless, it inspired us to combine non-overlapped narrowband LoRaWAN signals to increase the bandwidth for localisation, as discussed in Chapter 4. However, the resolution of the combined bandwidth signal was still poor (i.e., 125 m), which cannot be used in localisation directly. Bansal et al. proposed OwLL [52] to exploit TV whitespace band (up to hundreds of MHz) to increase the accuracy of localisation. There are two major differences between OwLL and Seirios. First, OwLL sends hundreds of packets to cover up to tens or hundreds of MHz, while Seirios uses limited bandwidth (i.e., 1.6 MHz with eight channels). Thus, there are energy consumption implications for transmitting such a large number of packets for localisation (80 to 120 packets).

In comparison, *Seirios* transmits eight packets only (a fraction, i.e., 1/15 to 1/10, as that of OwLL). For limited bandwidth scenarios (e.g., 1.6 MHz), this thesis argues that ToF-related algorithms are less effective, and, thus, *Seirios* is designed with AoA algorithms. Second, for synchronisation, OwLL follows Chime [62] and uses an extra transmitter to synchronise the phase of multiple base stations (i.e., gateways), whereas *Seirios* exploits the microstructure of chirps to synchronise the phase of multiple channels instead of synchronising base stations. See Table. 2.3 for details.

Table 2.3: Comparison of OwLL and Seirios

Features	OwLL [52]	Seirios
Bandwidth	400 MHz	1.6 MHz
Localisation time	20.97s	0.24s
Localisation technique	TDoA	AoA
Packets per localisation	80-120	8
Battery life (request twice a day)	1-1.8 years	10+ years
Synchronisation	Base stations	Multiple channels
Range	500 m	100 m
Accuracy	$\approx$ 9 m	$\approx$ 5 m (outdoors)

Abbreviations: time difference of arrival (TDoA), angle of arrival (AoA)

2.3.3 Virtual Antennas

Kotaru et al. proposed SpotFi to create a virtual antenna array with the number of virtual antennas greater than the number of radio signal multipaths, thus, overcoming the constraint posed by a limited number of antennas [40]. That said, the model proposed in SpotFi was designed for ToF-AoA joint estimation, which produced poor accuracy for LoRaWAN. Therefore, this study proposes a novel model for accurate AoA estimation only to avoid unreliable ToF estimation. Moreover, this study proposes to utilise the conjugates of the channel measurements to further increase the number of virtual antennas (Chapter 5), which can further improve localisation accuracy in radio signal multipath rich environments (e.g., cluttered indoor environments).

2.3.4 Spatial Smoothing

The spatial smoothing scheme was proposed by Evan et al. to solve coherent signal classification [74]. ArrayTrack [68] is a uniform linear array (ULA) with eight antennas that utilises spatial smoothing by averaging two adjacent antennas to resolve multipaths to improve the accuracy of AoA estimation. Theoretical studies by Pillai et al. [75] and Pan et al. [76] showed that using both forward and conjugated backward spatial smoothing can further improve the number of coherent signals that can be resolved. However, this method does not work for ULAs with a small number of antennas (e.g., two or three only), which are available in low-cost hardware. To this end, SpotFi [40] proposed to use a special Wi-Fi signal model with multiple channels for spatial smoothing with three antennas. We note that SpotFi does not use the conjugate information because of a significantly larger number of communication channels available in Wi-Fi (e.g., 30, compared with eight in LoRaWAN). Therefore, the bandwidth constraint problem is unique to the LoRa signals studied in this thesis. *Seirios* is inspired by both SpotFi and conjugated-backward techniques and proposes a novel LoRa signal model, which solves coherent multipath signals with a small number of antennas (i.e., two) and a limited number of channels (i.e., eight).

2.4 Background

2.5 Chapter Summary

This chapter reviewed the foundation of LoRaWAN, relevant techniques for PHY sample compression and conventional algorithms for device localisation. PHY sample compression is an enabler for a Cloud-RAN architecture for LP-WAN, such as LoRaWAN. Localisation is an important service for LoRaWAN devices that can benefit from Cloud-RAN architecture to improve performance. The work in this thesis is inspired by the prior research to develop novel algorithms based on Cloud-RAN architecture to enable efficient packet delivery and accurate device localisation.

Chapter 3

Nephelai: Towards LPWAN Cloud-RAN with Physical Layer Compression

In this chapter, we propose *Nephelai*, a Compressive Sensing-based Cloud Radio Access Network (Cloud-RAN), to reduce the uplink bit rate of the physical layer (PHY) between the gateways and the cloud server for multi-channel LPWANs. Recent research shows that single-channel LPWANs suffer from scalability issues. While multiple channels improve these issues, data transmission is expensive. Furthermore, recent research has shown that jointly decoding raw physical layers that are offloaded by LPWAN gateways in the cloud can improve the signal-to-noise ratio (SNR) of week radio signals. However, when it comes to multiple channels, this approach requires high bandwidth of network infrastructure to transport a large amount of PHY samples from gateways to the cloud server, which results in network congestion and high cost due to Internet data usage. In order to reduce the operation's bandwidth, we propose a novel LPWAN packet acquisition mechanism based on Compressive Sensing with a *custom design dictionary that exploits the structure of LPWAN packets*, reduces the bit rate of samples on each gateway, and demodulates PHY in the cloud with (joint) sparse approximation. Moreover, we propose an adaptive compression method that takes the Spreading Factor (SF) and SNR into account. Our empirical evaluation shows that up to 93.7% PHY samples can be reduced by *Nephelai* when $SF = 9$ and SNR is high without degradation in the packet reception rate (PRR). With four gateways, 1.7x PRR can be achieved with 87.5% PHY samples compressed, which can extend the battery lifetime of embedded IoT devices to 1.7.

3.1 Introduction

Low-Power Wide Area Networks (LPWANs) are emerging wireless technologies with features such as comprehensive signal coverage, low bandwidth, potentially small packet sizes, and long battery life [1]. One of the representatives is LoRa, which has been widely used in commercial and industrial applications, such as logistical tracking, smart agriculture and intelligent building [3].

LoRaWAN is a recognised MAC-layer LoRa protocol for reliable data transfer, and it is generally deployed on unlicensed ISM bands with 125 kHz or 500 kHz narrow band channels. Such narrow bands limit the bit rate down to several kilo-bits or hundred-bits per second, while they benefit the demodulator's sensitivity, making it possible to detect and decode LoRa signals significantly lower than noise floor.

Previous research demonstrates that if only one channel is used, LoRaWAN coverage drops exponentially as the number of end devices grows [4] and may only support approximately 120 nodes for a typical smart city deployment [55]. Some other research similarly indicates that LoRaWAN can support from 200-

1000 nodes in different applications [8, 10], which raises concerns about the scalability of LoRaWAN. To this end, by extending from single to multiple channels similar to frequency division multiple access (FDMA), the scalability can be increased [8]. Typical LoRaWAN gateways equipped with Semtech SX1301 chips[1] can operate with up to 8 $\times$ 125kHz channels, which provides greater network capacity than a single channel network by eight times. Furthermore, in the USA, up to 64 $\times$ 125kHz narrow-band channels are allocated on unlicensed ISM bands for LoRaWAN. A naive approach to cover more than eight channels is to use several gateways simultaneously in one spot. A commercial outdoor LoRaWAN gateway costs approximately US$1,000. Therefore, covering all 64 channels would be expensive and difficult to maintain.

Beyene et al. propose the implementation of NB-IoT via Cloud-RAN, which are easy to implement and cost-efficient to deploy [16]. NB-IoT and LoRa/LoRaWAN are both LPWAN technologies and share many common features. Inspired by the Cloud-RAN of NB-IoT, we propose a Cloud-RAN architecture for LoRaWAN as an affordable solution to support as many LoRaWAN channels as possible. Thus, with the help of software-defined ratios (SDR), parallel gateways are replaced with a single remote radio head, and PHY processing is offloaded to the cloud.

As an extra benefit of Cloud-RAN, the opportunity to increase the battery life for end devices is provided. Some other approaches such as optimal frequency selection [62] and backscatter [12] have been proposed, while our approach is based on spatial diversity gains. Similar to the architecture of cellular networks [19], multiple LoRaWAN gateways are commonly deployed to provide wide-area network coverage. Therefore, the signal from one end

[1]SX1301 datasheet. https://www.semtech.com/products/wireless-rf/lora-gateways/sx1301

device can be received by multiple gateways and processed jointly. In a recent research, Dongare et al. implemented such a system to exploit the spatial diversity gain to improve SNR by coherently combining PHY samples captured by various gateways in different locations [15]. Thus, an end device may transmit with a faster bit rate, which results in a shorter transmission duration for a fixed packet/data payload length. Their evaluation shows that increasing the number of received gateways improves the SNR of packets in an approximately logarithmic manner.

Although the aforementioned Cloud-RAN is a promising architecture with many benefits for IoT wireless networks, such a system has a huge impact on the PHY offloading network between the gateways and the cloud. According to Charm [15], when a moving average compressed technique is applied for PHY, 9 Mbps is required for each 500kHz channel and 2.25 Mbps is for each 125kHz channel respectively, which produces 2.25 Mbps $\times$ 64 = 144 Mbps data traffic to the cloud if a gateway supports 64 $\times$ 125kHz LoRa channels. For lossless Nyquist sampling and data stored as 24-bit I/Q samples (12-bit for I/Q each, same as SX1301), a minimal bit rate of 24 bit$\times$(64 $\times$ 125kHz) = 192 Mbps is required for the PHY offloading network. Both settings require gigabit bandwidth for reliable data transmissions, which is challenging in both outdoor or indoor scenarios such as pastures and buildings with sub-100-megabit Internet connections. Moreover, in some rural areas, Internet can only be provided via satellites, the bandwidth of which is very limited. On the other hand, a large-scale LoRaWAN (e.g., with hundreds of gateways) will pose a significant traffic to the data center. It may influence the real-time delivery of PHY samples and reduce the performance of joint decoding that requires synchronised PHY samples from different gateways.

One solution is to equip optical fibers as part of the infrastructure of the

PHY dispatching network. However, the cost is unaffordable for many low-cost or ad hoc IoT applications. Another solution is to upload active channels only. However, for large-scale deployment (i.e., tens of thousands of nodes), the probability of simultaneous multi-channel occupation is high. Moreover, because low SNR signals can benefit from joint processing in the cloud, the channel activity detector becomes more sensitive and uploads PHY samples of idle channels to the cloud due to 'false alarms'.

Therefore, PHY compression is the key enabler for LPWAN Cloud-RAN. To this end, we propose a Compressive Sensing (CS)-based technique, called *Nephelai*, to reduce the network bandwidth between gateways and the cloud. Figure 3.1 shows the overview of *Nephelai*, which leverages the sparsity of the PHY for signal compression and (joint) reconstruction.

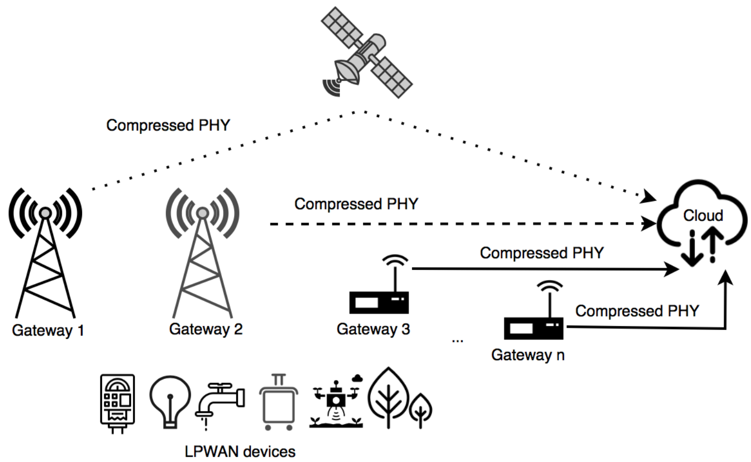

Fig. 3.1: The overview of *Nephelai* decoding in the cloud with compressed PHY samples.

Dictionaries and measurement matrices in *Nephelai* are custom-designed to *exploit the structure of LoRa radio signals* to achieve the best compression and reconstruction performance. *Nephelai* is designed to run in real-time and is implemented with SDR[2]. Our testbed evaluation in our campus has shown that, 1) up to 93.7% samples can be reduced without packet reception rate (PRR) reduction; 2) *Nephelai* can improve battery lifetimes to 1.7x with four gateways and 87.5% PHY samples compressed.

The contributions of this paper are as follows.

- We propose a novel CS-based compression technique for cloud-assisted LPWAN that significantly reduces the bandwidth between the gateways and the cloud.

- We propose a new dictionary to achieve high compression ratios without performance degradation. The proposed dictionary exploits the structure of LoRa radio signals, and achieves more than two orders-of-magnitude better sparse representation than standard Discrete Fourier transform (DFT) and Discrete Cosine transform (DCT) domains.

- We implement a prototype of *Nephelai* with software-defined radios, and our empirical evaluation demonstrates its superior performance on embedded devices.

3.2 Architecture

The *Nephelai* system has one cloud server equipped with GPU for ℓ_1 minimisation acceleration, and inexpensive single-board computers with SDRs as the edge gateways. Physical-layer radio samples are transferred from gateways to the cloud server via conventional Internet infrastructure. Figure 3.2 depicts the overall architecture of *Nephelai*.

[2]One limitation for *Nephelai* is the front-end hardware. Although our prototype discussed in Section 3.2 later can support 64 channels, if *Nephelai* is implemented on legacy front-end SX1257, it can support 8 channels only.

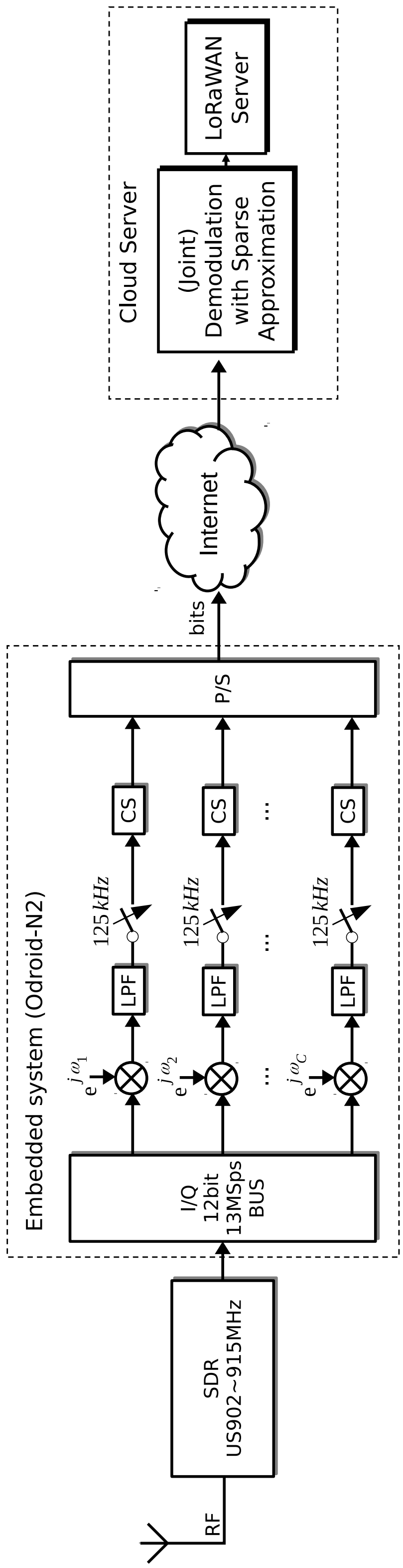

Fig. 3.2: Baseband block diagram showing the architecture of *Nephelai*

The gateway clocks are synchronised via PPS from GPS modules with the accuracy of several microseconds. The accurate timestamp can help synchronise LoRa chirp symbols (see Figure 2.2) and help the cloud server detect coherent LoRa packets easily. To analyze the complexity of our encoding algorithm in edge devices[3], suppose we have N samples per symbol (this will be discussed in Section 3.3.4.2, $N = 128$ in practice), M samples per compressed vector, C as the number of channels and P as the number of low pass filter (LPF) taps. Then, the frequency conversion block together with LPF is $O(NP)$, the down-sampler is $O(N)$, and the CS block is $O(MN)$. The overall complexity in the edge devices is $O(NPC + NC + NMC)$. Therefore, fewer taps for LPF and higher compression ratio for CS block can improve the performance of the embedded system. In order to support multiple 125 kHz channels as discussed in Section 3.1, the SDR of the gateway captures the whole 13 MHz LoRa spectrum, and the embedded system filters each channel and compresses using a shared measurement matrix. Compressed bits of each channel are packed together and uploaded to the cloud server. The cloud server then performs decompression and demodulation to recover the LoRa chirp symbols or jointly process all coherent symbols to improve their accuracy.

[3] We omit the complexity analysis of the proposed decoding algorithm in the cloud (i.e., ℓ_1 minimisation solver) since the cloud can be seen as having unlimited resources.

3.3 Compression

3.3.1 Lossless Compression

We compare the compression performance of *Nephelai* against a conventional lossless compression LZ77-based algorithm, *gzip* [20]. Gzip can only achieve a 7.5% compression ratio for Nyquist-sampled LoRa PHY, which means 92.5% of samples are not compressible. Such a low compression ratio is due to the fact that chirps spread across the whole spectrum, and general compression algorithms cannot exploit this sparsity in the frequency domain. In the following discussion, we consider the lossless compression ratio as the baseline, and investigate a novel CS-based algorithm to increase the compression ratio.

3.3.2 Compressive Sensing

CS is an information theory [77–79] that proposes an approach to recover high dimensional *sparse* signals from low dimensional measurements. Table 3.1 summarizes the mathematical symbols in this discussion.

For a predefined dictionary $\Psi \in \mathbb{C}^{N \times D}$, any signal $\mathbf{x} \in \mathbb{C}^N$ can be a linear combination of Ψ as:

$$\mathbf{x} = \Psi \mathbf{s} \tag{3.1}$$

where $\mathbf{s} \in \mathbb{C}^D$ is a coefficient vector of $\mathbf{x}$ in the Ψ domain. If $N < D$, given $\mathbf{x}$ and Ψ, we can not solve Equation (3.1) to obtain $\mathbf{s}$ in a general form because it is an undetermined problem.

CS imposes the requirement that vector $\mathbf{s}$ is sparse; namely, most of the elements in $\mathbf{s}$ are zeros. Let K denote the number of non-zeros in $\mathbf{s}$, then $\mathbf{s}$ is sparse if $K << D$. K in CS is termed as *sparsity*. CS theory states that vector $\mathbf{s}$ can be recovered accurately by solving the following *stable* ℓ_1 minimisation

Table 3.1: The summary of mathematical symbols used in this chapter.

Symbol	Definition
Ψ	CS dictionary
Φ	CS measurement matrix
U	Diagonal matrix for up-chirp
F_s	Sampling rate
T	LoRa symbol duration
$\mathbf{x}$	Raw samples before compression
$\mathbf{y}$	Compressed vector of measurement
$\mathbf{s}$	Sparse vector
α	Compression ratio
K	The degree of sparsity
D	The number of items in dictionary
N	The number of complex samples in LoRa symbol
M	The length of compressed vector y

problem:

$$\hat{\mathbf{s}} = \arg\min \|\mathbf{s}\|_1 \quad s.t. \quad \|\mathbf{x} - \Psi\mathbf{s}\|_2 < \epsilon \tag{3.2}$$

where ϵ is noise, and provided that Ψ satisfies the Restricted Isometry Property (RIP) condition. Note that RIP is only a sufficient but not a necessary condition. Therefore, ℓ_1-minimisation may still be able to recover the sparse $\mathbf{s}$ accurately, even if Ψ does not satisfy RIP. In fact, ℓ_1 minimisation has a rich history as it has been used to efficiently obtain useful *sparse* information in the signals from a compressed representation [80, 81].

Common ℓ_1 minimisation algorithms are Matching Pursuit (MP), Orthogonal Matching Pursuit (OMP), Homotopy, ℓ_1-magic, etc., and the reconstruction performance of the algorithms depends on the sparsity of the signal and the incoherence between the measurement (compression) matrix and the signal itself, which is application dependent. Therefore, *Nephelai* uses a custom-designed dictionary Ψ to exploit the structure of LoRa signal and a custom-designed measurement matrix Φ to maximize the incoherence between the matrix Φ and the dictionary Ψ. Furthermore, *Nephelai* features a unique joint decoding process to exploit the spatial diversity of the LoRa signals received by the gateways in different locations to further improve the signal reconstruction (i.e., the decoding of the LoRa packets) performance.

3.3.3 Dimension Reduction

Johnson-Lindenstrauss Lemma shows that random projections can preserve the ℓ_2 distance of vector $\mathbf{x} \in \mathbb{C}^N$ in a compressed domain $\mathbf{y} \in \mathbb{C}^M$, where $M < N$ with a high probability [77] as:

$$\mathbf{y} = \Phi\mathbf{x} = \Phi(\Psi\mathbf{s}) \tag{3.3}$$

where $\Phi \in \mathbb{C}^{M\times N}$ is a random compression matrix (recall that $\mathbf{x} = \Psi\mathbf{s}$ from Equation (3.1), $\Psi \in \mathbb{C}^{N\times D}$). Since the sparsity of $\mathbf{s}$ is K (see Section 3.3.2), Wright et al. show that the minimum dimension of M for a successful ℓ_1 minimisation recovery in practice is [82]:

$$M \geq 2Klog(D/K). \tag{3.4}$$

Substituting Equation (3.3) to (3.2), ℓ_1 minimisation can be used to recover sparse vector $\mathbf{s}$ from compressed measurement $\mathbf{y}$ as:

$$\hat{\mathbf{s}} = \arg\min \|\mathbf{s}\|_1 \quad s.t. \quad \|\mathbf{y} - \Phi(\Psi\mathbf{s})\|_2 < \epsilon. \tag{3.5}$$

Therefore, instead of uploading raw LoRa radio samples $\mathbf{x} \in \mathbb{R}^N$ to the cloud, a *Nephelai* edge gateway uploads compressed measurements $\mathbf{y} \in \mathbb{R}^M$, and achieves a **compression ratio** of α as:

$$\alpha = 1 - M \div N. \tag{3.6}$$

3.3.4 PHY Compression

LoRa gateways can compress physical layer radio samples with a predefined measurement matrix ($\Phi \in \mathbb{C}^{M \times N}$, where $M < N$) before transmitting the compressed samples ($\mathbf{y} \in \mathbb{C}^M$) to the cloud server, where (joint) demodulation is performed based on the compressed signals by solving an ℓ_1 minimisation problem, i.e., Equation (3.5).

For $SF \in \{7, 8, 9, 10\}$, we propose one dictionary for each SF covering two scenarios: 1) synchronised chirp symbol; 2) unsynchronised chirp symbol. Generally, scenario 2 is more common, and scenario 1 can be considered as a special case of scenario 2. Thus, a dictionary for unsynchronised should also be feasible for synchronised chirp symbols. However, based on our simulation and evaluation (see Sections 3.3.4.1 and 3.6.2.1), the compression ratio of the synchronised chirps is better than that of the unsynchronised, and thus we recommend the implementation of the synchronisation mechanism for LoRaWAN to achieve a better compression performance.

3.3.4.1 Dictionary Design

Rao et al. have proposed the *continuous*, direct compression of physical layer radio samples with non-overlapped windows, in an attempt to fully recover the signal from the cloud [83]. Normally, radio signals are sparse and compressible in conventional domains such as DFT and DCT. For LoRa, such methods are applicable but a more sparse domain can be obtained by exploiting the structure of the signals.

As discussed previously in Section 2.1.4, we demodulate the symbols by multiplying the symbols with an ideal down-chirp in the time domain and then by performing FFT on the de-chirped symbol. Both synchronised and unsynchronised blocks are sparse in frequency after being multiplied by a down-chirp. Here we define *block* as any T-length clip of a LoRa PHY, where T is equal to the duration of one chirp. A block is a combination of parts from two consecutive symbols. In the following sections, *block* and *unsynchronised symbols* are interchangeable. First, by letting $\varphi(t)$ stand for the phase of an ideal up-chirp, we define matrix $\mathbf{U}$ as having a diagonal made of an ideal down-chirp (opposite phase to an up-chirp),

$$\mathbf{U} = diag(e^{-j\varphi(\frac{0}{BW})}, e^{-j\varphi(\frac{1}{BW})}, ..., e^{-j\varphi(\frac{2^{SF}-1}{BW})}) \tag{3.7}$$

Second, we define $\mathbf{W}$ as the DFT matrix for $N = 2^{SF}$,

$$\mathbf{W} = (\frac{\omega^{ik}}{\sqrt{N}})_{i,k=0,...,N-1} \tag{3.8}$$

where $\omega = e^{-2\pi j/N}$. Therefore, we can write a sparse representation for any LoRa block $\mathbf{x}$ as,

$$\mathbf{s} = \mathbf{WUx} \tag{3.9}$$

where $\mathbf{s}$ represents the frequency domain and has only a few non-zeros. Comparing Equation (3.9) and (3.1), we can then derive the dictionary Ψ as,

$$\Psi = \mathbf{U}^H\mathbf{W}^H \tag{3.10}$$

where $(.)^H$ is the conjugate transpose. Therefore, the dictionary based on the sparsity of LoRa chirps is generated. We produce dictionaries according to $SF \in \{7, 8, 9, 10\}$, and store them in the cloud server.

As a comparison with DFT, DCT, and the proposed chirp dictionary, Figure 3.3a and 3.3c show the sparsity of typical synchronised and unsynchronised LoRa symbols ($SF = 9$) with channel noise in different domains by sorting the samples by order of magnitude. The fastest decay characteristic (or the smallest K) is observed in the proposed dictionary (Ψ), and therefore offers the most sparse representation; which means that the most accurate approximations (or LoRa symbol value estimations) can be obtained in this dictionary by using the smallest number of measurements M (Equation (3.4)). The sparsity in synchronised symbols is slightly better than the unsynchronised, which means that the accuracy in recovering synchronised symbols is better than the unsynchronised. The figure also shows that the proposed Ψ has two-order-of-magnitude fewer significant coefficients (e.g., the normalized magnitude is larger than 0.1) than those of DFT and DCT.

For the down-chirps in PHY, similar dictionaries can be obtained by replacing $\mathbf{U}$ with a matrix with a diagonal made of an ideal up-chirp. Due to the fact that most chirps in LoRa PHY are up-chirps, we first solve ℓ_1-minimisation with the up-chirp dictionary, and then try the down-chirp dictionary if no satisfactory result is obtained. Both dictionaries have similar features and performance. For brevity, we skip the discussion of the down-chirp dictionary.

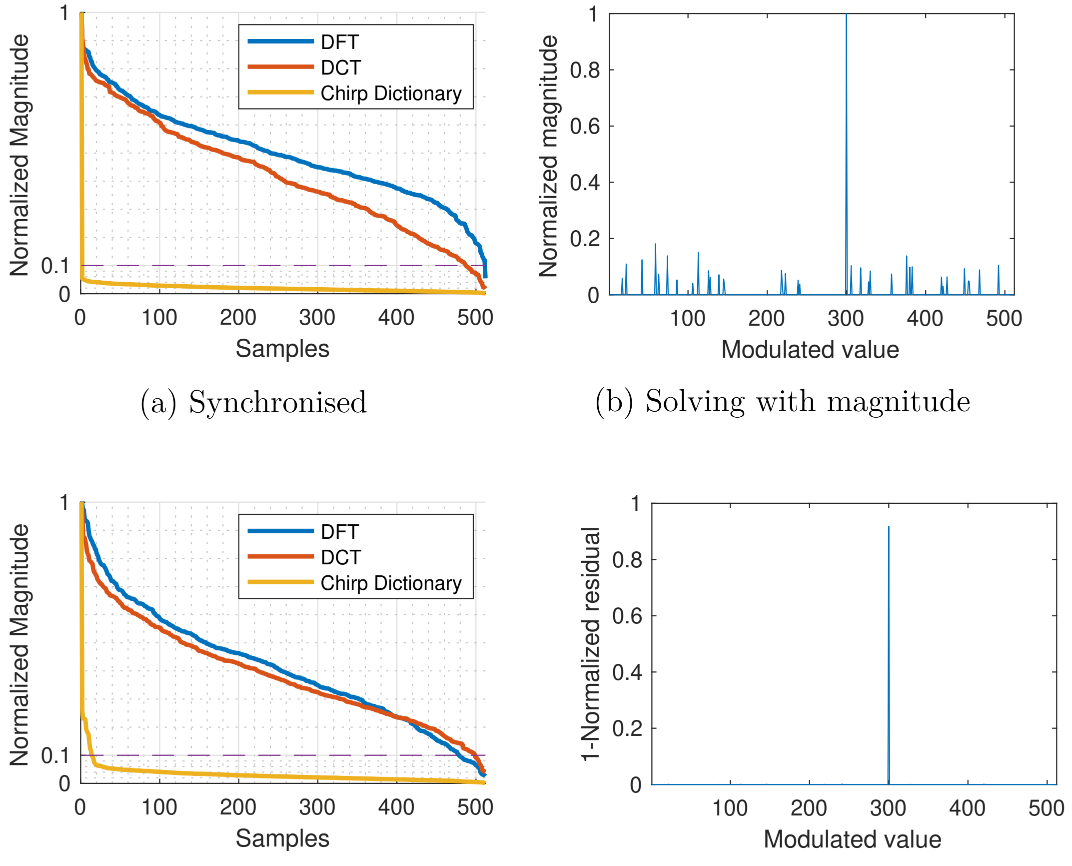

(a) Synchronised (b) Solving with magnitude

(c) Unsynchronised (d) Solving with residual

Fig. 3.3: (a) Sparsity for synchronised symbols based on DFT, DCT and the proposed chirp dictionary. It is more sparse in the proposed dictionary (Ψ) than the DFT and DCT by two orders-of-magnitude. The dashed line denotes the threshold for the coefficients with significant magnitude (0.1). (b) Sparse approximation with magnitude (Section 3.4.1). (c) Signal sparsity for unsynchronised chirps, less sparse than synchronised chirps but more sparse than the DFT and DCT. (d) Sparse approximation with residuals (Section 3.4.1); the residual domain is more sparse than the magnitude domain.

3.3.4.2 Measurement Matrix

As discussed in CS theory [77–79], zero-mean Gaussian matrix and balance symmetric random Bernoulli matrix achieve favorable compression performance. For the computational efficiency on embedded devices, we choose random Bernoulli(± 1) as the measurement matrix Φ with a fixed seed that is shared by both gateways and the cloud server.

Each symbol has $N = 2^{SF}$ samples, i.e., N =128, 256, 512, 1024 for $SF = 7, 8, 9, 10$ respectively. If we process SF separately, we have to compress PHY four times with Φ_7, Φ_8, Φ_9, Φ_{10} for each SF, which is against our motivation for compression. To solve this problem, we only measure with Φ_7. For $SF = 8$, we can simply concatenate two compressed vectors from Φ_7. Similarly, we concatenate four compressed vectors for $SF = 9$ and eight for $SF = 10$.

Thus, the gateway simply compresses every 128 samples with Φ_7 for each channel, and in the cloud the server concatenates compressed vectors for solving different SFs.

3.3.4.3 Compression Ratio

Compression ratios are defined by Equation (3.6), and thus a smaller M results in a better compression ratio. Theoretically, M should be bounded on its lower end by Equation (3.4). However, the noise from the original signal is hidden in compressed vectors, which may make it challenging to recover the original signals (i.e., ℓ_1 minimisation algorithm fails to solve Equation (3.5)). Thus, M is not only bounded by Equation (3.4), but is also affected by the signal SNR. We perform a simulation to investigate this phenomenon. As $N = 2^{SF}$ is an exponent of 2, to simplify the DSP process, M is selected among exponents of 2 (e.g., 16, 32, 64, etc.). Here, we define low, medium and high SNRs as -6, 0 and 6 dB.

Figure 3.4 shows that higher SFs outperform their lower counterparts, and increasing SNR can improve the compression ratio. When SNR is high, $SF = 9$ and $SF = 7$ can be compressed to 1/16 and 1/8 respectively without significant Symbol Error Rates (SERs), and the compression ratio is mainly bounded by Equation (3.4). When SNR is medium and low, $SF = 9$ can be

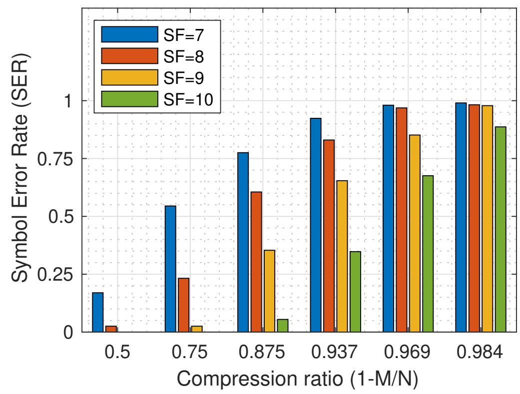

(a) SNR low (-6 dB)

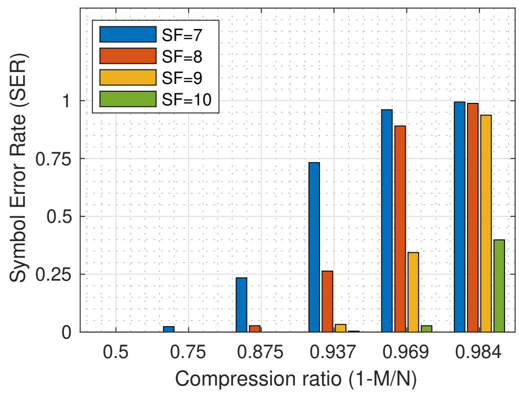

(b) SNR medium (0 dB)

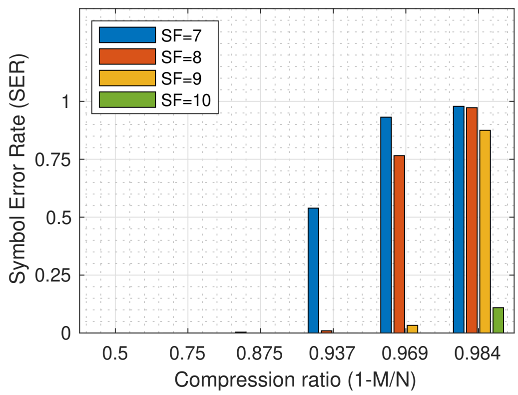

(c) SNR high (6 dB)

Fig. 3.4: Simulation with *synchronised* symbols: SER affected by compression ratio and SNR for different SF

compressed to 1/16 and 1/4 respectively without significant SERs, and the compression ratio is mainly affected by SNR.

We summarize M/N in Table 3.2 to represent the acceptable compression ratio α if SER is small (e.g., ≤ 0.04). Then, the empirical compression ratio based on Figure 3.4 and Table 3.2 can be derived as:

$$\alpha = max\{min\{1 - 2^{-\left\lfloor \frac{SNR_{dB}}{3} + SF - 5 \right\rfloor}, 1 - \frac{2 \cdot SF}{2^{SF}}\}, 0\}. \tag{3.11}$$

For unsynchronised symbols, as shown in Figure 3.5, the performance is

Table 3.2: Reliable compression ratios based on simulations of *synchronised* symbols represented by M/N

	SF7	SF8	SF9	SF10
low SNR (-6 dB)	1	1/2	1/4	1/8
medium SNR (0 dB)	1/4	1/8	1/16	1/32
high SNR (6 dB)	1/8	1/16	1/32	1/32

slightly poorer than that of the synchronised symbols. An unsynchronised symbol is composed of fractions of two consecutive chirp symbols (i.e., the last few samples from the first chirp and the first few samples from the second chirp). Thus, sparsity K is increased from 1 to 2, and the lower bound Equation (3.4) is slightly larger than that of the synchronised symbols. We modified Equation (3.11) to select an appropriate compression ratio for unsynchronised symbols accordingly:

$$\alpha = max\{min\{1 - 2^{-\left\lfloor \frac{SNR_{dB}}{3} + SF - 6 \right\rfloor}, 1 - \frac{4(SF-1)}{2^{SF}}\}, 0\}. \tag{3.12}$$

3.4 *Nephelai* in the cloud

3.4.1 Decoding (Single Gateway)

Most conventional ℓ_1-minimisation algorithms require real-valued vectors and dictionaries, while communication systems always use complex values for I/Q modulation. To solve this problem we transform the vectors from complex-

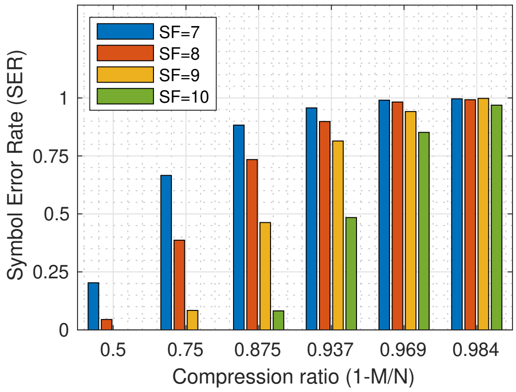

(a) SNR low (-6 dB)

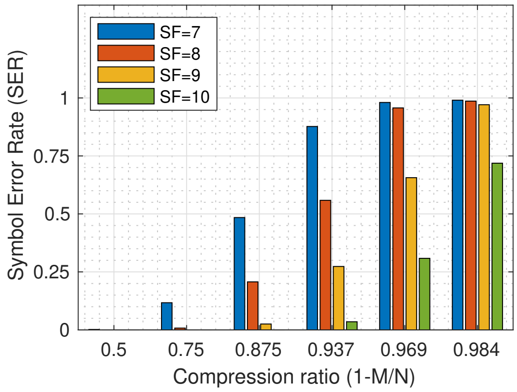

(b) SNR medium (0 dB)

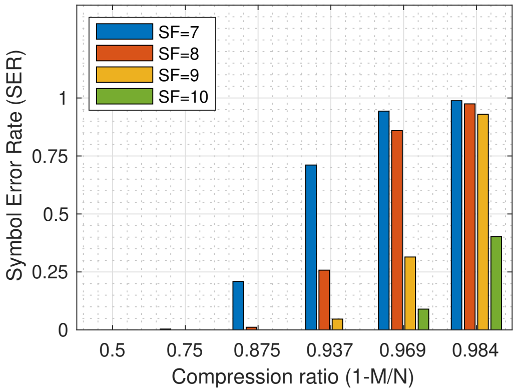

(c) SNR high (6 dB)

Fig. 3.5: Simulation with *unsynchronised* symbols: SER affected by compression ratio and SNR for different SF

valued to real-valued as,

$$\mathbf{y}' = [\Re\{\mathbf{y}\}^T \quad \Im\{\mathbf{y}\}^T]^T \tag{3.13}$$

$$\mathbf{s}' = [\Re\{\mathbf{s}\}^T \quad \Im\{\mathbf{s}\}^T]^T \tag{3.14}$$

$$\Theta' = \begin{bmatrix} \Re\{\Theta\} & -\Im\{\Theta\} \\ \Im\{\Theta\} & \Re\{\Theta\} \end{bmatrix} \tag{3.15}$$

where $\Theta = \Phi\Psi$. Then, we solve the problem with a real-valued ℓ_1-minimisation algorithm for Equation (3.5) as,

$$\hat{\mathbf{s}}' = \arg\min \|\mathbf{s}'\|_1 \quad s.t. \quad \|\mathbf{y}' - \Theta'\mathbf{s}'\|_2 < \epsilon \tag{3.16}$$

After obtaining the sparse vector $\hat{\mathbf{s}}'$ with Equation (3.16), we recover the complex-valued sparse vector $\mathbf{s_{opt}}$ by reversing Equation (3.14), and thus we solve not only the magnitude but the phase of the chirp symbol.

Instead of using FFT for demodulation as described in Section 2.1.4, we proceed to estimate the most likely value λ by using residual r. The residual for symbol candidate $i \in \{0, 1, ..., 2^{SF} \text{-}1\}$ is:

$$r^{(i)}(\mathbf{y}) = \left\| \mathbf{y} - \Phi\Psi\delta^{(i)}(\mathbf{s_{opt}}) \right\|_2, \forall i \tag{3.17}$$

where operator $\delta^{(i)} : \mathbb{R}^D \rightarrow \mathbb{R}^D$ indicates a vector containing the only coefficient related to candidates i (the coefficients related to other candidates are set to be zeros). Then the final symbol estimation is determined by:

$$\hat{\lambda} = \underset{i}{\operatorname{argmin}}\, r^{(i)}(\mathbf{y}), \forall i \tag{3.18}$$

i.e., the λ with the minimal residual representing the modulation value. Figure 3.3d shows the result of *Nephelai* decoding with Equation (3.17) for a noisy chirp symbol. The highest peak (i.e., $1 - r^{(i)}$, suppose $r^{(i)}$ is normalized) represents the modulated value (e.g., 300) of the LoRa symbol correctly. Note that in $\mathbf{s_{opt}}$, the phase of the highest peak may be used for radio-based ranging, which is beyond the scope of this paper.

3.4.2 Joint Decoding

We have discussed how *Nephelai* recovers value λ from single compressed measurement $\mathbf{y}$. In this section, we discuss how *Nephelai* exploits spatial diversity for gateways and improves performance with joint decoding.

Suppose that we have G gateways, and each gateway captures a transmitted copy of the same LoRa symbol independently. Next, *Nephelai* estimates the SNR level γ_g and produces residuals $r_g^{(i)}$ ($g \in \{0, 1, ...G-1\}$) for G gateways with Equation (3.17). One of the ways to fuse these residuals among gateways is to perform a weighted summation. Based on the selection of combining weights, we have four algorithms: 1) weighted equally, aka. equal gain combining (EGC); 2) weighted by the $\sqrt{SNR}$; 3) weighted by the SNR aka. the maximum ratio combining (MRC), and 4) weighted by the SNR^2. We evaluate the algorithms with collected samples by four gateways (further discussion in Section 3.6.2.3), and the results are shown in Figure 3.6. All algorithms succeed in improving the PRR, and the algorithm weighted by the SNR has the best performance especially when the compression ratio is high. Thus, we choose the MRC algorithm with SNR γ_g as the weight in the following evaluation.

Following this, the final symbol estimation is determined by:

$$\hat{\lambda} = \arg\min_i \sum_{g=0}^{G-1} \gamma_g r_g^{(i)}(\mathbf{y}), \forall i \tag{3.19}$$

Nephelai's joint decoding algorithm can be found in Algorithm 1.

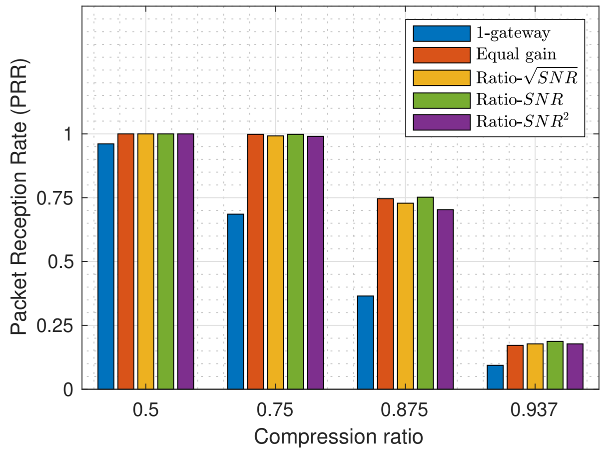

Fig. 3.6: Joint decoding algorithm comparison

Algorithm 1: JOINT-DECODING

Input: M-length measurements $\{\mathbf{y}_g\}_{g=0..G-1}$, estimated SNR $\{\gamma_g\}_{g=0..G-1}$

Output: An integer λ, the decoding result

for $g \leftarrow 0$ ***to*** $G-1$ **do**
  $\mathbf{s}_g \leftarrow \text{solve\_}\ell_1\text{\_minimisation}(\mathbf{y}_g, \Theta, \epsilon)$
  for $i \leftarrow 0$ ***to*** $2^{SF}-1$ **do**
    $r_g^{(i)}(\mathbf{y}) = \left\| \mathbf{y_g} - \Theta\delta^{(i)}(\mathbf{s_g}) \right\|_2$
  end
end
$\lambda \leftarrow \text{argmin}_i \sum_{g=0}^{G-1} \gamma_g r_g^{(i)}$
return λ

3.5 Prototype Implementation

The Edge Gateway The *Nephelai* gateway shown in Figure 3.7 has a radio front-end to capture signal samples on given LoRa channels, and an embedded computer to pre-process and compress the received signal samples before uploading to the cloud. In our prototype, we select BladeRF 2.0 SDR as the radio front-end to capture radio signals on LoRaWAN uplink channels (e.g., 902 MHz to 915 MHz in the USA). The output of SDR is a stream of I and Q components, which can be regarded as complex values where I denotes real and Q denotes imaginary parts respectively. The SDR can sample up to 61.44 mega samples per second (MSps), which are capable of capturing all the information in the whole 13 MHz upstream spectrum for USA defined by LoRaWAN. The Nyquist sampling rate for one channel is 125 kHz for complex samples (i.e., 250 kHz for real samples), and therefore the sample rate for 64 channels is 8 MSps (note the 75 kHz guard band between consecutive 125kHz channels, meaning that 8 MHz is for LoRa channels on a 13 MHz spectrum).

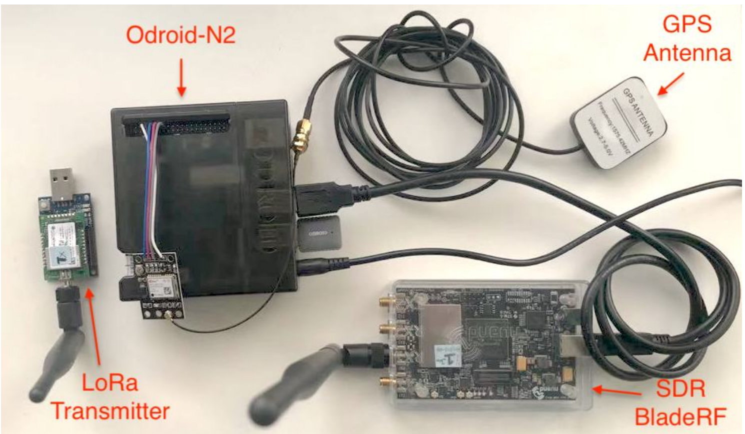

Fig. 3.7: *Nephelai* gateway and a LoRa transmitter

The SDR is connected to a Odroid-N2 (6-core single board computer with quad-core Cortex-A73@1.8GHz and dual-core Cortex-A53@1.9GHz) via a USB 3.0 port, through which the LoRa radio samples are transferred. Next, the Odroid-N2 processes (see Section 3.2) and compresses (see Section 3.3.4) the samples before transferring them to the cloud server. The sampling rate of our prototype is 13 MHz, which is sufficient to cover the 13 MHz LoRaWAN spectrum. Without loss of generality, we demonstrate the compression performance of *Nephelai* in a single LoRa uplink channel. If one single channel is compressible, so are 63 other channels.

We design and implement the software for *Nephelai* gateways, called *gr-Nephelai* based on the open-source software-defined ratio platform GNU-Radio. The frequency conversion and low pass filter shown in Figure 3.2 are implemented in C++ and complied with single instruction multiple data (SIMD) optimisation. Although there are 64 parallel branches in Figure 3.2, we implement one block for all 64 channels instead of one block for each of the 64 channels to reduce the handover between blocks. The low-pass filter taps are selected as 47 to maintain real-time performance. The passband is designed to be 275 kHz, which works well to avoid inter-channel interference. When the gateway is running at full capacity (processing 64 channels), the overall CPU usage is approximately 60%.

The transmitter We program Multitech mDot[4], which comprises a LoRa wireless chip (SX1272), to periodically transmit 4 predefined bytes. The mDot with STM32F411RET uses 31 mA @100 MHz in the maximum power setting.

The Cloud Server Although the *Nephelai* cloud server can be any kind of general server, we use a 12-core CPU, 32 GB RAM and Nvidia 2070 GPU server in our prototype. It can perform ℓ_1-minimisation algorithms for joint sparse LoRa signal reconstruction (i.e., LoRa packet decoding, see Section 3.4.2) in real-time.

[4]MDot datasheet. https://www.multitech.com/brands/multiconnect-mdot

3.6 Evaluation

3.6.1 Goals, Metrics and Methodologies

We deployed a *Nephelai* testbed with four *Nephelai* gateways (see Section 3.5) on our campus as shown in Figure 3.8, where gateways are connected to a *Nephelai* cloud server (see Section 3.5) via Wi-Fi. We programmed seven mDots (see Figure 3.7) as LoRa motes to periodically transmit predefined LoRa packets with power from 2 dBm to 14 dBm. We installed the LoRa motes in several representative positions in the campus to emulate real applications, and collected LoRa radio samples with each gateway simultaneously. During our evaluation, we collected more than one million LoRa chirp symbols among SF7 to SF10 to evaluate the performance of *Nephelai*.

We deployed LoRa motes to emulate real use cases. Mote-1 was an indoor temperature and humidity sensor; mote-2 acted as a passive infrared sensor (PIR), which functioned as an occupancy detector for the warehouse; mote-3 behaved as a smart water meter; mote-4 represented a simple outdoor weather station; mote-5 was attached to a stair handrail and counted people; and mote-6 and mote-7 measured the soil's humidity to control a watering system for the lawn. In this evaluation we were not interested in application data but instead focused on PHY compression and potential battery lifetime improvement with joint decoding.

Nephelai is designed to implement the physical layer compression for cloud-assisted LoRa demodulation/decoding and to potentially improve transmitters' energy efficiency. Therefore, the **goals** of our evaluation were:

1. to study whether *Nephelai* can reduce the network bandwidth of the front-haul in LPWAN Cloud-RAN,

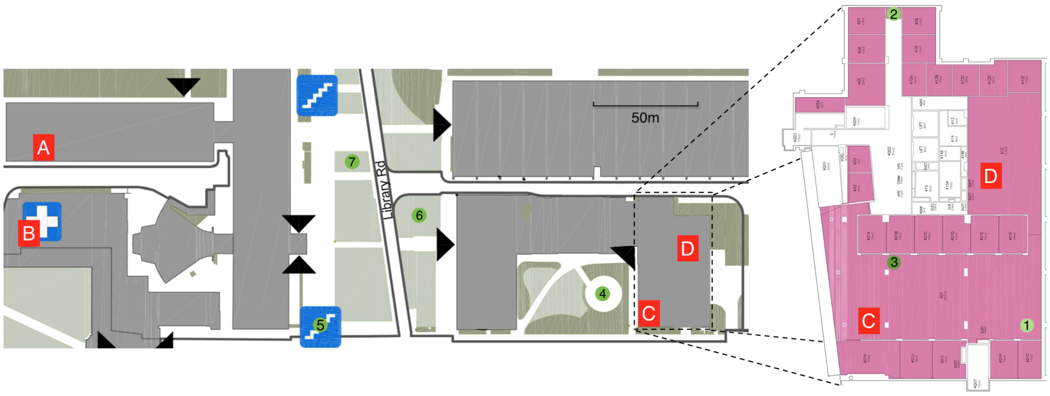

Fig. 3.8: *Nephelai* test-bed on our campus. The gateways are marked with the letter A/B/C/D and stationed inside buildings near windows to simulate a customer-deployed scenario. The transmitters (motes) are labeled from 1 to 7, and marked with green circles. Mote-1 is on the same floor (the 4th floor) as gateway C; mote-2 is on the 3rd floor; mote-3 is hidden in the basement, 5 floors below gateway C. Motes-4/5/6/7 are placed outdoor without any cover.

2. to study the impact of compression ratio (α) on the system's performance, and

3. to study whether *Nephelai* can demonstrate similar energy improvements for the LoRa transmitter as the state-of-the-art LPWAN Cloud-RAN, but with fewer front-haul data rates.

The **metric** for network bandwidth reduction is bits per second (bps), and that for energy reduction is battery lifetime extension. For **methodologies**, firstly, on the symbol level we evaluate how SNR and compression ratios affect SER in order to compare these with the simulation in Section 3.3.4.3. And then on packet level, we evaluated the PRR for single gateway scenarios with three LoRa motes and different power transmission levels. Furthermore, we evaluated the joint processing gain with four gateways and four transmitters to demonstrate that an equivalent SNR improvement can be achieved as the state-of-the-art [15], i.e., to extend the battery lifetime to approximately 1.7x (equivalent to 2.3 dB SNR improvement) with four gateways, but with greater

PHY compression. As there are different SFs resulting in different PRRs, we assumed that each SF was equal likely to be selected, and we calculated the expected PRR by averaging the PRRs of all SFs.

3.6.2 Empirical Results

3.6.2.1 Compression ratio

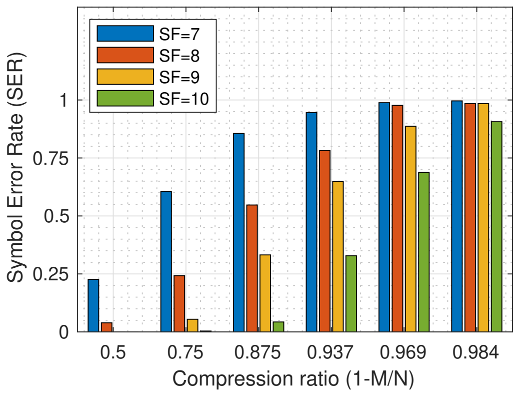

(a) SNR low (-6 dB)

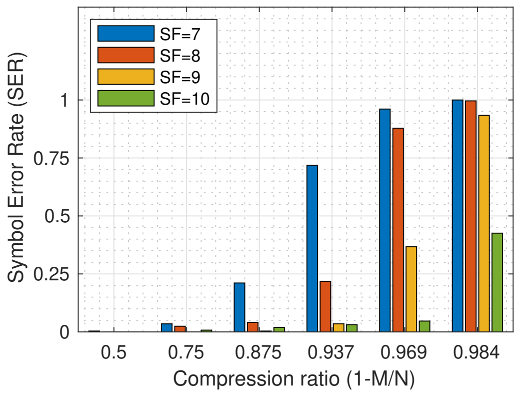

(b) SNR medium (0 dB)

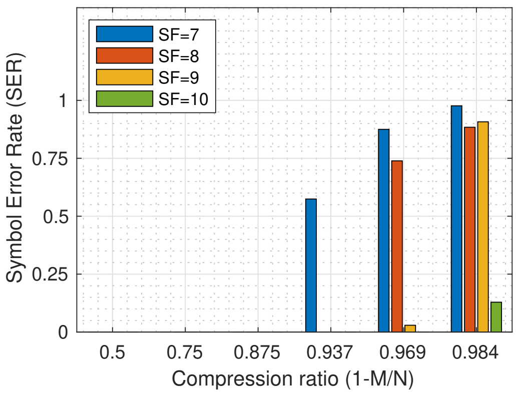

(c) SNR high (6 dB)

Fig. 3.9: Synchronised symbols from testbed: SER affected by compression ratio and SNR for different SFs

As discussed in Section 3.3.4.2, the compression ratio (α) is calculated using the dimension of measurement matrix $\Phi \in \mathbb{C}^{M \times N}$ (see Equation (3.3)). In this section, we are only interested in how SNR affected the compression ratios, and in evaluating the compression ratio determination equations (i.e., Equation (3.11) and (3.12)) for synchronised and unsynchronised symbols. We programmed motes-1/2/3 to transmit with power varying from 2 dB to 14 dB, and collected 50,000 synchronised and unsynchronised symbols respectively. We grouped symbols with respect to their low (-6 dB), medium (0 dB) and high (6 dB) SNR. Figure 3.9 and 3.10 compare the compression performance of different SFs and SNRs based on the symmetric Bernoulli matrix(Φ) of ± 1 and our proposed chirp dictionary Ψ (see Section 3.3.4). For example, for medium SNR (0 dB, i.e., the signal energy is equivalent to the noise floor) with synchronised symbols in Figure 3.9, SF9 achieves an SER below 0.04 with a compression ratio of 93.7%. This represents approximately 16 times the bandwidth reduction in the Cloud-RAN front-haul.

With a small SER value (e.g., ≤ 0.04) as the reliable transmission threshold, we can summarize that the evaluation matches the simulation, when referring to M/N in Table 3.3 based on Figure 3.9, which compares Table 3.3 to Table 3.2. Therefore, we can use Equation (3.11) in compression ratio selection. We observed similar patterns in the results of unsynchronised symbols in Equation (3.12), however we omit the discussion here for brevity.

Furthermore, we performed PRR evaluation for synchronised packets with different SNRs, SFs and compression ratios as shown in Figure 3.11. The LoRa packets transmitted in the evaluation had fixed length and their payloads consisted of 4 bytes (equivalent to 8 symbols). We defined PRR 75% as the threshold for reliable transmission [84] and used it in our compression ratio selection. With the PRR criteria, Figure 3.11 implies a similar compression ratio selection as that with SER in Table 3.3. Thus, we can use Equation (3.11)

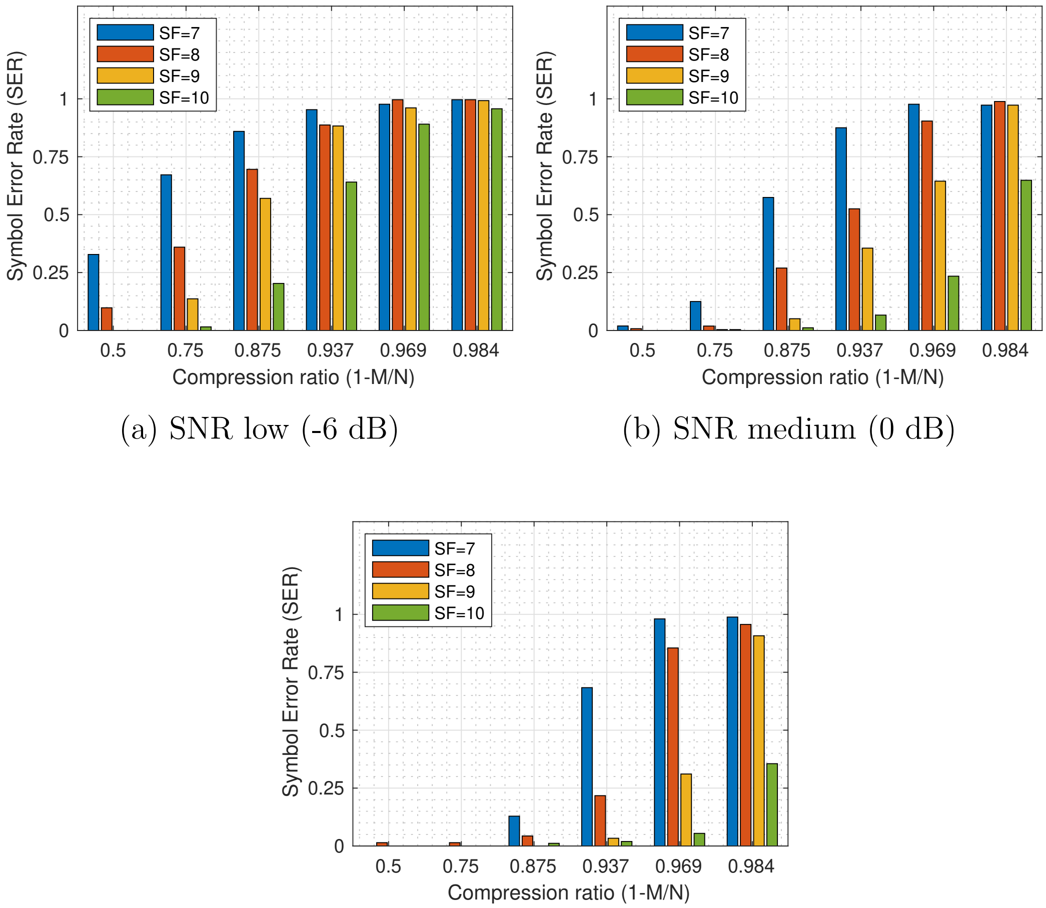

(a) SNR low (-6 dB)

(b) SNR medium (0 dB)

(c) SNR high (6 dB)

Fig. 3.10: Unynchronised symbols from testbed: SER affected by compression ratio and SNR for different SFs

in compression ratio selection. For unsynchronised symbols, similar to the discussion with SER, Equation (3.12) is used for compression ratio selection.

In summary, compared to the benchmark of lossless algorithm LZ77 that achieves a compression ratio of 7.5% (see Section 3.3.1 for more details), the proposed approach can improve the compression ratio by approximately 10 times, depending on the parameter settings. For example, when SNR is high, a compression ratio up to 93.7% can be achieved for most SFs. Therefore, *Nephelai* achieves a significant reduction in traffic between gateways and the cloud server, which makes the cloud-assisted LoRa decoding scheme more scal-

Table 3.3: Reliable compression ratio based on testbed collected data represented by M/N.

	SF7	SF8	SF9	SF10
low SNR (-6 dB)	1	1/2	1/4	1/8
medium SNR (0 dB)	1/4	1/8	1/16	1/32
high SNR (6 dB)	1/8	1/16	1/32	1/32

able.

3.6.2.2 The performance of single gateway

In the single gateway evaluation using a real case, our goal was to compress PHY without PRR degradation. As discussed in Section 3.3, over-compression means that the ℓ_1 minimisation algorithm fails to solve Equation (3.16), which increases SERs and decreases PRRs.

Firstly, as shown in Figure 3.8, LoRaWAN transmitter motes-1, 2 and 3 were installed in a fixed position and were programmed to transmit 4 bytes with different spreading factors ($SF = 7, 8, 9, 10$) at 2 dBm, 8 dBm and 14 dBm respectively. We collect packets via one gateway in either synchronised or unsynchronised mode. Secondly, with the algorithm proposed in Section 3.4.1, we calculated the PRR for different compression ratios. Instead of SER, we were more interested in PRR which describes the performance of end-to-end data transmissions. For example, if PRR is halved, the energy required to successfully deliver one packet is doubled, as the embedded node needs to transmit the packet twice. Therefore, the battery lifetime is halved. It is evident that PRR is more intuitive than SER in describing battery lifetime.

In our synchronised scenario, the compression ratio of 87.5% for motes-1 and 2 produced more than 90% PRR when power transmission was medium.

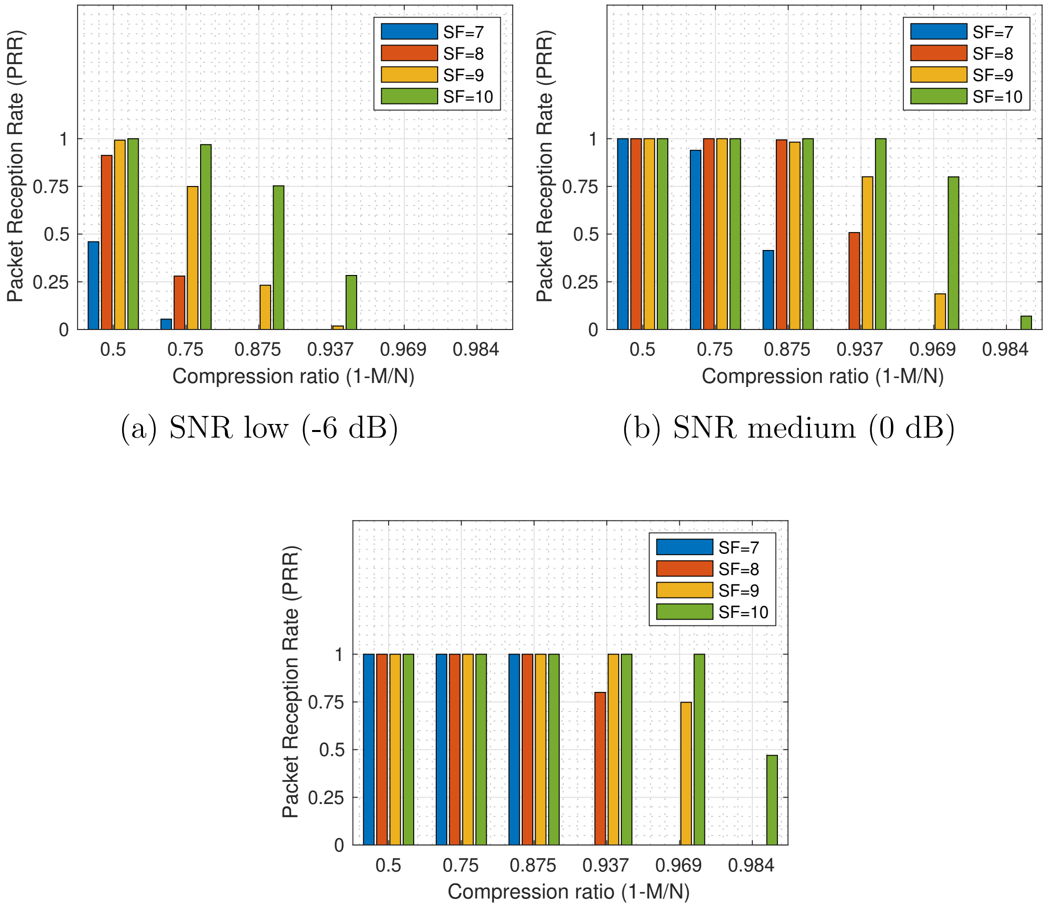

(a) SNR low (-6 dB)

(b) SNR medium (0 dB)

(c) SNR high (6 dB)

Fig. 3.11: PRR affected by SNR, SFs and compression ratios for synchronised symbols/packets

For mote-3 in the basement, the compression ratio of 75% produced more than 50% PRR. We note that mote-3 was over-compressed with the compression ratio of 87.5% because the PRR is only 30% (see Figure 3.12). Increasing power transmission could have increased the compression ratio for mote-3 from 75% to 87.5%, allowing it to maintain its PRR above 50% (Figure 3.12(c)). According to the mDot datasheet, increasing power transmission from medium to high consumes 3.7% extra energy, which provides another acceptable option for scalability improvement.

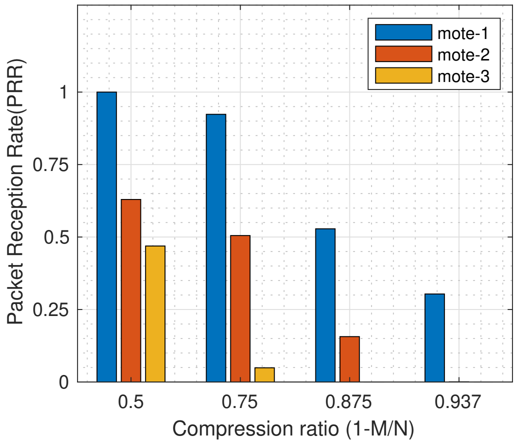

(a) Tx power low (2 dBm)

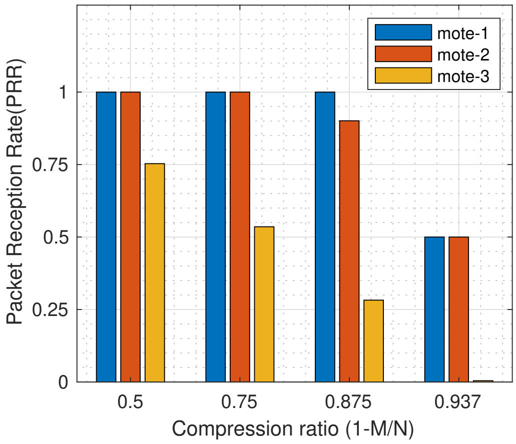

(b) Tx power medium (8 dBm)

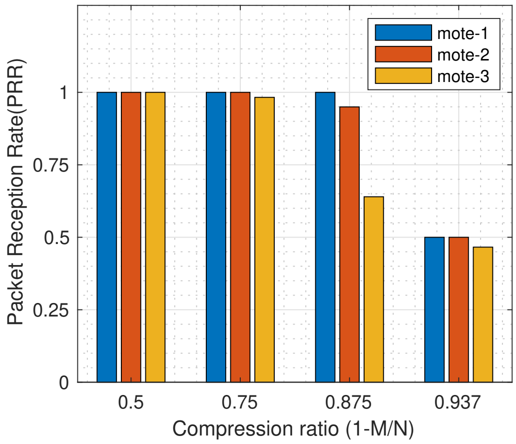

(c) Tx power high (14 dBm)

Fig. 3.12: The single gateway evaluation with 3 transmitters and **synchronised** symbols shows that PRR is affected by compression ratios in different power transmission scenarios. Motes-1/2/3 were placed according to Figure 3.8.

In summary, Figure 3.12 shows that PRR does not decrease with appropriate compression ratios, and increasing power transmission can improve the compression performance of *Nephelai*. Therefore, if all motes transmit at 14 dBm, we can select 87.5% as the compression ratio. For 64 channels, only $64 \times 24 \times 125000 \times (1 - 0.875) = 24$ Mbps is required for a single gateway in LPWAN Cloud-RAN. Consequently, such a gateway can operate with bandwidth-limited Internet connections, widely extending the deployment region and application scenarios.

3.6.2.3 The performance of joint decoding

Compressing PHY without PRR degradation is possible as shown in Section 3.6.2.2 above. In this section, we evaluate the improvement of PRR with joint decoding under compression. Our goal was to achieve an equivalent performance to the state-of-the-art Charm system (i.e., 2.3 dB SNR improves with four gateways, see Section 3.1 for the details), but with less front-haul bandwidth between the gateway and the cloud.

Firstly, we programmed motes-4,5,6 and 7 to be in synchronised mode and to send 4 byte messages periodically with high transmission power[5] (14 dBm). We collected LoRa radio samples simultaneously via gateways-A,B,C and D with different compression ratios (see Section 3.6.1 and Figure 3.8 for testbed deployment in details). The number of packets for each SF was equal. Secondly, we calculated the PRR for single gateway decoding and coherent joint decoding with 4 gateways (according to the algorithm discussed in Section 3.4 under different compression ratios). We averaged PRR for all SFs to get an expected PRR as discussed previously in Section 3.6.1.

Figure 3.13 shows how much improvement can be seen by joint decoding with four gateways compared to a single gateway. For battery-powered LoRa motes, the expected energy consumption per packet is reversely proportional to the PRR, and thus the expected battery lifetime is proportional to the PRR. When the compression ratio was 87.5%, mote-4 had PRR above 99% (since the position of mote-4 was very close to one of the gateways), while motes-5,6 and 7 had poor PRR with a single gateway. After joint decoding

[5]We define 14 dBm as high transmission power in this paper, but in fact 14 dBm is a moderate choice compared to the maximum 22 dBm.

with four gateways, the PRR of mote-5 was improved from 70% up to 93%, while mote-6 went from 47% to 77%, and mote-7 went from 36% to 76%. The improvement factors are 1.33, 1.64 and 2.11 respectively, and the average is about 1.70. Therefore, on average, joint decoding extends battery lifetime to approximately 1.70 with four gateways when the compression ratio is 87.5%. We note that the least improved PRR occurred when the compression ratio is 75%, which is equivalent to a good quality, low power wireless link with a high Cloud-RAN bit rate. Therefore, 87.5% is the recommended trade-off between compression ratio and PRR.

For compression up to 93.7%, single gateways experience severe packet loss for each mote. After joint decoding, the PRR of mote-4 was improved from 40% to 58%, while mote-5 improved from 16% to 22%, mote-6 from 13% to 22%, and mote-7 from 10% to 20%. However, this compression ratio is not recommended because most of the PRRs are still poor (i.e., less than 50%) even with joint decoding. Particularly, increasing the compression ratio from 87.5% to 93.7% for mote-4 causes PRR to decrease from more than 99% to 40%, meant that the mote had a shorter battery lifetime by approximately 60%. Finally, we note that when the compression ratio is 75%, with joint decoding, all PRRs are increased to more than 99%.

In summary, *Nephelai* with 4 gateways improves the PRR and the battery lifetime of a LoRa transmitter by 1.7 times on average, with the recommended compression ratio of 87.5% compared to a single gateway, which is equivalent to 2.3 dB SNR improvement ($10log_{10}1.7$). The compression ratio of 87.5% also means that the PHY is compressed from 3 Mbps down to 375 kbps for one channel, while that of Charm is 2.25 Mbps per channel (see Section 3.1 for details). This demonstrates that *Nephelai* has similar functionality in improving the battery lifetime of embedded IoT devices as Charm [15], while *Nephelai* reduces the bandwidth between gateways and the cloud by $1 - 0.375/2.25 = 83.3\%$.

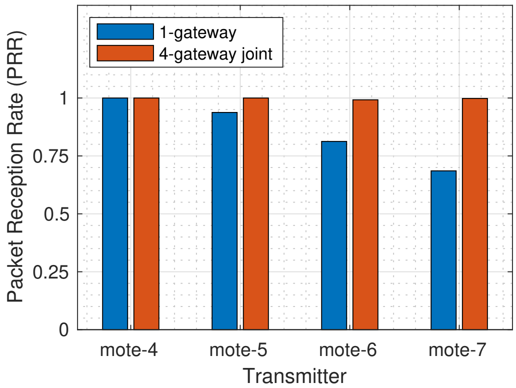

(a) Compression ratio = 0.750

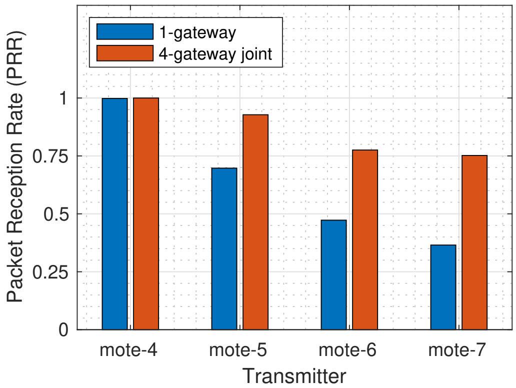

(b) Compression ratio = 0.875

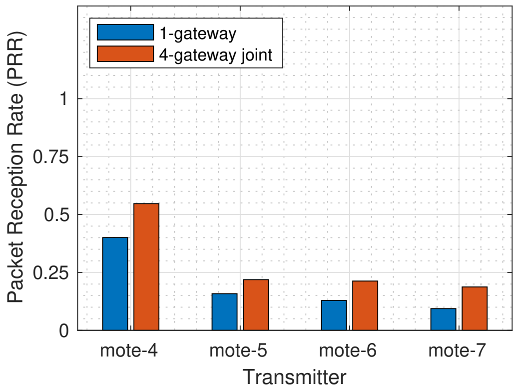

(c) Compression ratio = 0.937

Fig. 3.13: PRR improvement by 4-gateway joint decoding with compression ratio

3.6.2.4 Cloud computing overhead

Solving ℓ_1 minimisation is computationally intensive, but can be handled with parallel implementation using multi-threading, GPU, FPGA, etc. in the cloud. If the demodulation of one symbol is performed in real-time, and the delay caused by data transmission and computation (from the gateway to the cloud, and back to the gateway) meets the LoRaWAN requirement for an ACK, the

Nephelai system is feasible.

We evaluated cloud computing overhead by performing single-threading tests with MATLAB on Intel Core i7-8700 CPU @ 3.20GHz with 32GB RAM for 1000 times calculation per case as shown in Table. 3.4. The worst case is SF10 with a 50% compression ratio. One symbol for SF10 can be solved in less than 500 ms with a single thread. The length of one symbol for SF10 is 8.2 ms, and in 500 ms the gateway can receive at most 61 of these symbols. Therefore, a 64 core server can be used in the cloud to dispatch demodulation tasks to each core in order to obtain real-time demodulation within 500 ms. For other SFs and compression ratios, the computational demand is even lower. Note that the computation can be further optimised for higher efficiency.

LoRaWAN has a relatively loose requirement for ACK delays due to low bit rates (e.g., 300 bps). There is a parameter called ACK_TIMEOUT in the LoRaWAN settings with a default value of "2 $\pm$ 1s (i.e., a random delay between 1 and 3 seconds)". The demodulation latency is less than 500ms as discussed above, and the Internet latency is typically less than 100 milliseconds one way. Processing latency caused by gateways and radio propagation delays can be ignored. Thus, an ACK can easily be generated in one second to meet the LoRaWAN requirements discussed above.

Table 3.4: ℓ_1-minimisation overhead testing for different SFs and compression ratios. Unit: millisecond.

α	SF7	SF8	SF9	SF10
0.5	5.1$\pm$ 2.5	10.8$\pm$2.7	66.8 $\pm$61.9	297.7$\pm$180.5
0.75	2.0$\pm$ 0.6	4.7$\pm$ 1.0	16.3$\pm$13.7	71.2$\pm$32.6
0.875	1.0$\pm$ 0.2	2.2$\pm$ 0.4	5.5$\pm$ 3.3	16.1$\pm$6.1
0.937	0.6$\pm$ 0.1	1.1$\pm$ 0.2	2.3$\pm$ 0.9	5.1$\pm$1.8

3.6.2.5 Influence of concurrent transmission

Theoretically, multi-channel concurrent transmission may reduce the system's performance by leaking energy as noise to other channels. However, through our evaluation, we have found that concurrent transmission does not cause system degradation.

We established a LoRa transmitter that sent packets with SF=8 and a packet length of 41.5 ms every 50 ms periodically in one 125kHz channel, and another transmitter that sent in the neighbouring channels. We calculated the PRR based on the collected samples in different interference environments: no interference, concurrent transmission on a +200kHz channel, concurrent transmission on a +400kHz channel, ... , and concurrent transmission on a +1000kHz channel. Our evaluation results show that no significant PRR reduction is caused by concurrent transmissions. If we have a well designed filter for each 125kHz channel, the noise caused by concurrent transmissions can be prevented. In summary, *Nephelai* is robust against the interference caused by concurrent transmissions.

3.7 Conclusion

We introduce *Nephelai*, which is based on CS-theory, to reduce the bandwidth requirement between edge gateways and the cloud server for cloud-assisted LoRaWAN. *Nephelai* exploits: 1) the physical layer structure of LoRa symbols for a custom designed *dictionary* to significantly improve its compression performance, 2) the relationship between compression ratios, SNR and SFs to select an appropriate compression ratio, and 3) radio signal spatial diversity by joint decoding to improve the PRR as well as the battery lifetime for end devices. Our empirical results with an edge gateway prototype consisting of

SDR and Odroid-N2 show that *Nephelai* can reduce traffic between gateways and cloud servers by up to 93.7% and can significantly improve the scalability of cloud assisted LoRaWAN.

Chapter 4

Seirios: Leveraging Multiple Channels for LoRaWAN Outdoor Localisation

4.1 Abstract

Geolocation is an important context for a large number of IoT end-point devices connected by LoRaWAN. Due to the bandwidth limitations of narrowband LPWANs, existing localisation methods that do not require specialised hardware (e.g., GPS) produce poor performance. To increase the localisation accuracy, we propose a super-resolution localisation method, called *Seirios*, which features a novel algorithm to synchronise multiple **non-overlapped** communication channels by exploiting the unique features of radio physical layer to increase the overall bandwidth. We design a *Seirios* prototype and evaluate its performance in an outdoor area of 100 m $\times$ 60 m, which shows that *Seirios* can achieve a median error of 4.4 m (80% samples $<$ 6.4 m). The results show that *Seirios* produces 36.2% less localisation errors than the

baseline approaches.

Our evaluation also shows, in contrast to previous studies in Wi-Fi localisation systems with wider bandwidth, that ToF is less effective for AoA in narrowband LPWAN localisation.

4.2 Introduction

Low-Power Wide-Area Network (LPWAN) is providing wide-range wireless network coverage for low-power embedded devices. In order to meet the requirements of long range and power efficiency, LPWAN is designed to transmit at low bit-rates (e.g. in the order of 100 bps) in narrowband radio. In addition to low-power communication, geolocation is another important service that can enable a wide range of IoT applications that require the location information of the embedded IoT devices. GPS is a popular technology to acquire such location information outdoors. However, it requires additional hardware (i.e., GPS receiver) and cost, as well as is power intensive because a GPS receiver takes a significant amount of time (e.g., in the order of 10 seconds) to acquire GPS satellite signals and navigation data from a sleep state (i.e., "cold start"). Technologies such as assisted GPS and cloud-offloaded GPS [20,85] can reduce the acquisition time significantly, but they need to download/upload a significantly amount of data from/to the Internet, which is challenging for low bit-rated LPWAN.

An alternative is to exploit common localisation algorithms with existing infrastructure (i.e., gateways) of LPWANs, such as RSS-based fingerprinting, and TDoA or AoA-based triangulation, to localise embedded IoT devices, which requires no extra hardware (e.g., GPS module) and may work **indoors**. However, one major disadvantage of these approaches is their undesirable localisation accuracy. Taking LoRaWAN as an example, according to LoRaWAN geolocation whitepaper[1], RSS-based localisation can only provide 1,000 - 2,000 metre accuracy. While TDoA-based localisation algorithms claim to provide 20 - 200 m accuracy, an outdoor evaluation in a public LoRaWAN shows that such algorithms achieved a median accuracy of 200 m only [51]. Such poor localisation accuracy can't meet the requirements of many applications such as geofencing and asset tracking.

A major performance bottleneck of narrowband LPWAN radio-based localisation is the radio multipath effect. Previous research shows that both RSS and TDoA-based localisation methods suffer from significant errors due to the multipath effect [5]. Recently, researchers have proposed a number of approaches to improve the localisation accuracy for LPWANs [5, 48, 53, 64]. However, super-resolution algorithms [17, 22, 40, 41, 59, 68, 86] that have been well investigated to resolve the multipath effect and improve the accuracy of Wi-Fi-based localisation have not been studied for LPWANs yet. The key behind these algorithms is to extract the significant reflectors (though strongly coherent) from incoherent channel state measurements, and resolve the direct path. Incoherent channel state measurements can be provided by an antenna array [68], multiple sub-carriers in wideband signal [40], and/or multiple dimensions [59]. Specifically, The radio signals in different communication channels naturally *out of sync*, making it difficult to utilise multiple channels to increase bandwidth and decrease localisation errors. To this end, Chronos [22] proposes stitching multiple Wi-Fi channels via two-way CSI measurements and communications. However, such approach is difficult to apply in LPWANs since their data rates can be very slow (e.g., 300 bps) that makes two-way

[1]https://lora-alliance.org/sites/default/files/2018-04/geolocation_whitepaper.pdf

CSI communication costly and, to be the best of our knowledge, embedded LPWAN radio transceivers can't measure CSI yet.

To this end, we propose *Seirios*, which exploits the channel state information of multiple channels as incoherent measurements and utilises super-resolution algorithms on multiple anchors (i.e., gateways) to provide accurate localisation for LPWAN devices. It works with legacy LoRaWAN devices, and the specialised hardware is required for gateways or Access Points (APs) only, making it cost-effective to deploy.

Seirios exploits the unique structure of the radio signal, i.e., linear chirps that sweeps the whole band (see Section 2.1.3 for the details), to synchronise the radio signal in multiple LoRaWAN[2] channels without two-way communications and CSI measurements like Chronos [22]. The contributions of this paper are as follows.

- We propose *Seirios* for narrowband LPWAN localisation, which achieves significantly higher accuracy than state-of-the-art approaches and does not require special hardware in the legacy embedded LPWAN devices.
- We propose a novel inter-channel synchronisation algorithm to obtain the synchronised Channel State Information (CSI) of multiple channels by exploiting the unique structure of LoRaWAN physical layer. Compared to prior work [22], our approach **does not require two-way communications and CSI measurements**, which is more applicable to LPWAN architecture.
- We design and implement a prototype of *Seirios* with software-defined radios (SDRs) as the APs and off-the-shelf embedded LoRaWAN devices,

[2]LoRaWAN, NB-IoT and Sigfox are the major standards of LPWAN.

and our evaluation in a 100 m $\times$ 60 m outdoor area shows that *Seirios* achieves a median localisation error of 4.4 m, which is 36.2% smaller than the baseline approaches. Different to the observation in previous studies with Wi-Fi localisation systems, our results show that Time-of-Fight (ToF) estimation is harmful to narrowband LPWAN localisation.

4.3 Background

Table 4.1: The summary of mathematical symbols used in this Chapter 4

Symbol	Definition
SF	LoRa Spreading Factor
BW	LoRa bandwidth
F_s	Sampling rate
T	LoRa symbol duration
M	Number of channels
P	Number of multipaths
$\boldsymbol{R}$	Covariance matrix
$\boldsymbol{A}$	Steering matrix
$\boldsymbol{\Phi}$	Diagonal matrix of AoA
$\boldsymbol{B}$	Diagonal matrix of random phase offset
$\boldsymbol{\Gamma}$	Matrix of path attenuation
λ	Chirp rate in linear chirps
c	Speed of light
d	Sensor spacing, i.e., distance between two antennas
f_c	Carrier frequency
f_δ	Channel spacing, i.e., frequency between two channel

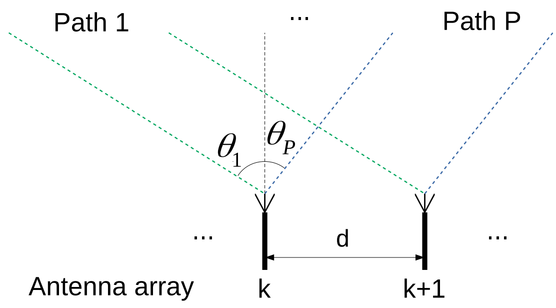

Fig. 4.1: A pair of adjacent antennas in a uniform linear array (ULA). The AoA is defined as the angle between an incident signal and the array's normal. Antenna spacing d is the distance between adjacent antennas. The source is far from the array, and thus the incident signals of the same path are parallel.

4.3.1 Signal Model

Before discussing LoRa, note Table 4.1, which summarizes the mathematical symbols used in the following sections.

Suppose there are P significant paths between a sender and a receiver. Since the signal is narrowband, the channel response of each path can be modeled as a complex value $\alpha_p (p = 1 \dots P)$, representing the amplitude attenuation and phase shift compared to the original signal $u(t)$ that has been sent. The received signal $r(t)$ is the sum of multipath replicas of the original signal $u(t)$ as,

$$r(t) = \sum_{p=1}^{P} \alpha_p u(t - \tau_p), \tag{4.1}$$

where τ_p is the ToF of the p-th path. With a Fourier transform, we can transfer Eq (4.1) into the frequency domain as,

$$R(f) = U(f) \sum_{p=1}^{P} \alpha_p e^{-j2\pi f \tau_p}, \tag{4.2}$$

where f is the frequency. Therefore, we can obtain the channel response by

$$H(f) = \frac{R(f)}{U(f)} = \sum_{p=1}^{P} \alpha_p e^{-j2\pi f \tau_p}, \tag{4.3}$$

Suppose we have M equally spaced channels with frequency spacing f_δ and K antennas. We use the central frequency to represent the frequency of the whole narrowband channel, and $H_{k,i}$ to represent the channel response of the i-th ($i = 1 \ldots M$) channel measured by the k-th ($k = 1 \ldots K$) antenna. Each path has an AoA $\theta_p (p = 1 \ldots P)$, as depicted in Figure 4.1. Therefore, $H_{k,i}$ can be represented by

$$H_{k,i} = \sum_{p=1}^{P} \alpha_p e^{-j2\pi[f_c+(i-1)\cdot f_\delta]\tau_p} e^{-j(k-1)2\pi d sin(\theta_p) f_c/c}, \tag{4.4}$$

where d is the antenna spacing—that is, the distance between the adjacent antennas (k and $k+1$)—and c is the speed of light. For simplicity, we use $\Phi(\theta_p)$ or Φ_p to represent the phase shift caused by the AoA θ_p and $\Omega(\tau_p)$ or Ω_p caused by the ToF τ_p. We have

$$\Phi_p = \Phi(\theta_p) = e^{-j2\pi d sin(\theta_p) f_c/c}, \tag{4.5}$$

$$\Omega_p = \Omega(\tau_p) = e^{-j2\pi f_\delta \tau_p}, \tag{4.6}$$

$$\gamma_p = \alpha_p e^{-j2\pi f_c \tau_p}, \tag{4.7}$$

$$H_{k,i} = \sum_{p=1}^{P} \gamma_p \Phi_p^{k-1} \Omega_p^{i-1}. \tag{4.8}$$

If the central frequency is increased by 2 MHz on 915 MHz spectrum, for $\tau_p = 100$ ns (i.e., 30m), there is a significant phase change for Ω_p of 1.26 radian. However, Φ_p is less affected by f_δ. For example, if $d = 0.14$ m, $\theta = 80°$, an increment of 2 MHz on 915MHz spectrum causes Φ_p to change by 0.006 radian only, which is negligible.

For linear chirps, as suggested by Eq. (2.3), frequency increases linearly and monotonically with time. With Eq. (4.3), the channel response for continuous frequency can be measured with linear chirps. For example, 125 kHz LoRa chirp with central frequency 920 MHz can be used to measure the channel response from 919.9375 MHz to 920.0625 MHz. *Seirios* utilises this microstructure of LoRa signals to obtain the channel response of continuous frequency and perform interchannel synchronisation (see Section 4.4.3 for details).

4.3.2 MUSIC and ESPRIT

MUSIC [40, 86–88] and ESPRIT [89, 90] are known as super-resolution algorithms, and have been shown to resolve the multipath effect in wider-band radio (e.g., Wi-Fi) localisation system.

Previous research has shown that increasing the number of antennas (e.g., up to eight) can increase the localisation accuracy [68]. However, *Seirios* can work with only two antennas but provides acceptable localisation accuracy, which achieves low-cost for the hardware. For a pair of antennas (k and $k+1$) with M LoRa channels, the measurements matrix $\boldsymbol{X}_{MU}$ for MUSIC can be organised as,

$$\boldsymbol{X}_{MU} = [H_{k,1} \cdots H_{k,M}, H_{k+1,1} \cdots H_{k+1,M}]^T \tag{4.9}$$

The steering vector required by MUSIC is,

$$\vec{\boldsymbol{a}} = \begin{bmatrix} 1 \\ \Omega(\tau) \\ \cdots \\ (\Omega(\tau))^{M-1} \\ \Phi(\theta) \\ \Phi(\theta)\Omega(\tau) \\ \cdots \\ \Phi(\theta)(\Omega(\tau))^{M-1} \end{bmatrix} \tag{4.10}$$

To this end, we can utilise the measurement matrix $\boldsymbol{X}_{MU}$ and steering vector $\vec{\boldsymbol{a}}$ to estimate each paths by searching the AoA and ToF that can generate peaks on the pseudo-spectrum span of MUSIC.

Alternatively, we can also use ESPRIT to solve multipaths. The measurement matrices $\boldsymbol{X}_{ES,k}$, $\boldsymbol{X}_{ES,k+1}$ for either antenna in a pair can be organised as,

$$\boldsymbol{X}_{ES,k} = [H_{k,1} \cdots H_{k,M}]^T \tag{4.11}$$

$$\boldsymbol{X}_{ES,k+1} = [H_{k+1,1} \cdots H_{k+1,M}]^T \tag{4.12}$$

Therefore, we can compose a model to exploit the rotational invariance to solve AoA,

$$\begin{bmatrix} \boldsymbol{X}_{ES,k} \\ \\ \boldsymbol{X}_{ES,k+1} \end{bmatrix} = \begin{bmatrix} \boldsymbol{A} \\ \\ \boldsymbol{A\Phi} \end{bmatrix} \boldsymbol{\Gamma} + \boldsymbol{\epsilon}, \tag{4.13}$$

where $\boldsymbol{\Phi} = diag(\Phi_1 \dots \Phi_P)$, $\boldsymbol{\Gamma} = [\gamma_1 \dots \gamma_P]^T$, $\boldsymbol{\epsilon}$ is the noise (can be ignored for high SNR signal), and $\boldsymbol{A}$ is a steering matrix. By solving $\boldsymbol{\Phi}$, the AoAs are estimated.

4.4 Design

As discussed in Section 4.2, *Seirios* utilises triangulation with multiple APs. The key to improving localisation accuracy is improving AoA estimation. In this section, we will discuss interchannel packet synchronisation (Section 4.4.3) and extended super-resolution algorithms (Section 4.4.6 and Section 4.4.5) to overcome the challenges posed in Section 4.2 to improve the accuracy of AoA estimation as well as the performance of the system.

4.4.1 System Design

Seirios is designed to exploit multiple LoRaWAN APs to locate a transmitter. The location and antenna direction of APs are known in advance and stored in the cloud. Here, the APs sense the radio signal transmitted from the transmitter before relaying them to the cloud server. We assume that there is only one transmitter and no concurrent transmission at the same channel. Then, the cloud server synchronise the channels and performs an AoA estimation from the radio signal measured at each AP and locate the transmitter via triangulation. Each AP in *Seirios* has at least two synchronised antennas. The distance between the two antennas is slightly less than the half of the wavelength. If there is one path only between the transmitter and an AP, the AoA can be calculated directly by comparing the phase difference of the received signal between two antennas. However, in reality, there are multiple paths due to radio signal reflection. Even though the Line-of-Sight (LoS) path exists, other paths may cause significant errors in the AoA estimation due to radio signal self-interference.

Prior studies show that the number of significant reflectors in an indoor environment is 5.05 on average, with a standard deviation 1.95 [22]. For an outdoor or uncluttered indoor environment, there will be even less number of significant reflectors (e.g., four). Therefore, one of our research questions is how to accurately estimate the AoA of a limited number paths in such environments (both indoor and outdoor) with narrowband radio signal (e.g., LoRa). We will first discuss indoor localisation in this chapter, and then outdoor localisation in the next chapter.

Figure 4.2 shows an illustrated example that *Seirios* decomposes the radio wave multipaths generated by the tree reflectors, estimates the AoA of the radio wave in different APs and localises the target successfully.

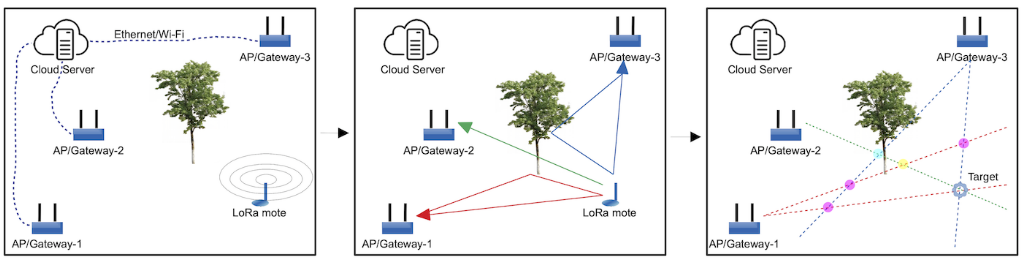

Fig. 4.2: An example of *Seirios*. *Seirios* selects the direct paths via a maximum likelihood gateway fusion introduced in Section 4.4.7.

4.4.2 Channel State

Channel state information (CSI) represents how signals at certain carrier frequencies propagate from the transmitter to the receiver along multiple paths [60]. It has been widely used in Wi-Fi signal based localisation systems [17, 40, 41, 58, 59]. To measure CSI, a Wi-Fi transmitter sends packets whose preamble contains pre-defined training symbols for each subcarrier. When the training symbols are received, the receiver can measure CSI by comparing the amplitude and phase of the received symbols with the pre-defined training symbols.

For LoRa, similar CSI can be obtained. At the receiver, the radio signal can be sampled as a complex sequence of I and Q components. *Seirios* detects the preamble and applies the digital processing algorithms introduced in [28] for precise carrier frequency offset (CFO) and sampling time offset (STO) calibration. In the following discussion, we assume that all LoRa chirps are well calibrated. Since both the sender and the receiver know the preamble, this can be regarded as a training sequence. Here, LoRa CSI can be obtained by comparing the received preambles with the pre-defined preambles (i.e., linear up-chirps).

Furthermore, we can sum up the repeating up-chirps in the preamble to improve signal-to-noise ratio (SNR) in CSI estimation. There are two reasons ensuring that the up-chirps can be summed up as follows. Firstly, since the frequency modulation for up-chirp is symmetric (see Equation (2.3)), the phase will roll back to its initial state after the period of one chirp, and thus **all these up-chirps have the same phase**. Moreover, the preamble only lasts for a small amount of time and the channel response does not change during this period, and thus **all these up-chirps have the same CSI**. Therefore, we can combine all the up-chirps by

$$\bar{r}(t) = \frac{1}{N_{Preamble}} \sum_{l=1}^{N_{Preamble}} r^{(l)}(t), \tag{4.14}$$

where $N_{Preamble}$ stands for the number of up-chirps in the preamble, $r^{(l)}(t)$ is the l-th up-chirp received, and $\bar{r}(t)$ represents the summation of received up-chirps.

To this end, LoRa CSI can be measured by,

$$CSI = \frac{1}{T} \int_0^T \bar{r}(t) \cdot u^*(t) dt, \tag{4.15}$$

where $u(t)$ is the zero-phased up-chirp defined in Equation (2.5), and $(.)^*$ denotes the conjugate transpose. Equation (4.15) is similar to the pulse compression technique, which is used in LoRa demodulation to significantly increase the SNR.

Different to Chronos [22],which estimates the CSI of a wireless link by comparing the CSI measurements in the two end nodes of the link, *Seirios* estimates the CSI by comparing the received up-chirps in the preamble with the reference on the receivers only. The advantage of our approach is two-fold. First, none of the embedded LoRaWAN devices (transmitters) is capable of measuring CSI. *Seirios* requires CSI measurements in one end (i.e., LoRaWAN gateway) only, while Chronos requires both ends to measure CSI. This makes *Seirios* cost-effective to deploy because the number of embedded devices is orders of magnitude more than that of gateways. Second, the data rates of LoRaWAN (can be as low as 300 bps) are orders of magnitude smaller than those of Wi-Fi (the lowest is 1 Mbps). Therefore, transmitting the CSI measurements between two ends incurs significantly more time and (energy) costs in LoRaWAN.

We have discussed the method for LoRa CSI measurements above. Below, we will discuss how CSI can be used in localisation.

Recall that both MUSIC and ESPRIT utilise channel response to resolve radio signal multipaths (see Section 4.3.1 and Section 4.3.2). The main difference between CSI and channel response is a random phase shift that is introduced in CSI because the transmitter and the receiver are not synchronised. For wideband Wi-Fi signals, CSIs for each subcarrier are measured at the same time. The phase shift is the same for each subcarrier, so it does not affect the results of super-resolution algorithms. Therefore, CSI can be used directly by the super-resolution algorithms.

However, for the i-th narrowband channel of LoRa measured by antenna k, $CSI_{k,i}$ is phase-shifted from $H_{k,i}$ (see Equation (4.4)) as

$$CSI_{k,i} = H_{k,i} \cdot e^{j2\pi(\phi_i^{tx} - \phi_i^{rx})}, \tag{4.16}$$

where ϕ_i^{tx} and ϕ_i^{rx} are the initial phases of the transmitter and the receiver, respectively. Since each channel (here LoRa channels may be viewed as the Wi-Fi subcarriers) is measured individually, the random phase shift is different for each channel. Therefore, unlike Wi-Fi signals, LoRa CSI must be calibrated before it can be used with super-resolution algorithms.

To calibrate phase shift is equivalent to synchronise channels by solving $\phi_i^{tx} - \phi_i^{rx}$ in Equation (4.16). However, solving the synchronisation problem between a transmitter and a receiver is challenging. Chronos [22] proposed measuring CSI on both the transmitter and the receiver to eliminate the phase shift, yet the method requires extra hardware to measure CSI in embedded LoRaWAN transmitters, which is undesirable.

Conversely, in the context of localisation, we do not need to estimate the absolute value of the phase shifts. Instead, we need an identical phase shift—say, the phase shift of the first channel—for all calibrated channels to be used by super-resolution algorithms.

Taking M LoRa channels into consideration, we assume the multipaths are stable during a short period of time. An AP stores the CSI estimation (see Section 4.4.2) based on the latest LoRa packet in each channel. Since the transmitter and the receiver are not synchronised, there is a random phase offset between the received signals of two packets in the adjacent channels. We model this random phase offset as a unit complex number $\beta_i (i = 1 \dots M)$. However, since the antennas are synchronised, they share the same phase offset. Therefore, the received signal $\boldsymbol{X}_k$, $\boldsymbol{X}_{k+1}$ for two antennas can be modeled as,

$$\begin{bmatrix} \boldsymbol{X}_k \\ \\ \boldsymbol{X}_{k+1} \end{bmatrix} = \begin{bmatrix} \boldsymbol{BA} \\ \\ \boldsymbol{BA\Phi} \end{bmatrix} \boldsymbol{\Gamma} + \boldsymbol{\epsilon}, \tag{4.17}$$

where $\boldsymbol{B} = diag(\beta_1, \beta_2 \dots \beta_M)$, $\boldsymbol{\Phi} = diag(\Phi_1, \Phi_2 \dots \Phi_P)$, $\boldsymbol{\Gamma} = [\gamma_1, \gamma_2 \dots \gamma_P]^T$, $\boldsymbol{\epsilon}$ is the noise, and $\boldsymbol{A}$ is a steering matrix:

$$\boldsymbol{A} = \begin{bmatrix} 1 & \dots & 1 \\ \Omega_1 & \dots & \Omega_P \\ \vdots & & \\ (\Omega_1)^{M-1} & \dots & (\Omega_P)^{M-1} \end{bmatrix}. \tag{4.18}$$

Note that, since random phase offset $\boldsymbol{B}$ exists, it is difficult to solve $\boldsymbol{\Phi}$ directly by super-resolution algorithms. Figure 4.3 shows an example of the CSI in synchronised and unsynchronised channels collected by the *Seirios* prototype introduced in Section 4.5. In the next section, we will discuss how to exploit the microstructure of LoRa signal for interchannel synchronisation.

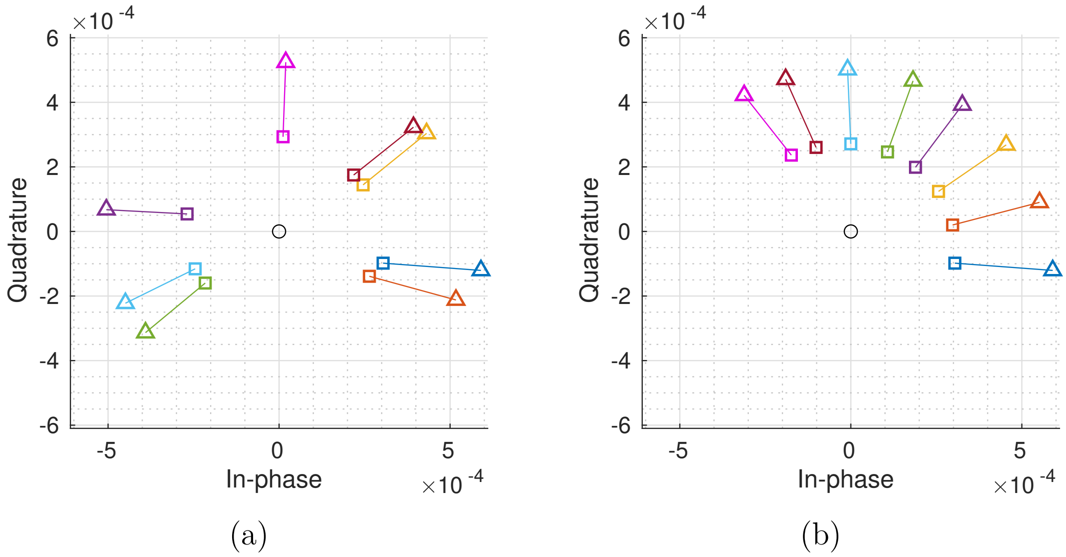

Fig. 4.3: (a) CSI of unsynchronised channels. Triangles denote the CSI of antenna k, and squares denote the CSI of antenna $k+1$. Eight different colors represent eight adjacent channels. (b) CSI of synchronised channels. Only synchronised CSI can be used in spatial smoothing.

After synchronisation, we have $\beta_i = \beta_j(\forall i, \forall j)$. Without loss of generality, we assume $\beta_i = 1, \forall i$. Therefore, the signal model in Equation (4.17) becomes

$$\begin{bmatrix} \boldsymbol{X}_k \\ \boldsymbol{X}_{k+1} \end{bmatrix} = \begin{bmatrix} \boldsymbol{A} \\ \boldsymbol{A\Phi} \end{bmatrix} \boldsymbol{\Gamma} + \boldsymbol{\epsilon}. \tag{4.19}$$

4.4.3 Interchannel Synchronisation

First of all, let us briefly review the related work discussed in Section 2.3.2. ToneTrack [17] has proposed a method to align overlapped Wi-Fi channels. (Adjacent channels are regarded as the special forms of the overlapped channels in this paper, to be differentiated from non-overlapped channels.) It first equalises the phase slope in the frequency domain; then, it aligns the phase of the last subcarrier of the first wideband channel and the first subcarrier of the second wideband channel. With these two steps, the second wideband channel can be concatenated to the first channel to form a wider band. However, this method only works for overlapped channels. By contrast, *Seirios* improves the method to operate on non-overlapped narrowband channels.

Different to a Wi-Fi signal, which has multiple subcarriers to form a phase slope, a narrowband LoRaWAN signal has only one carrier. To form a similar phase slope for the LoRaWAN signal, we exploit the microstructure of LoRa chirps. For illustration, we define $g(f)$ as the channel state for a continuous frequency range from the lower bound to the upper bound of the bandwidth. Figure 4.4a shows an example of the phase slopes for three channels (915.2 MHz, 915.3 MHz, and 915.4 MHz). Note the random phase shift in between is caused by lack of synchronisation (see the discussion in Section 4.4.2). Equation (2.3) shows that frequency f and time t have a linear relationship.

Therefore, we can estimate $g_i(f)$ for channel i as

$$g_i(f) = \bar{r}_i(t(f))u^*(t(f)) = \bar{r}_i(\frac{f - f_i + \frac{BW}{2}}{\lambda})u^*(\frac{f - f_i + \frac{BW}{2}}{\lambda}), \tag{4.20}$$

where $f \in [f_i - \frac{BW}{2}, f_i + \frac{BW}{2}]$, f_i is the carrier frequency of channel i. Figure 4.4a depicts the phase of $g_i(f)$ for $i = 1, 2, 3$.

However, unlike the stable phase slope illustrated by [17], the phase slope of the LoRa narrowband channel is full of noise even when the SNR is high (see Figure 4.4b, where the SNR is 10 dB). This is because that the phase change in a narrowband (e.g., in channel 1 the phase decreases by approximately 0.05 rad, as shown in Figure 4.4b) is much less than that of a Wi-Fi wideband (e.g., approximately 3.0 rad in [17]), and, thus, the narrowband is less robust to the noise than Wi-Fi even with the same noise level. To better estimate the phase offset between two channels, *Seirios* **averages** the phase offset within the overlapped frequency to reduce the noise. By compensating the phase offset of the second channel to align with the first channel, the second channel can now be concatenated to the end of the first channel, as shown in Figure 4.4b.

For non-overlapped channels, ToneTrack states that estimating the correct amount of phase offset is challenging. To this end, for narrowband radio signals, we propose to generate a (**virtual**) intermediate channel response as a bridge to assist the synchronisation. In the microbenchmark (See Section 5.4), we show that the channel response varies slowly with frequency, making it possible to generate the virtual intermediate channel with small errors by averaging the two adjacent channels. Taking Figure 4.4c as an example, we can obtain the (virtual) intermediate channel response (shown as a bridging channel in the figure) by averaging the phases of (co-phased) channel 1 and channel 2. Similar to the overlapped channels, non-overlapped channels can now be synchronised with the (virtual) intermediate channel (Figure 4.4d).

Unlike Wi-Fi wideband, which measures multiple CSIs in one packet, a LoRa narrowband can only measure one CSI per packet. To measure the CSI of multiple channels, at least one packet on each channel should be transmitted within the coherence time. A LoRaWAN end device has eight channels of 125 kHz with 200 kHz spacing. Eight packets should be transmitted on eight different channels to measure their CSI. LoRaWAN channels are separated by 75 kHz guard bands, and the (virtual) intermediate channel has a 25 kHz overlap with the adjacent channels. In practice, *Seirios* leaves out the first and the last 4 kHz because the quality of phase estimation in transient is poor. Thus, the overlapped frequency of one LoRaWAN channel (with the virtual bridging channel) is 17 kHz (13.6% of the bandwidth), which is sufficient for synchronisation (see our evaluation in Section 5.4.2 for more details). The synchronised CSI can later be used in super-resolution algorithms for multipath resolution.

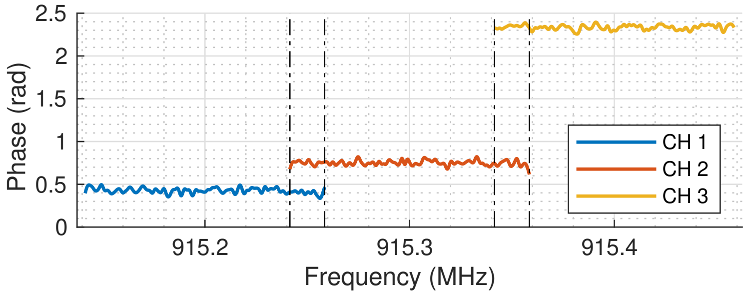

(a)

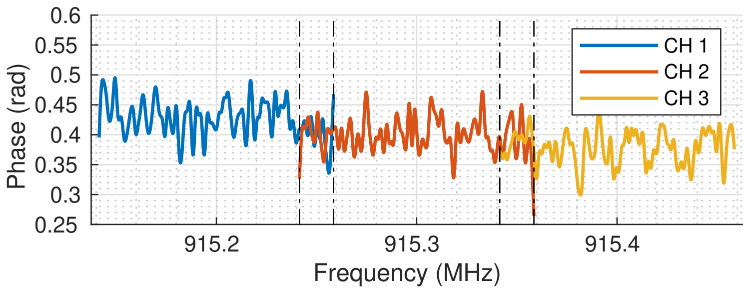

(b)

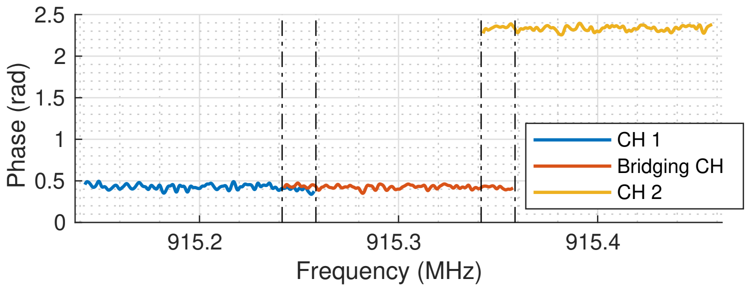

(c)

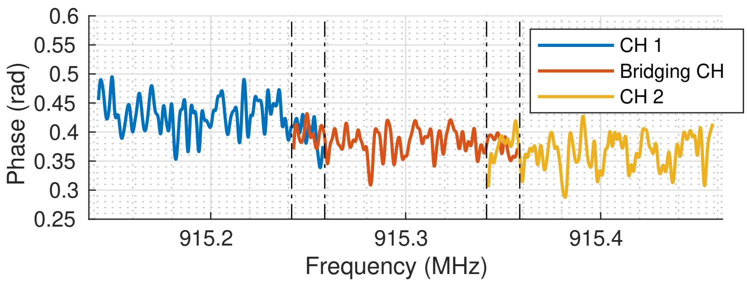

(d)

Fig. 4.4: (a) Lack of synchronisation between transmitters and receivers introduces random phase shift. (b) Interchannel synchronisation exploits the overlapped band to eliminate the phase shift. (c) For non-overlapped channel, a bridging channel can be generated by averaging two adjacent (co-phased) channels. (d) Using a generated bridging channel to synchronise two adjacent channels.

4.4.4 Estimating AoA with MUSIC

In the the multipath multi-channel model for MUSIC and ESPRIT as shown in Section 4.3.2, multipath reflectors are highly correlated so that $R_\Gamma = E\{\mathbf{\Gamma}\,\mathbf{\Gamma}^H\}$ is rank-deficient. It will result in failure for the MUSIC algorithm [87]. To solve this problem, we follow the spatial smoothing approach proposed in SpotFi [40]. Specifically, *Seirios* smooths $L = 6$ consecutive channels in $M = 8$ synchronised LoRa channels since a typical configuration of LoRaWAN has 8 $\times$ 125kHz channels with the channel spacing of 200kHz between the centre frequencies (f_c) of adjacent channels.

Therefore, we first measure the CSI for each channel by two antennas k and $k+1$ (see Section 4.4.2) as

$$CSI\ Matrix = \begin{bmatrix} csi_{k,1} & csi_{k,2} & \cdots & csi_{k,8} \\ csi_{k+1,1} & csi_{k+1,2} & \cdots & csi_{k+1,8} \end{bmatrix}. \tag{4.21}$$

Then, we can generate $\boldsymbol{X}_k$ as a 3×6 matrix

$$\boldsymbol{X}_k = \begin{bmatrix} csi_{k,1} & csi_{k,2} & \cdots & csi_{k,6} \\ csi_{k,2} & csi_{k,3} & \cdots & csi_{k,7} \\ csi_{k,3} & csi_{k,4} & \cdots & csi_{k,8}. \end{bmatrix} \tag{4.22}$$

with $L - 1 = 5$ CSI measurement overlaps. Similar structure can be applied to $\boldsymbol{X}_{k+1}$. Therefore, the $\boldsymbol{A}$ and $\boldsymbol{\Gamma}$ become

$$\boldsymbol{A} = \begin{bmatrix} 1 & 1 & \dots & 1 \\ \Omega_1 & \Omega_2 & \dots & \Omega_P \\ (\Omega_1)^2 & (\Omega_2)^2 & \dots & (\Omega_P)^2 \end{bmatrix} \tag{4.23}$$

and

$$\boldsymbol{\Gamma} = \begin{bmatrix} \gamma_1 & \Omega_1\gamma_1 & \cdots & (\Omega_1)^5\gamma_1 \\ \gamma_2 & \Omega_2\gamma_2 & \cdots & (\Omega_2)^5\gamma_2 \\ \vdots & \vdots & & \vdots \\ \gamma_P & \Omega_P\gamma_P & \cdots & (\Omega_P)^5\gamma_P \end{bmatrix}, \tag{4.24}$$

respectively.

Since the number of significant multipaths in outdoor or uncluttered indoor environment is small (e.g., $P \leq 4$), the covariance matrix $R_\Gamma = E\{\boldsymbol{\Gamma}\,\boldsymbol{\Gamma}^H\}$ now has full rank because the number of columns and the number of rows in $\boldsymbol{\Gamma}$ (Equation (4.24)) are six and four respectively.

To estimate AoA and ToF with MUSIC, we first calculate the covariance matrix $\boldsymbol{R}_X$ of $\begin{bmatrix} X_k \\ X_{k+1} \end{bmatrix}$,

$$\boldsymbol{R}_X = E\{\begin{bmatrix} X_k \\ X_{k+1} \end{bmatrix} \begin{bmatrix} X_k^H & X_{k+1}^H \end{bmatrix}\} \tag{4.25}$$

With the eigen-analysis of covariance matrix $\boldsymbol{R}_X$, we can get L eigenvectors $\boldsymbol{E} = [\vec{e}_1 \dots \vec{e}_L]$ sorted with their eigenvalues. The first P significant eigenvectors $\boldsymbol{E}_S = [\vec{e}_1 \dots \vec{e}_P]$ represent the signal subspace, and the remaining $L - P$

eigenvectors $\boldsymbol{E}_N = [\vec{e}_{P+1} \dots \vec{e}_L]$ represent the noise subspace.

We further define the column of steering matrix $\boldsymbol{A}$ as a steering vector $\vec{a}(\theta, \tau)$,

$$\vec{a}(\theta, \tau) = \begin{bmatrix} 1 \\ \Omega(\tau) \\ (\Omega(\tau))^2 \\ \Phi(\theta) \\ \Phi(\theta)\Omega(\tau) \\ \Phi(\theta)(\Omega(\tau))^2 \end{bmatrix}. \tag{4.26}$$

Then, we can estimate AoA and ToF by maximising the following equation,

$$P_{MUSIC}(\theta, \tau) = \frac{1}{\vec{a}(\theta, \tau)^H \boldsymbol{E}_N \boldsymbol{E}_N^H \vec{a}(\theta, \tau)} \tag{4.27}$$

With the MUSIC algorithm, AoA and ToF can be estimated. However, previous research shows that the estimation of ToF is unreliable [40, 91]. Our evaluation shows that ToF is sensitive to noise. Thus, we only keep the AoA estimation for localisation.

4.4.5 Estimating AoA with ESPRIT

ESPRIT [89, 90, 92] is another subspace algorithm for AoA estimation but there was little study about ESPRIT in previous super-resolution localisation research with Wi-Fi because of its inferior performance compared to MUSIC [93]. One of the possible reasons is that ESPRIT doesn't estimate ToF as MUSIC. However, since LoRa has orders of magnitude less bandwidth than Wi-Fi (see Section 4.4.1), our results in Section 4.6 show that the AoA and localisation performance of ESPRIT is slightly better than those of MUSIC because of the poor ToF estimation of MUSIC with LoRa.

ESPRIT uses the same signal model Equation (4.19) as MUSIC. Note that we abuse the notations in this section against those in Section 4.4.4 to help simplify the exposition.

Firstly, similar to MUSIC in Section 4.4.4, we apply spatial smoothing to have a fully ranked covariance matrix. In order to smooth L consecutive channels from total M channels, we define a partial covariance matrix as

$$\boldsymbol{R}_{i,j}^{(q)} = E\{\boldsymbol{X}_i[q:l,q:l]\,\boldsymbol{X}_j^H[q:l,q:l]\}, \quad l = M - L + q \tag{4.28}$$

where $q = 1 \ldots L$ and $i, j \in \{k, k+1\}$. Therefore, the smoothed covariance matrix is calculated by

$$\boldsymbol{R}_{smooth} = \frac{1}{L} \cdot \begin{bmatrix} \sum_{q=1}^{L} R_{k,k}^{(q)} & \sum_{q=1}^{L} R_{k,k+1}^{(q)} \\ \sum_{q=1}^{L} R_{k+1,k}^{(q)} & \sum_{q=1}^{L} R_{k+1,k+1}^{(q)} \end{bmatrix} \tag{4.29}$$

The number of channels for smoothing L should not be less than the number of path (P). For cluttered indoor environment, P is between six and eight [94–96]. Therefore, $L \geq 8$ and $M \geq 16$. we choose $L = 4$ since $M = 8$ for typical LoRaWAN gateway configuration. Therefore, *Seirios* is designed for outdoor or uncluttered indoor environment.

Secondly, we apply the TLS-ESPRIT algorithm [90,97] to estimate the AoA for all significant radio paths. We further define partial covariance matrix $\boldsymbol{R}_{ii}$ as the left-up quarter of $\boldsymbol{R}_{smooth}$ and $\boldsymbol{R}_{ij}$ as the right-up quarter. Then we have,

$$\boldsymbol{R}_{ii} = \frac{1}{L}\sum_{q=1}^{L} R_{k,k}^{(q)}, \tag{4.30}$$

$$\boldsymbol{R}_{ij} = \frac{1}{L}\sum_{q=1}^{L} R_{k,k+1}^{(q)}. \tag{4.31}$$

The smallest eigenvalue of $\boldsymbol{R}_{ii}$ can be regarded as the noise term σ^2, and we further define a new matrix $\boldsymbol{C}_{ii}$ with noise subtracted as,

$$\boldsymbol{C}_{ii} = \boldsymbol{R}_{ii} - \sigma^2\boldsymbol{I}. \tag{4.32}$$

Similarly, we can have $\boldsymbol{C}_{ij}$ calculated from $\boldsymbol{R}_{ij}$. Then we perform eigen-analysis for $\boldsymbol{C}_{ii}$,

$$\boldsymbol{U}\boldsymbol{\Sigma}\boldsymbol{V}^H = \boldsymbol{C}_{ii}. \tag{4.33}$$

Eigenvalues and eigenvectors are sorted in non-increasing order, and we take the first P significant eigenvalues and eigenvectors to form new matrics as $\boldsymbol{U}_1$, $\boldsymbol{\Sigma}_1$ and $\boldsymbol{V}_1$. After solving the generalised eigenvalues of matrices $\boldsymbol{\Sigma}_1$ and $\boldsymbol{U}_1^H\boldsymbol{C}_{ij}\boldsymbol{V}_1$, we can solve the phases of $\Phi(\theta)$ with the phases of the eigenvalues. Finally, we can estimate AoAs of the multipaths with Equation (4.5).

4.4.6 Limitation of ToF Estimation

In this section, we discuss the limitation of ToF estimation. A typical configuration of LoRaWAN has 8 $\times$ 125 kHz channels with the channel spacing of 200 kHz between two adjacent channels. Therefore, we can measure the CSI for each channels with a pair of antennas k and $k+1$ (see Section 4.4.2) as

$$\begin{bmatrix} x_{k,1} & x_{k,2} & \cdots & x_{k,8} \\ x_{k+1,1} & x_{k+1,2} & \cdots & x_{k+1,8} \end{bmatrix}. \tag{4.34}$$

Following the spatial smooth approach used in SpotFi [40] to maximise the incoherence of measurements for better multipath resolution, we form $\boldsymbol{X}_k$ for CSI measured on antenna k as a 3×6 matrix

$$\boldsymbol{X}_k = \begin{bmatrix} x_{k,1} & x_{k,2} & \cdots & x_{k,6} \\ x_{k,2} & x_{k,3} & \cdots & x_{k,7} \\ x_{k,3} & x_{k,4} & \cdots & x_{k,8} \end{bmatrix}. \tag{4.35}$$

$\boldsymbol{X}_{k+1}$ can be formed similarly. By putting $\boldsymbol{X}_k$ and $\boldsymbol{X}_{k+1}$ together, the measurement matrix for MUSIC is,

$$\boldsymbol{X}_{MUSIC} = \begin{bmatrix} \boldsymbol{X}_k \\ \boldsymbol{X}_{k+1} \end{bmatrix}. \tag{4.36}$$

We can obtain a steering vector $\vec{\boldsymbol{a}}$ according to Equation (4.10) with $M = 3$. With $\boldsymbol{X}_{MUSIC}$ and the steering vector $\vec{\boldsymbol{a}}$, we can use MUSIC to estimate AoA and ToF jointly. The super-resolution algorithm searches all combinations of θ and τ for the steering vector, and calculate the value of a pseudo-spectrum function to find the peaks where locate the most likely estimations.

Nevertheless, in our practical evaluation, the performance is far from satisfactory and sometimes even worse than the baseline. We investigate the phenomenon with simulation, and find two main reasons.

- ToF resolution is 625 *ns* (125 m), making the paths indistinguishable with ToF difference. On the pseudo-spectrum, those estimations merge into one peak which is away from the ground truth. Therefore, the attempt to resolve multipaths fails. With wider bandwidth (e.g., 20 MHz as Wi-Fi), the accuracy can be improved.

- AoA estimation is sensitive to ToF accuracy. If ToF is estimated poorly, it will be noisy for AoA estimation, making AoA estimation worse than the baseline.

Therefore, we look for other algorithms that can avoid using ToF estimation for direct path resolution.

4.4.7 Multiple-AP Fusion

Previous research proposes to determine the direct path based on ToFs [17, 22, 40]. However, the ToFs measured with LPWAN is not reliable as discussed in Section 4.4.6. Therefore, *Seirios* does not resolve the direct path at the beginning. Instead, *Seirios* utilise triangulation with the AoA estimation of multiple APs to locate the transmitter directly. This method is based on the

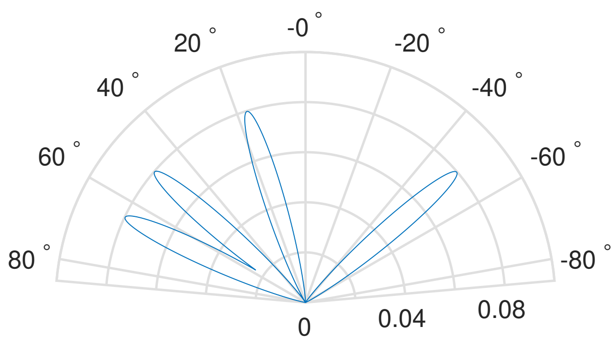

Fig. 4.5: An example for likelihood function with $\sigma = 5$. This figure shows four significant paths. The likelihood function can be translated into a heatmap in Figure 4.6a given the locations of the APs.

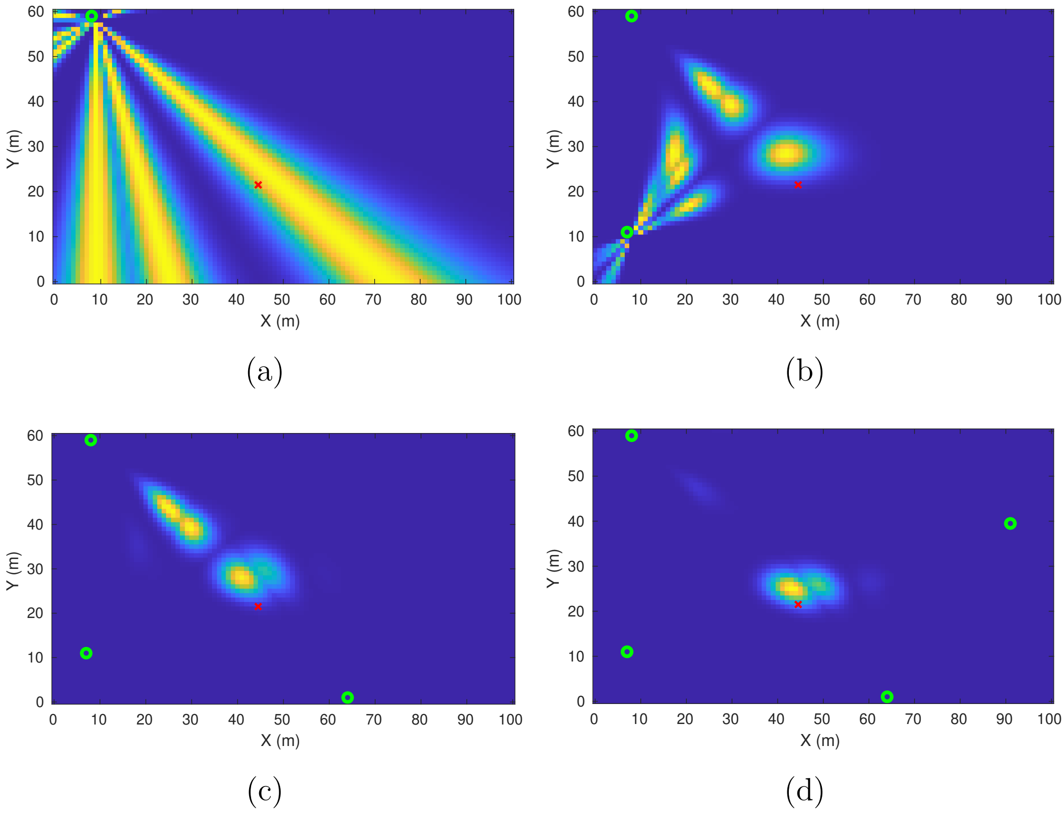

Fig. 4.6: (Picture view best in color) A heatmap example for multiple-AP fusion. Green circles indicate the APs, and the red cross indicates the ground-truth of the transmitter. (a) One AP. Multiple AoAs exist. (b) 2 APs. 7 clusters exist after fusion. (c) 3 APs. 4 clusters exist after fusion. (d) 4 APs. 2 clusters exist. The one with stronger likelihood is the location estimation for the transmitter, which is very close to the ground truth.

fact that the origins of the direct paths are congregated to the transmitter, but that of the reflectors are diverged (see examples in Figure 4.2 and Figure 4.6). Different to the classical triangulation algorithm that minimises the 2-norm of localisation errors, *Seirios* utilises maximum likelihood algorithm to simplify the calculation.

First of all, *Seirios* deals with all estimated AoAs equally, as they can be either the direct paths or the reflectors. The errors of AoA estimation are modeled as Gaussian distribution $\mathcal{N}(0, \sigma^2)$. Therefore, *Seirios* can apply a function $\ell(\theta)$ with Gaussian distribution's probability density function (PDF)

$f(\theta|\mu, \sigma^2)$ to represent the likelihood of a correct estimation for angle θ. $l(\theta)$ is defined as,

$$\ell(\theta) = \max_{i=1..P} f(\theta|\hat{\theta}_i, \sigma^2), \quad -85^\circ < \theta < 85^\circ. \tag{4.37}$$

where $\hat{\theta}_i$ is the AoA of the ith path, and σ is determined by the noise level and is a tunable parameter of *Seirios*. We found that the 'good' values of σ are between 3° and 5° empirically. Figure 4.5 shows an example for the likelihood function $\ell(\theta)$.

Since the position of APs and the directions of antennas are known, we can translate the likelihood function into a heatmap $\mathcal{L}(x, y)$ demonstrating the likelihood of the transmitter's location as shown in Figure 4.6a. As the size of the antenna array is relatively small compared to the distance between the transmitter and the receiver, instead of using hyperbolas to translate the AoAs to the heatmap, we use straight lines to simplify the calculation. To fusion the likelihood estimated by multiple APs, *Seirios* merges the heatmaps by multiplication. Therefore, the heatmap $\hat{\mathcal{L}}(x, y)$ as the fusion of G APs is generated by

$$\hat{\mathcal{L}}(x, y) = \prod_{g=1}^{G} \mathcal{L}_g(x, y). \tag{4.38}$$

However, there might be multiple clusters if the number of APs is not enough. The ambiguity can be reduced with the increase of APs. Figure 4.6 shows the refining of location estimation as the number of APs increases. On the heatmap with two APs (Figure 4.6b), there are many possible locations for the transmitter. With four APs (see Figure 4.6d), the transmitter's location is estimated as the center of a cluster, which is very close to the ground truth (i.e., the red cross). With multiple-AP fusion algorithm, it is not necessary to determine the direct path for each AP, which can avoid inaccurate ToF estimation discussed in Section 4.4.6.

LPWAN signals are good at penetration, and thus in most of the cases there exist direct paths. For the cases that direct paths are completely blocked, we leave the study and evaluation as future work.

4.5 Implementation

(a) (b)

Fig. 4.7: (a) AP implementation for data acquisition; (b) AP for outdoor deployment.

Seirios is designed for the transmitter localisation in an outdoor or uncluttered indoor environment. According to the architecture shown in Figure 4.2, we have implemented a *Seirios* prototype with the APs for wireless data acquisition and the cloud service for data processing.

Seirios AP prototype. We use BladeRF 2.0 SDR, which supports 2×2 MIMO as the AP prototype to receive LoRa radio signals between 902 and 928 MHz. The SDR can generate two synchronised I and Q streams of two antennas with 12-bit resolution. The distance between antennas is fixed as 14cm, which is slightly less than the half of the radio wavelength. Prior calibration is performed to eliminate the phase offset caused by connectors or cables. The SDR is connected to a general-purpose processor (GPP) via USB 3.0, which can be either a PC or a single board embedded computer. To operate *Seirios* prototype in a mobile manner (e.g., in an outdoor environment), we choose to use a low-power embedded system Raspberry Pi 4 as the GPP, which is deployed with signal processing program for LoRa packet detection. The detection algorithm is implemented in C++ with GNU Radio for high efficiency. Once a LoRa packet is detected, the GPP uploads the packet to the *Seirios* cloud service prototype via high-speed Wi-Fi. The devices are shown in Figure 4.7a. For outdoor deployment, the devices are packed in a case (see Figure 4.7b).

Cloud server. The cloud has a TCP server for incoming LoRa PHY that is uploaded by multiple APs. The server stores the data with its timestamp and maintains a time window to group the relevant packets for further processing. For each AP, when at least one packet for each channel is recorded in the window, the server will start to process the data. It first estimates the CSI for each channel, and then synchronises the channels. After that, it performs either MUSIC or ESPRIT for the AoA estimation. After the AoA estimations for multiple APs are produced, the server will perform multiple-AP fusion to estimate the location of the transmitter. The flowchart of the the process is shown in Figure 4.8.

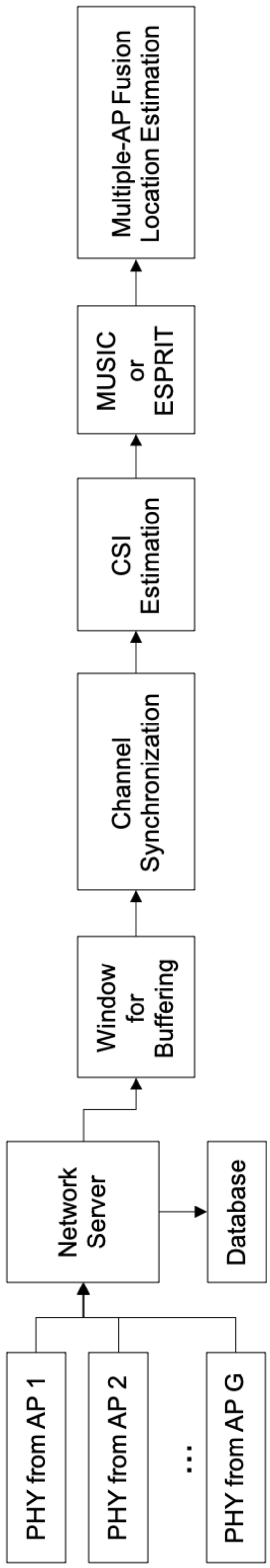

Fig. 4.8: Flowchart for signal processing in the *Seirios* cloud service.

4.6 Evaluation

4.6.1 Goals, Metrics and Methodology

Our goal in this evaluation is to show that *Seirios* can locate LoRa transmitter accurately outdoors. For this purpose, we evaluate the performance of our *Seirios* prototype developed in Sec 4.5 in a 100m $\times$ 60m lawn with a number of trees and is surrounded by buildings (see Figure 4.9). This is the largest outdoor space available in our campus.

Fig. 4.9: Outdoor evaluation on 100 m $\times$ 60 campus lawn. Red squares marked with A/B/C/D and antenna direction indicate the APs. Green circles indicate the ground-truth of transmitter's locations.

We deployed four APs in the lawn, one of which is shown in Figure 4.7b. A pair of 5 dBi antennas were mounted on each AP. The devices were battery-powered and each of them sampled at 2 MSps to cover the 1.6 MHz LoRaWAN spectrum. We used mDots[3] as our transmitters (i.e., the LoRa devices to be localised), which were configured with frequency hopping at eight LoRaWAN

[3]MDot datasheet. https://www.multitech.com/brands/multiconnect-mdot

channels. Specifically, each of them transmitted packets for $SF = 7$ at 8×125 kHz channels with the channel spacing of 200 kHz. It took a device approximately 30 ms to send a pre-defined packet; therefore, it took approximately $30 \times 8 = 240$ ms to cover all the channels.

During the evaluation, we recorded the locations of the transmitters (see the green dots and the red squares in Figure 4.9 for the locations of the transmitters and APs respectively). Then, a transmitter transmitted LoRa packets in all channels for three times. We collected two datasets with different transmission power levels, 14 dBm and 27 dBm respectively to study the impact of different transmission power levels to localisation accuracy.

The metrics that we use to evaluate the performance of *Seirios* are the errors of AoA (in degrees) and localisation (in metres), which are simply the absolute differences between estimation and ground truth.

Apart from overall AoA and localisation performance in both MUSIC (see Section 4.4.4) and ESPRIT (see Section 4.4.5), we had also investigated the performance of different components of *Seirios* such as the synchronisation algorithms in both overlapped and non-overlapped channels as discussed in Section 4.4.3, and fusion algorithm (see Section 4.4.7).

4.6.2 The accuracy of AoA estimation

The accuracy of AoA estimation determines that of localisation. Therefore, we start with the AoA accuracy. Figure 4.10 and 4.11 show the Cumulative Distribution Function (CDF) for AoA estimation errors of ESPRIT and MUSIC at transmit power levels 27 dBm and 14 dBm respectively. When the transmit power level is low (e.g., 14 dBm), the median errors with ESPRIT and MUSIC are 3.2 and 6.7 degrees, respectively, and the 80% percentile are

12.0 and 17.4 degrees, respectively (see Figure 4.11). When the transmit power level is high, the median error of ESPRIT is the same as that of low transmit power level (i.e., 3.2 degrees), but the 80% percentile of the estimation errors is improved to 6.0 degrees (vs. 12.0 degrees at the low transmission power level). For MUSIC, the high transmit power level (i.e., 27 dBm) reduces the AoA estimation error to 6.0 degrees (from 6.7 degrees produced by the low transmit power level). Similarly, and the 80% percentile of estimation errors is reduced to 12.0 degrees (from 17.4 degrees).

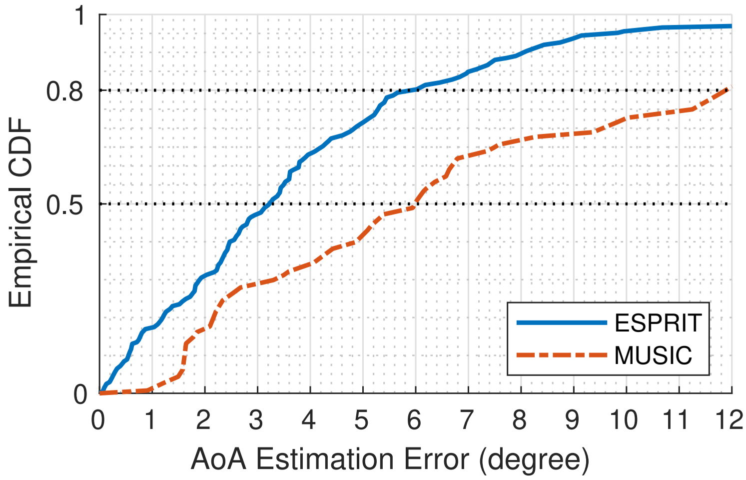

Fig. 4.10: AoA estimation error (Tx: 27 dBm)

Therefore, a higher transmit power level can increase the accuracy of AoA estimation of *Seirios*. At the same transmit power level, **ESPRIT has better performance than MUSIC, which is different to the results reported in Wi-Fi localisation literature**. This phenomenon is due to the foundation of MUSIC model discussed in Section 4.4.4 that an accurate AoA estimation with MUSIC relies on an accurate ToF estimation, while the ToF estimation is sensitive to noise and sometimes unreliable in narrow band LoRa channels that is different to orders-of-magnitude wider band Wi-Fi channels.

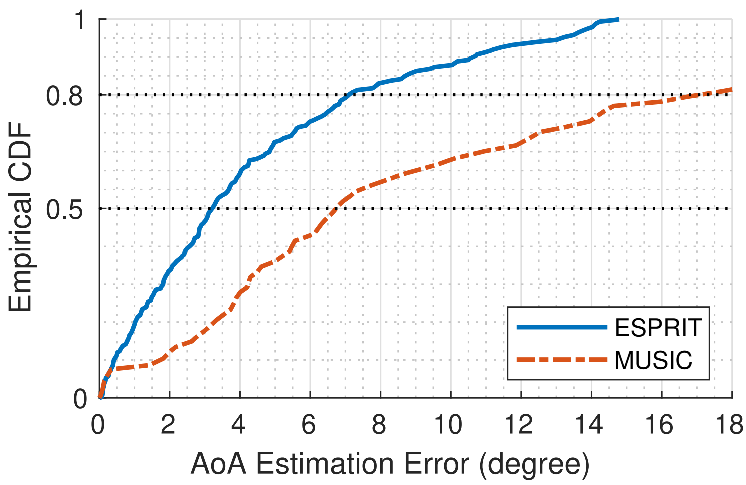

Fig. 4.11: AoA estimation error (Tx: 14 dBm)

An AoA estimation error of 3.2 degrees can be translated to a theoretical localisation error of 5.5 m at a distance of 100 m. In the next section, we will evaluate such end-to-end localisation errors with multiple-AP fusion empirically.

4.6.3 Localisation Accuracy

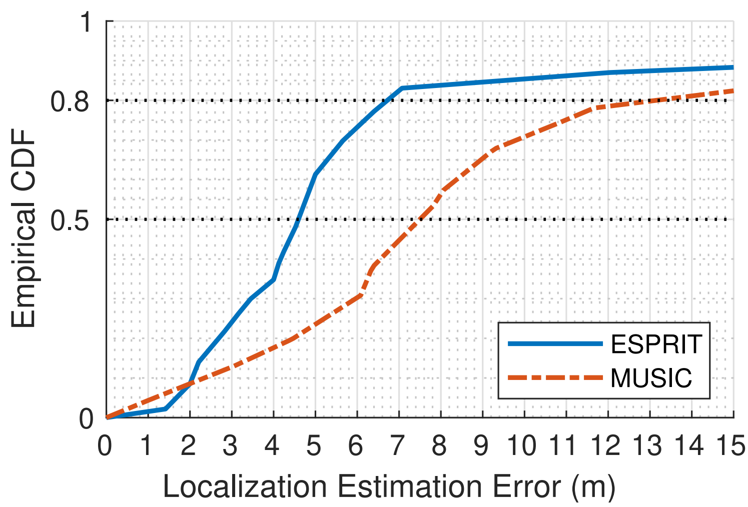

Fig. 4.12: Localisation error (Tx: 27 dBm)

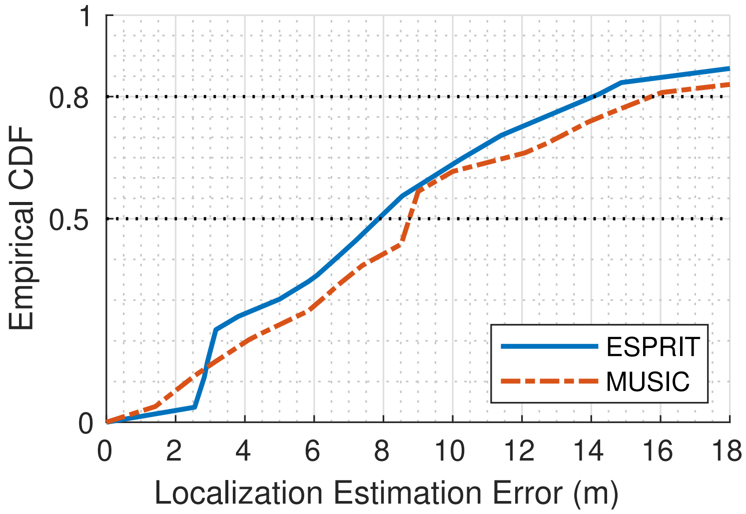

Fig. 4.13: Localisation error (Tx: 14 dBm)

The overall performance of *Seirios* is shown in Figure 4.12 (at the transmit power level of 27 dBm) and Figure 4.13 (at the transmit power of 14 dBm), respectively. Similar to Section 4.6.2, at the transmit power of 14 dBm, the performance of ESPRIT is slightly better than that of MUSIC with the median localisation errors of 7.8 m and 8.8 m for ESPRIT and MUSIC respectively. The 80% percentiles are 14.3 m and 17.1 m for ESPRIT and MUSIC respectively. When the transmit power level is 27 dBm, the median and 80% percentile errors (5.0 m and 7.0 m respectively) of ESPRIT are significantly better than those of MUSIC (7.8 m and 14.8 m respectively). From these figures, we can also observe that the transmit power levels have a significant impact to the localisation accuracy, especially with ESPRIT, where the 80% percentile of estimation error reduced from 14.3 m to 7.0 m (a more than half reduction) when the transmit power level increased from 14 dBm to 27 dBm.

4.7 Conclusion

We introduce *Seirios*, an AoA based localisation system for LPWAN. Despite the huge success and popularity of AoA based localisation methods in wide band radio systems such as Wi-Fi, there is no prior studies of such method in the emerging narrowband LPWAN because of the bandwidth limitation that results in poor multipath and location estimation. *Seirios* addresses this limitation by a novel interchannel packet synchronisation method that exploits the unique structure of the PHY. Our empirical evaluation shows that *Seirios* can achieve 4.4 m accuracy in an area of 100m $\times$ 60m.

Chapter 5

Seirios+: Leveraging Multiple Channels for LoRaWAN Indoor Localisation with Conjugates

5.1 Abstract

The *Seirios* localisation system proposed in Chapter 4 can improve the accuracy of outdoor localisation; however, it does not work for indoor localisation due to the increase of multiple radio propagation paths. Therefore, novel algorithms are proposed in this chapter to improve the localisation accuracy for indoor environment. By exploiting both the original and the **conjugate** of the physical layer, the improved *Seirios+* can resolve multiple reflectors in both **indoor** and outdoor environments. We upgraded the *Seirios* prototype to *Seirios+* and evaluate its performance in an indoor area of 25 m $\times$ 15 m, which shows that *Seirios+* can achieve a median error of 2.4 m indoors (80% samples <6.1 m).The results show that *Seirios+* produces 47.8% and 38.5% less error than the baseline approach and the approach without using

the conjugate information, respectively.

5.2 Introduction

In Chapter 4, we have proposed *Seirios* system for LoRaWAN device outdoor localisation. Channel combination and super-resolution algorithms are proposed to improve the localisation accuracy. In the evaluation (Section 4.6), *Seirios* achieves superior outdoor localisation accuracy. However, it does not support indoor localisation due to the fact that the number of significant multipaths indoors is more than that outdoors, making it challenging to resolve multipaths in clutter indoor environments.

To overcome the challenge, we propose improving *Seirios* to *Seirios+* for indoor localisation with and upgraded super-resolution algorithm. The key is, in addition to the original channel state measurements themselves, *Seirios+* utilises the conjugate of the measurements, which doubles the total amount of information for multipath resolution. The number of multipath that can be resolved by *Seirios+* is increased by 50% compared to original *Seirios* system without extra measurements, which does not increase energy consumption. In our evaluation (Section 5.5), *Seirios+* can significantly improve the localisation accuracy for indoor environment compared to *Seirios*. Therefore, *Seirios+* can provide accurate localisation estimation for LoRaWAN devices both **indoors** and **outdoors**. The contributions of this chapter are as follows.

- We propose doubling the amount of channel information by utilizing both **the original and the conjugate** of the CSI to increase the numbers of multipaths that the super-resolution algorithms can resolve (up to six reflectors), and thus improve the accuracy of localisation.

- We upgrade the prototype of *Seirios* with novel super-resolution algorithms, and our evaluation in a 25 m $\times$ 15 m indoor area shows that *Seirios* achieves a median localisation error of 2.4 m, which is 47.8% smaller than the baseline approaches and 38.5% smaller than the algorithm without conjugate (i.e., the algorithm proposed in Chapter 4).

5.3 Multi-channel Model with Conjugate

ESPRIT [89, 90, 92] takes advantage of rotational invariance for AoA estimation. However, there was little application about it in previous super-resolution localisation with Wi-Fi due to its inferior performance compared to MUSIC [93]. One of the possible reasons is that ESPRIT does not estimate ToF as MUSIC does. Since LoRa has orders-of-magnitude less bandwidth than Wi-Fi (see Sec 4.4.1), ToF estimation is inaccurate and may impair the overall performance. With ESPRIT, we can exploit all the information for AoA estimation only, which may have better performance than AoA-ToF joint estimation. Our results in Section 5.4.1 and Section 5.5 prove that AoA estimation alone has better performance than AoA-ToF joint estimation.

The signal model for ESPRIT is shown as Equation (4.17). Measurements are organised in two matrices $\boldsymbol{X}_k$ and $\boldsymbol{X}_{k+1}$ (we abuse the notations as in Section 4.4.6 for brevity). A naïve approach is to follow Equation (4.11) and (4.12) to form matrices with dimension 8×1. However, their covariance matrix $\boldsymbol{R} = E\{\boldsymbol{X}_k \boldsymbol{X}_{k+1}\}$ is rank-deficient with rank only one. The rank indicates that the number of multipaths the algorithm can solve is only one. With spatial smoothing, the rank can be increased to four. Our evaluation shows that solving four paths is acceptable for outdoor environment, but results in poor accuracy for indoor. To meet the system design (see Section 4.4.1), the rank should be increased to six at a minimum.

To this end, we propose to exploit both the original and the conjugate of the measurements. For convenience, we call this algorithm *conjugated ESPRIT*. $\boldsymbol{X}_k$ and $\boldsymbol{X}_{k+1}$ become,

$$\boldsymbol{X}_k = \begin{bmatrix} x_{k,1} & x_{k,2} & x_{k,3} & x^*_{k+1,8} & x^*_{k+1,7} & x^*_{k+1,6} \\ x_{k,2} & x_{k,3} & x_{k,4} & x^*_{k+1,7} & x^*_{k+1,6} & x^*_{k+1,5} \\ \vdots & \vdots & \vdots & \vdots & \vdots & \vdots \\ x_{k,6} & x_{k,7} & x_{k,8} & x^*_{k+1,3} & x^*_{k+1,2} & x^*_{k+1,1} \end{bmatrix} \tag{5.1}$$

as a 6 × 6 matrix, and symmetrically,

$$\boldsymbol{X}_{k+1} = \begin{bmatrix} x_{k+1,1} & x_{k+1,2} & x_{k+1,3} & x^*_{k,8} & x^*_{k,7} & x^*_{k,6} \\ x_{k+1,2} & x_{k+1,3} & x_{k+1,4} & x^*_{k,7} & x^*_{k,6} & x^*_{k,5} \\ \vdots & \vdots & \vdots & \vdots & \vdots & \vdots \\ x_{k+1,6} & x_{k+1,7} & x_{k+1,8} & x^*_{k,3} & x^*_{k,2} & x^*_{k,1} \end{bmatrix}. \tag{5.2}$$

With Equation (4.17)(5.1)(5.2), A is a 6 × 6 steering matrix,

$$\boldsymbol{A} = \begin{bmatrix} 1 & 1 & \dots & 1 \\ \Omega_1 & \Omega_2 & \dots & \Omega_P \\ \vdots & \vdots & \ddots & \vdots \\ (\Omega_1)^5 & (\Omega_2)^5 & \dots & (\Omega_P)^5 \end{bmatrix}. \tag{5.3}$$

and we can derive $\boldsymbol{\Gamma}$,

$$\boldsymbol{\Gamma} = \begin{bmatrix} \boldsymbol{\Gamma}_k & \boldsymbol{\Gamma}_{k+1} \end{bmatrix}, \tag{5.4}$$

where

$$\mathbf{\Gamma}_k = \begin{bmatrix} \gamma_1 & \gamma_1\Omega_1 & \gamma_1(\Omega_1)^2 \\ \gamma_2 & \gamma_2\Omega_2 & \gamma_2(\Omega_2)^2 \\ \vdots & \vdots & \vdots \\ \gamma_P & \gamma_P\Omega_P & \gamma_P(\Omega_P)^2 \end{bmatrix}, \tag{5.5}$$

$$\mathbf{\Gamma}_{k+1} = \begin{bmatrix} \gamma_1^*(\Omega_1^*)^7\Phi_1^* & \gamma_1^*(\Omega_1^*)^6\Phi_1^* & \gamma_1^*(\Omega_1^*)^5\Phi_1^* \\ \gamma_2^*(\Omega_2^*)^7\Phi_2^* & \gamma_2^*(\Omega_2^*)^6\Phi_2^* & \gamma_2^*(\Omega_2^*)^5\Phi_2^* \\ \vdots & \vdots & \vdots \\ \gamma_P^*(\Omega_P^*)^7\Phi_P^* & \gamma_P^*(\Omega_P^*)^6\Phi_P^* & \gamma_P^*(\Omega_P^*)^5\Phi_P^* \end{bmatrix}. \tag{5.6}$$

The rows of $\mathbf{\Gamma}$ represent multipath signals. Normally, multipath signals (defined in Equation (4.7)) are highly correlated. With Equation (5.5) and (5.6), the signals are decoupled. As shown in Equation (5.1)(5.2), the amount of measurement is doubled. Therefore, the rank of covariance matrix is increased from four to six to deal with six multipaths (70% indoor cases, see discussion in Section 5.2). Generally, given measurements of M channels, the multipaths that ESPRIT can solve is $\lfloor \frac{2(M+1)}{3} \rfloor$. Our evaluation show that this algorithm can increase the accuracy of LPWAN indoor localisation.

This approach can also be applied to Wi-Fi signals where CSI of multiple subcarriers can be used for localisation. For a pair of antennas with W consecutive subcarriers, similar to Equation (5.1) and (5.2), the CSI measurements can be organised as

$$\boldsymbol{X}_k^W = \begin{bmatrix} x_{k,1} & \cdots & x_{k,\lceil\frac{W+1}{3}\rceil} & x^*_{k+1,W} & \cdots & x^*_{k+1,\lfloor\frac{2(W+1)}{3}\rfloor} \\ x_{k,2} & \cdots & x_{k,\lceil\frac{W+1}{3}\rceil+1} & x^*_{k+1,W-1} & \cdots & x^*_{k+1,\lfloor\frac{2(W+1)}{3}\rfloor-1} \\ \vdots & \vdots & \vdots & \vdots & \vdots & \vdots \\ x_{k,\lfloor\frac{2(W+1)}{3}\rfloor} & \cdots & x_{k,W} & x^*_{k+1,\lceil\frac{W+1}{3}\rceil} & \cdots & x^*_{k+1,1} \end{bmatrix} \tag{5.7}$$

and symmetrically,

$$\boldsymbol{X}_{k+1}^W = \begin{bmatrix} x_{k+1,1} & \cdots & x_{k+1,\lceil\frac{W+1}{3}\rceil} & x^*_{k,W} & \cdots & x^*_{k,\lfloor\frac{2(W+1)}{3}\rfloor} \\ x_{k+1,2} & \cdots & x_{k+1,\lceil\frac{W+1}{3}\rceil+1} & x^*_{k,W-1} & \cdots & x^*_{k,\lfloor\frac{2(W+1)}{3}\rfloor-1} \\ \vdots & \vdots & \vdots & \vdots & \vdots & \vdots \\ x_{k+1,\lfloor\frac{2(W+1)}{3}\rfloor} & \cdots & x_{k+1,W} & x^*_{k,\lceil\frac{W+1}{3}\rceil} & \cdots & x^*_{k,1} \end{bmatrix}. \tag{5.8}$$

5.4 Microbenchmark

So far, we have discussed interchannel synchronisation (Section 4.4.3) and conjugated ESPRIT (Section 5.3) as the key algorithms of *Seirios* to improve the accuracy of AoA estimation as well as the localisation of LoRaWAN IoT devices. To understand the performance of the algorithms on one AP, we conducted a microbenchmark indoors (25 m × 15 m) with LoS and non-line of sight (NLoS) to evaluate the AoA estimation accuracy. We compared three algorithms (i.e., AoA-conjugated using conjugated ESPRIT, Section 5.3; AoA-ToF joint estimation using MUSIC, Section 4.4.6; and the baseline). The baseline algorithm is similar to TDoA, but instead of synchronising multiple

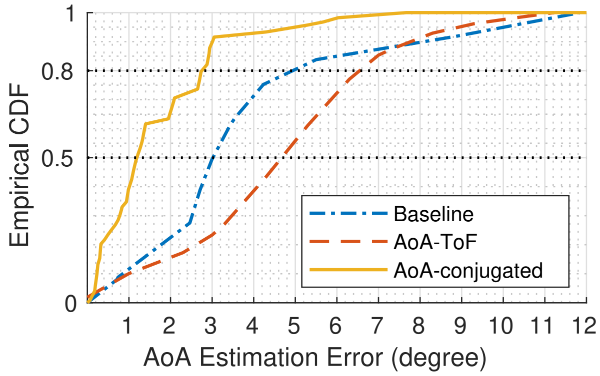

(a) Line-of-sight (LoS)

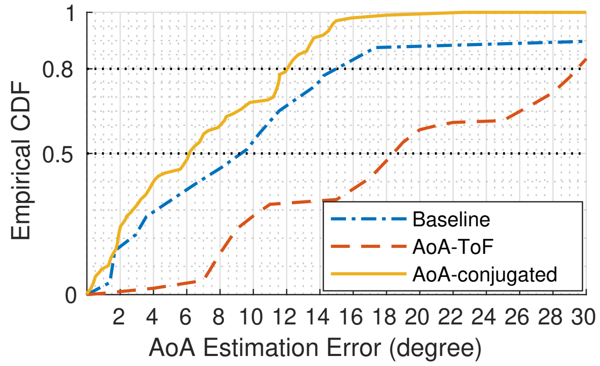

(b) Non-line-of-sight (NLoS)

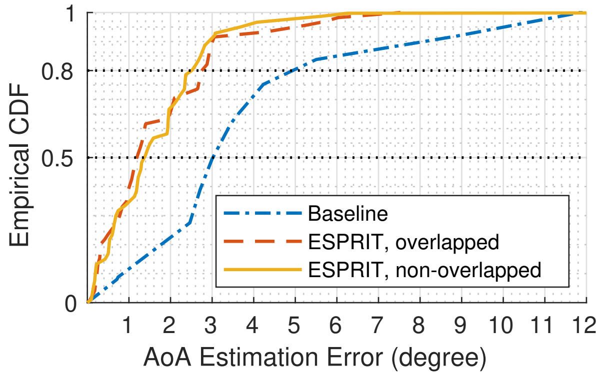

(c) Overlapped and non-overlapped

Fig. 5.1: Microbenchmark: (a) LoS, (b) NLoS, and (c) overlapped and non-overlapped channels. The accuracy of the two cases is close, with half the error as the baseline. The performance of the interchannel synchronisation algorithm for non-overlapped channels is comparable to that for overlapped channels.

AoA: angle of arrival; CDF: cumulative distribution function; ToF: time of flight

APs for timestamp measurement, we synchronised two antennas of one AP to extract the time difference based on the phase difference and further calculated AoA based on the measurements.

5.4.1 AoA Estimation Accuracy

Figs. 5.1a and 5.1b show the cumulative distribution function (CDF) for AoA estimation errors of the AoA-conjugated, AoA-ToF, and the baseline, for LoS and NLoS, respectively. The lab where the data were collected is a typical cluttered indoor environment. For LoS, AoA-conjugated (median error 1.2°) has 3 times superior accuracy compared to AoA-ToF (4.7°) and 1.5 times compared to the baseline (3.0°). Compared to the previous observation in a Wi-Fi localisation system is that AoA-ToF joint estimation has even worse performance than the baseline (see Section 4.4.6 for an explanation of this result). For NLoS, the radio path is completely blocked by walls so that only penetrated radio (with much noise) can reach the receiver. The median error (6.0°, 18.2°, and 9.2° for AoA-conjugated, AoA-ToF and the baseline, respectively) is larger than those under LoS, but AoA-conjugated still has the best performance. Therefore, we can conclude that AoA estimation with conjugated ESPRIT can, on average, improve the accuracy by two times compared to the baseline.

5.4.2 Interchannel Synchronisation

If using customised LoRa protocol [98] instead of LoRaWAN, one may define overlapped LoRa channels, and exploit them to improve localisation accuracy. However, the communication channels defined by LoRaWAN do not overlap (to avoid interchannel interference and improve transmission performance);

therefore, a virtual intermediate channel must be synthesised to synchronise LoRaWAN channels, as discussed in Section 4.4.3. Theoretically, synchronisation for non-overlapped channels may introduce extra errors compared to overlapped channels, which may increase the AoA estimation and localisation errors. In practice, the extra error is relatively small.

For demonstration, we conducted a microbenchmark to compare the performance of *Seirios* in non-overlapped and overlapped LoRa channels. To have overlapped channels, a LoRa transmitter is programmed to transmit packets in 15 channels of 125 kHz with the channel spacing of 100 kHz, 30 times over. We selected the odd number of channels (i.e., 1st, 3rd, … 15th) from the overlapped dataset to form a 'new' dataset of non-overlapped channels.

Then, we performed conjugated ESPRIT on both datasets for AoA estimation. Figure 5.1c shows that there is insignificant difference between the two datasets (i.e., overlapped and non-overlapped). Taking the median error for comparison, the loss (0.2°) of the non-overlapped dataset is very small and is only one-eighth of its improvement from the baseline. Therefore, the error introduced by non-overlapped channels has little effect on AoA estimation.

5.5 Evaluation

5.5.1 Goals, Metrics and Methodology

Our goal in this evaluation is to show that *Seirios* can locate LoRa transmitter accurately for both indoor and outdoor with the algorithm proposed in this chapter. For this purpose, we reuse our *Seirios* prototype developed in Section 4.5 and evaluate its performance in a 100 m × 60 m lawn with a number of trees and is surrounded by buildings (see Figure 4.9), and in a 25 m× 15 m large room with concrete pillar and surrounded by walls (see Figure 5.2).

For outdoor, we deployed four APs in the lawn with the same configurations as discussed in Section 4.6.1. Each of the transmitters transmitted LoRa packets in all channels for three times. At the same time, we logged the locations of the transmitters as the ground truth (see the green dots and the red squares in Figure 4.9 for the locations of the transmitters and APs respectively).

Similarly, we deployed APs and transmitters in our lab for indoor evaluation. The lab is a cluttered environment with furniture and walls (see Figure 5.2), and thus all APs and transmitters were placed at the height above 1.5 metres to best avoid obstacles. The transmitters were configured similar to those for outdoor evaluation.

The metrics that we use to evaluate the performance of *Seirios* is error of localisation (in metres), which is simply the absolute difference between the estimation and the ground truth.

Besides overall localisation performance with conjugated ESPRIT (Section 5.3), AoA-ToF joint estimation (Section 4.4.6) and the baseline (Section 5.4), we had also investigated the performance of different components of *Seirios* such as fusion algorithm (Section 4.4.7), and the effectiveness of conjugated ESPRIT.

5.5.2 Outdoor Localisation

For the outdoor evaluation on the campus lawn as shown in Figure 4.9, the overall performance of *Seirios* is shown in Figure 5.3. The performance of conjugated ESPRIT is better than that of AoA-ToF joint estimation and the baseline with the median localisation errors of 4.4 m, 6.4 m and 6.9 m for

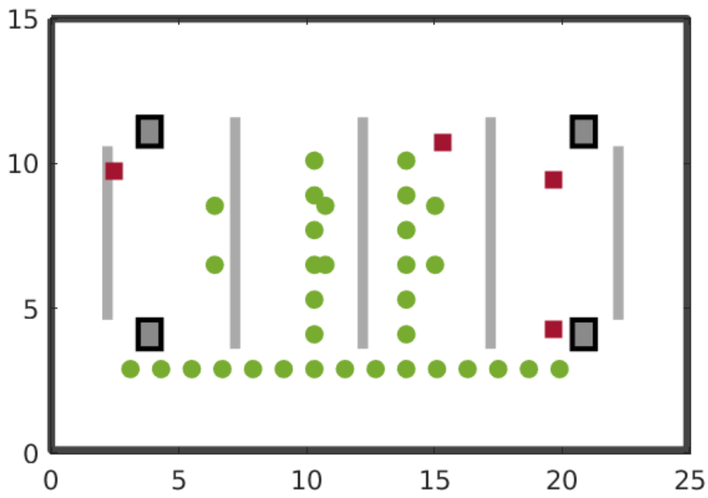

Fig. 5.2: Indoor evaluation on 25 m× 15 large room. The red squares indicate the APs, and the green circles indicate the ground-truth of transmitter's locations. The four black rectangles filled in gray are concrete pillar that may cause strong reflection. The gray bars are 1.5-metre-high barriers to split the lab into several zones, which may block the LOS.

Note: Values are measured in metres.

conjugated ESPRIT, AoA-ToF joint estimation and the baseline respectively. The 80% percentiles are 6.4 m, 10.5 m and 9.4 m for conjugated ESPRIT, AoA-ToF joint estimation and the baseline respectively.

The results show that the localisation error is reduced by 36.2% comparing conjugated ESPRIT with the baseline. Furthermore, **conjugated ESPRIT has better performance than AoA-ToF joint estimation, which is different to the results reported in Wi-Fi localisation literature**. This phenomenon is due to the foundation of the model discussed in Section 4.4.6 that an accurate AoA estimation with AoA-ToF joint estimation relies on an accurate ToF estimation, while the ToF estimation is sensitive to the raw resolution limited by the overall bandwidth of LoRa channels that is orders-of-magnitude smaller than Wi-Fi channels. AoA-ToF joint estimation is even worse than the baseline, which proves that the error introduced by inaccurate

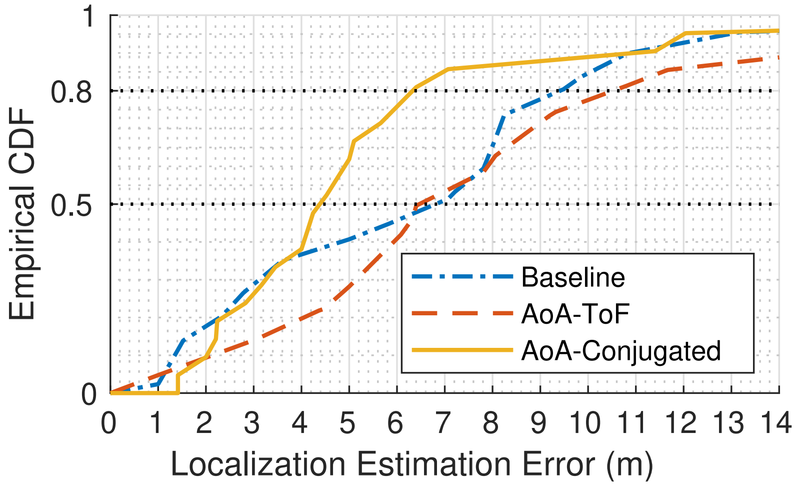

Fig. 5.3: Outdoor localisation error

ToF estimation can affect AoA estimation.

The results also indicate that super-resolution algorithms are still useful for outdoor environment. Even though the number of multipaths is less than that of indoor, strong reflection can be caused by trees and building, which may increase the localisation error.

5.5.3 Indoor Localisation

For the indoor evaluation in our lab, as shown in Fig. 5.2, the overall performance of *Seirios* is shown in Fig. 5.4. The median errors with conjugated ESPRIT, AoA-ToF joint estimation, and the baseline are 2.4 m, 4.0 m, and 4.6 m, respectively, and the 80th percentiles are 6.1 m, 8.8 m, and 11.6 m, respectively. The results show that with the conjugated ESPRIT, the localisation error is reduced by 47.8% compared to the baseline, which is slightly more than that of outdoor evaluation (36.2%, see Section 5.5.2). This is because the multipath effect is more severe indoors than outdoors, which affects the baseline algorithm but can be resolved by the conjugated ESPRIT. On average (indoors

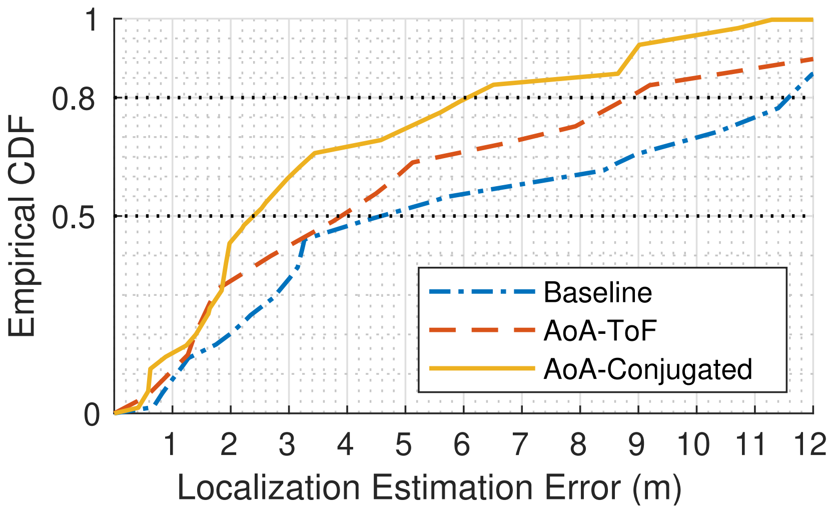

Fig. 5.4: Indoor localisation error

and outdoors), the localisation improvement is 42%, which demonstrates the superior localisation performance of *Seirios* (i.e., conjugated ESPRIT) on narrow bandwidth radio signals with commercial off-the-shelf (COTS) hardware, which has two antennas only.

Unlike outdoor evaluation, AoA-ToF joint estimation is better than the baseline indoors. The reason behind this phenomenon is that ToF estimation is apt to average the ToF of multipaths if they are not distinguishable, and indoor paths have relatively similar ToF, so the estimation is relatively more accurate than those of outdoors evaluations (with significantly larger different ToF for each path). The relatively accurate ToF estimation can improve the accuracy of AoA estimation, so that the localisation performance of AoA-ToF joint estimation is better than the baseline. Nevertheless, multipaths are not resolvable with AoA-ToF joint estimation, so its performance is worse than that of conjugated ESPRIT.

5.5.4 Comparison with RSS and TDoA

As discussed in Section 4.2, RSS and TDoA based LoRaWAN localisation systems have poor performance. In this section, we evaluate these techniques in both indoor and outdoor environments as a comparison to *Seirios*. For the RSS-based approach, we follow a general path-loss model proposed in [99,100] with triangulation for evaluation. For the TDoA-based approach, we use the phase difference of two synchronised antennas in each gateway to calculate TDoA.

The median **outdoor** localisation errors are 15.3 m and 6.9 m for RSS and TDoA based approaches, respectively, while the median **indoor** localisation errors are 6.3 m and 4.6 m with for RSS and TDoA based approaches, respectively. Therefore, the AoA-based conjugated ESPRIT of *Seirios* produces significantly better performance (4.4 m outdoors, 2.4 m indoors) than these of RSS and TDoA based approaches.

5.5.5 Impact of AP Fusion

AoA estimation proposes the possible directions of all incoming paths regardless of direct path or reflectors. AP fusion is a effective technique to determine the direct path as well as the location of the transmitter. It is based on the fact that the direct paths are congregated but the reflectors are diverged.

Seirios uses multiple-AP fusion for localisation. As shown in Figure 4.6, fusing more number of APs can reduce the ambiguity of localisation estimation and increase the accuracy. To investigate how the number of APs affects the overall performance, we evaluate the localisation errors with two, three and four APs respectively with the collected data.

For outdoor, we first evaluate two APs with C and D as shown in Fig 4.9,

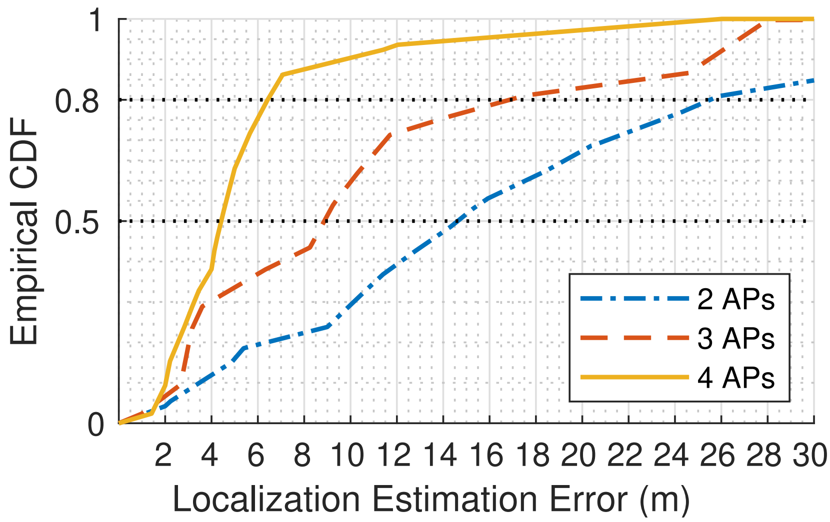

Fig. 5.5: The impact of APs evaluated for outdoor

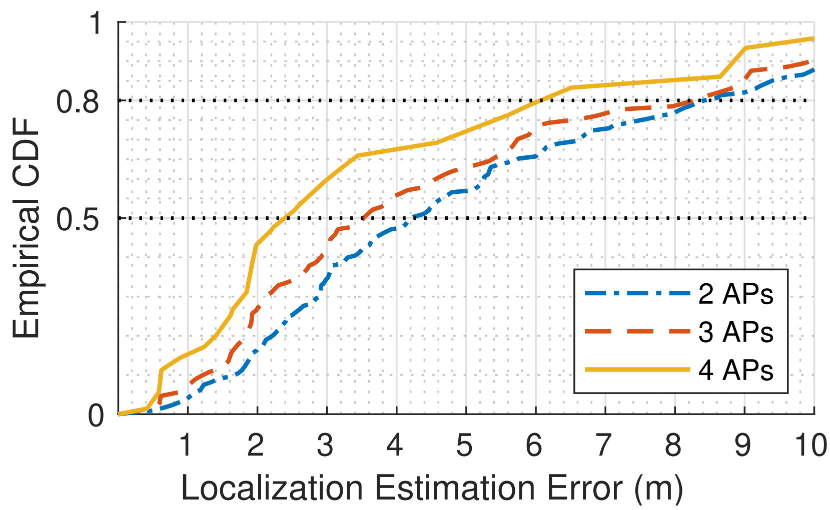

Fig. 5.6: The impact of APs evaluated for indoor

and then add AP B and A sequentially for the evaluation of three and four APs. The results are shown in Figure 5.5. With two APs, the median and 80% percentile errors are 14.8 m and 26.0 m respectively. By increasing the number of APs from two to three, the median and 80% percentile errors are reduced to 8.8 m and 17.0 m, respectively. With four APs, the median error is reduced by the 50% of those with three APs and 70% of two APs to 4.4 m, and 80% percentile error is reduced to 6.4 m.

For indoor, we observe similar behaviour as shown in Figure 5.6, but the error reduction for indoor is 31% of three APs and 42% of two APs, which is less than that of outdoor. The reason is that the indoor area is smaller than the outdoor, but both are equipped with the same amount of APs, which means that the indoor area has stronger coverage than the outdoor. Thus, the improvement with an extra AP for the indoor is not as significant as that for the outdoor. Based on this phenomenon, we can predict that with more APs, the localisation error for outdoor can be further reduced significantly.

Overall, the evaluation shows that localisation accuracy relates to the density of APs (gateways) and proves the effectiveness of AP fusion algorithm introduced in Section 4.4.7.

5.5.6 Effectiveness of Conjugated ESPRIT

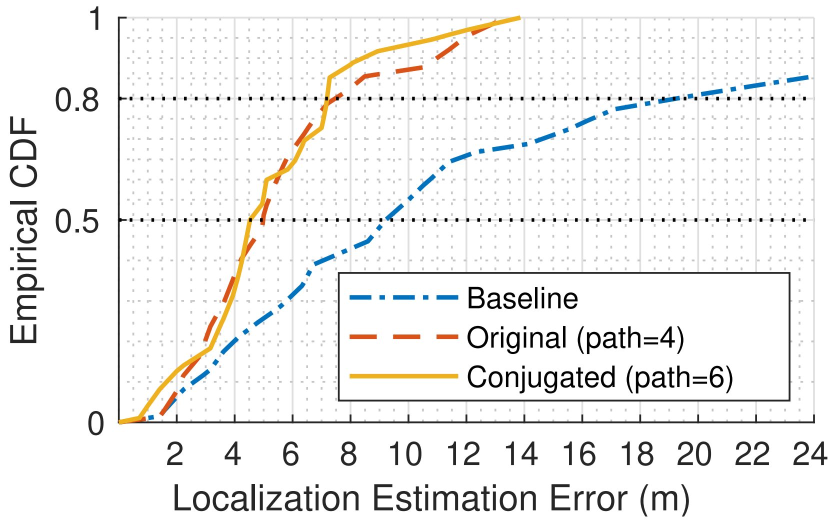

Fig. 5.7: The impact of multipath for outdoor

In Section 5.3, we propose to use conjugated ESPRIT to handle more

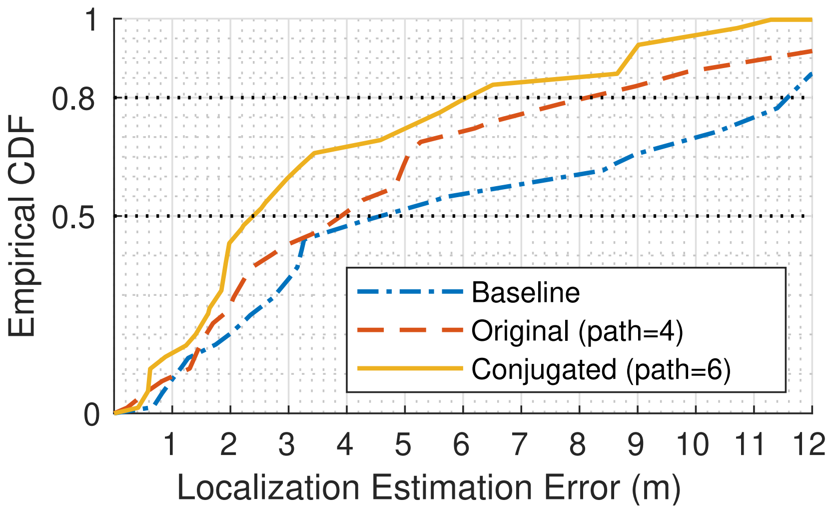

Fig. 5.8: The impact of multipath for indoor

multipaths. Theoretically, the proposed algorithm can increase the capacity for multipaths resolution from four to six. In this section, we will evaluate and compare the performance of the conjugated ESPRIT with the conventional ESPRIT to prove the effectiveness of our proposed algorithm.

Figure 5.8 shows the localisation accuracy achieved by the conventional ESPRIT with spatial smoothing, the conjugated ESPRIT, and the baseline for the indoor evaluation. The median error for three algorithms are 2.4 m, 3.9 m and 4.6 m, respectively. It is obvious that the conjugated ESPRIT has reduced the error significantly. However, for outdoor, Figure 5.7 shows the conjugated ESPRIT does not have significant improvement compared to the conventional ESPRIT. It is due to the fact that outdoor environment has only a small number of multipath that can even be solved by the conventional ESPRIT supporting four paths.

Furthermore, Figure 5.8 and Figure 5.7 imply that the number of significant multipath for indoor is more than four, while that for the outdoor is less than or equal to four.

5.6 Conclusion

We introduce *Seirios+*, an AoA based localisation system for LPWAN. Despite the huge success and popularity of AoA based localisation methods in wide band radio systems such as Wi-Fi, there is no prior studies of such method in the emerging narrowband LPWAN technologies because of the bandwidth limitation that results in poor multipath and location estimation. *Seirios+* addresses this limitation by a novel interchannel synchronisation method and ESPRIT algorithm that exploits both the original and the conjugate of the channel state measurements. Our empirical evaluation shows that *Seirios+* can reduce localisation error by 41.6%, and can achieve 4.4 m accuracy in an open area of 100 m $\times$ 60 m as well as 2.4 m accuracy in an indoor area of 25 m $\times$ 15 m.

Chapter 6

Conclusion and Future Work

This thesis proposed a Cloud-RAN architecture to improve the performance of LoRaWAN network and provide localisation service. It first discussed PHY compression as a key technique to facilitate the deployment and maintenance for the system. Then, it discussed channel combining technique and super-resolution algorithms to improve the localisation accuracy.

In the study of PHY compression (Chapter 3), we introduce *Nephelai*, which is based on CS-theory, to reduce the bandwidth requirement of the infrastructure of Cloud-RAN. This work has discovered the relationship between compression ratios, SNR and SFs to select an appropriate compression ratio, and it proves that joint decoding can improve the PRR as well as the battery lifetime for end devices. In an empirical evaluation, 93.7% of PHY can be compressed which can significantly improve the scalability of cloud assisted LoRaWAN.

In the second work, we introduce *Seirios* (Chapter 4), an AoA based localisation system for LoRaWAN. It addresses the limitation of the bandwidth of narrow band signals by a novel interchannel packet synchronisation method that exploits the unique structure of the packets. Our empirical evaluation shows that the system can reduce localisation errors by 36.2% compared to the baseline and achieve 4.4 m median accuracy in an area of 100m × 60m.

In the third work, we further improve the localisation system for indoor environment. We propose *Seirios+* (Chapter 5), exploiting both the original and the conjugate of the channel state measurements with super-resolution algorithms to improve the localisation accuracy. Our empirical evaluation shows that *Seirios+* can reduce localisation errors by 47.8% compared to the baseline, and can achieve 2.4 m median accuracy in an indoor area of 25 m × 15 m.

This thesis proposes to focus on LoRaWAN Cloud-RAN as a humble step towards greener and more flexible wireless network for IoT devices. However, there are limitations for future work.

One limitation of our research is that *Seirios* and *Seirios+* focus on one transmitter only and does not support concurrent transmissions from other LoRaWAN devices. However, since LoRa networks benefit hugely from the innate orthogonality of SFs, we believe that concurrent transmissions can be regarded as the noise and suppressed by the super-resolution algorithms [87, 89, 90]. In this regard, *Seirios* and *Seirios+* can potentially locate multiple transmitters at the same time. Nevertheless, we leave further research in this direction as future work.

Another limitation is the number of gateways in practice. Normally, one LoRaWAN gateway can cover up to 10 km and thus the density of deployment is low, which is different to our evaluation setup in Sec.5.5.5 with multiple gateways for high localisation accuracy. However, our research about *Nephelai* shows that a dense deployment of LoRaWAN gateways is beneficial in improving signal quality, battery lifetime and network scalability and robustness. We envision the dense deployment of LoRaWAN gateways in the future and leave how the gateway deployment density influences localisation performance as future work.

Bibliography

[1] S Farrell. Low-Power Wide Area Network (LPWAN) Overview. Technical report, RFC Editor, may 2018.

[2] LoRa Alliance. LoRaWAN 1.1 Specification. *LoRa Alliance*, (1.1):101, 2017.

[3] Rashmi Sharan Sinha, Yiqiao Wei, and Seung-Hoon Hwang. A survey on lpwa technology: Lora and nb-iot. *Ict Express*, 3(1):14–21, 2017.

[4] Orestis Georgiou and Usman Raza. Low Power Wide Area Network Analysis: Can LoRa Scale? *IEEE Wireless Communications Letters*, 6(2):162–165, oct 2017.

[5] Chaojie Gu, Linshan Jiang, and Rui Tan. LoRa-Based Localization: Opportunities and Challenges. 2018.

[6] Norman Abramson. The aloha system: Another alternative for computer communications. In *Proceedings of the November 17-19, 1970, fall joint computer conference*, pages 281–285, 1970.

[7] Christian Namislo. Analysis of mobile radio slotted aloha networks. *IEEE Journal on Selected Areas in Communications*, 2(4):583–588, 1984.

[8] Jansen C Liando, Amalinda Gamage, Agustinus W Tengourtius, and Mo Li. Known and unknown facts of lora: Experiences from a large-scale

measurement study. *ACM Transactions on Sensor Networks (TOSN)*, 15(2):1–35, 2019.

[9] Ferran Adelantado, Xavier Vilajosana, Pere Tuset-Peiro, Borja Martinez, Joan Melia-Segui, and Thomas Watteyne. Understanding the Limits of LoRaWAN. *IEEE Communications Magazine*, 55(9):34–40, 2017.

[10] Weitao Xu, Jun Young Kim, Walter Huang, Salil S Kanhere, Sanjay K Jha, and Wen Hu. Measurement, characterization, and modeling of lora technology in multifloor buildings. *IEEE Internet of Things Journal*, 7(1):298–310, 2019.

[11] Yao Peng, Longfei Shangguan, Yue Hu, Yujie Qian, Xianshang Lin, Xiaojiang Chen, Dingyi Fang, and Kyle Jamieson. PLoRa: a passive long-range data network from ambient LoRa transmissions. In *Proceedings of the 2018 Conference of the ACM Special Interest Group on Data Communication - SIGCOMM '18*, SIGCOMM '18, pages 147–160, Budapest, Hungary, 2018. ACM.

[12] *LoRa Backscatter: Enabling The Vision of Ubiquitous Connectivity*, number 3, 2017.

[13] Nick Iliev and Igor Paprotny. Review and Comparison of Spatial Localization Methods for Low-Power Wireless Sensor Networks. *IEEE Sensors Journal*, 15(10):5971–5987, 2015.

[14] Bashima Islam, Md Tamzeed Islam, Jasleen Kaur, and Shahriar Nirjon. Lorain: Making a case for lora in indoor localization. In *2019 IEEE International Conference on Pervasive Computing and Communications Workshops (PerCom Workshops)*, pages 423–426. IEEE, 2019.

[15] Adwait Dongare, Revathy Narayanan, Akshay Gadre, Anh Luong, Artur Balanuta, Swarun Kumar, Bob Iannucci, and Anthony Rowe. Charm: Exploiting Geographical Diversity Through Coherent Combining in Low-power Wide-area Networks. In *Proceedings of the 17th ACM/IEEE International Conference on Information Processing in Sensor Networks*, IPSN '18, pages 60–71, Piscataway, NJ, USA, 2018. IEEE Press.

[16] Yihenew Dagne Beyene, Riku Jantti, Olav Tirkkonen, Kalle Ruttik, Sassan Iraji, Anna Larmo, Tuomas Tirronen, and Johan Torsner. NB-IoT Technology Overview and Experience from Cloud-RAN Implementation. *IEEE Wireless Communications*, 24(3):26–32, jun 2017.

[17] Jie Xiong and Kyle Jamieson. ToneTrack : Leveraging Frequency-Agile Radios for Time-Based Indoor Wireless Localization Categories and Subject Descriptors. In *Proceedings of the Annual International Conference on Mobile Computing and Networking, MOBICOM*, pages 537–549, 2015.

[18] China Mobile. C-RAN: the road towards green RAN. *White Paper, ver 2.5*, 5:15–16, 2011.

[19] Aleksandra Checko, Henrik L. Christiansen, Ying Yan, Lara Scolari, Georgios Kardaras, Michael S. Berger, and Lars Dittmann. Cloud RAN for Mobile Networks - A Technology Overview. *IEEE Communications Surveys & Tutorials*, 17(1):405–426, 2015.

[20] Prasant Misra, Wen Hu, Yuzhe Jin, Jie Liu, Amanda Souza De Paula, Niklas Wirström, and Thiemo Voigt. Energy efficient GPS acquisition with Sparse-GPS. In *IPSN 2014 - Proceedings of the 13th International*

Symposium on Information Processing in Sensor Networks (Part of CPS Week), pages 155–166. IEEE, 2014.

[21] Fusang Zhang, Zhaoxin Chang, Kai Niu, Jie Xiong, Beihong Jin, Qin Lv, and Daqing Zhang. Exploring lora for long-range through-wall sensing. In *Proceedings of the ACM on Interactive, Mobile, Wearable and Ubiquitous Technologies*, volume 4, pages 1–27. ACM New York, NY, USA, 2020.

[22] Deepak Vasisht, Swarun Kumar, and Dina Katabi. Decimeter-level localization with a single WiFi access point. In *Proceedings of the 13th USENIX Symposium on Networked Systems Design and Implementation, NSDI 2016*, number ii, pages 165–178, 2016.

[23] Marco Centenaro, Lorenzo Vangelista, Andrea Zanella, and Michele Zorzi. Long-range communications in unlicensed bands: The rising stars in the iot and smart city scenarios. *IEEE Wireless Communications*, 23(5):60–67, 2016.

[24] M. Saari, A. Muzaffar bin Baharudin, P. Sillberg, S. Hyrynsalmi, and W. Yan. LoRa — A survey of recent research trends. In *2018 41st International Convention on Information and Communication Technology, Electronics and Microelectronics (MIPRO)*, pages 0872–0877, Opatija, may 2018. IEEE.

[25] Olivier BA SELLER and Nicolas Sornin. Low power long range transmitter, February 2 2016. US Patent 9,252,834.

[26] Matthew Knight. Decoding LoRa : Realizing a Modern LPWAN with SDR. In *Proceedings of the 6th GNU Radio Conference,*, volume 1, 2016.

[27] Pieter Robyns, Peter Quax, Wim Lamotte, and William Thenaers. A multi-channel software decoder for the lora modulation scheme. In *IoTBDS*, 2018.

[28] Reza Ghanaatian, Orion Afisiadis, Matthieu Cotting, and Andreas Burg. Lora digital receiver analysis and implementation. In *ICASSP 2019-2019 IEEE International Conference on Acoustics, Speech and Signal Processing (ICASSP)*, pages 1498–1502. IEEE, 2019.

[29] Olivier Bernard André Seller and Nicolas Sornin. Low complexity, low power and long range radio receiver, January 4 2018. US Patent App. 15/620,364.

[30] Lorenzo Vangelista, Andrea Zanella, and Michele Zorzi. Long-range IoT technologies: The dawn of LoRaTM. In *Lecture Notes of the Institute for Computer Sciences, Social-Informatics and Telecommunications Engineering, LNICST*, volume 159, pages 51–58. Springer, Cham, 2015.

[31] Lorenzo Vangelista. Frequency Shift Chirp Modulation: The LoRa Modulation. *IEEE Signal Processing Letters*, 24(12):1818–1821, dec 2017.

[32] Semtech Corporation. LoRa Modulation Basics. (May):1–26, 2015.

[33] LoRa Alliance. LoRaWAN Regional Parameters v1.1 REV B. pages 7–11, 2016.

[34] Tommaso Polonelli, Davide Brunelli, Achille Marzocchi, and Luca Benini. Slotted ALOHA on LoRaWAN-design, analysis, and deployment. *Sensors (Switzerland)*, 19(4), 2019.

[35] D. G. Brennan and D.G.BRENNAN. Linear Diversity Combining Technique. *Proceedings of the IRE*, 10(6):1075–1102, jun 1959.

[36] Kun Tan, He Liu, Ji Fang, Wei Wang, Jiansong Zhang, Mi Chen, and Geoffrey M. Voelker. SAM: Enabling Practical Spatial Multiple Access in Wireless LAN. In *Proceedings of the 15th annual international conference on Mobile computing and networking - MobiCom '09*, MobiCom '09, page 49, New York, NY, USA, 2009. ACM.

[37] Xiufeng Xie and Xinyu Zhang. Scalable user selection for MU-MIMO networks. In *Proceedings - IEEE INFOCOM*, pages 808–816, apr 2014.

[38] Dirk Wübben, Peter Rost, Jens Steven Bartelt, Massinissa Lalam, Valentin Savin, Matteo Gorgoglione, Armin Dekorsy, and Gerhard Fettweis. Benefits and impact of cloud computing on 5g signal processing: Flexible centralization through cloud-RAN. *IEEE Signal Processing Magazine*, 31(6):35–44, nov 2014.

[39] You Li, Yuan Zhuang, Xin Hu, Zhouzheng Gao, Jia Hu, Long Chen, Zhe He, Ling Pei, Kejie Chen, Maosong Wang, et al. Location-enabled iot (le-iot): A survey of positioning techniques, error sources, and mitigation. *arXiv preprint arXiv:2004.03738*, 2020.

[40] Manikanta Kotaru, Kiran Joshi, Dinesh Bharadia, and Sachin Katti. SpotFi: Decimeter level localization using WiFi. In *SIGCOMM 2015 - Proceedings of the 2015 ACM Conference on Special Interest Group on Data Communication*, pages 269–282, 2015.

[41] Elahe Soltanaghaei, Avinash Kalyanaraman, and Kamin Whitehouse. Multipath triangulation: Decimeter-level WiFi localization and orientation with a single unaided receiver. In *MobiSys 2018 - Proceedings of the 16th ACM International Conference on Mobile Systems, Applications, and Services*, pages 376–388. ACM, 2018.

[42] Xiaoyue Hou and Tughrul Arslan. Monte carlo localization algorithm for indoor positioning using bluetooth low energy devices. In *2017 International Conference on Localization and GNSS (ICL-GNSS)*, pages 1–6. IEEE, 2017.

[43] Patrick Lazik, Niranjini Rajagopal, Oliver Shih, Bruno Sinopoli, and Anthony Rowe. Alps: A bluetooth and ultrasound platform for mapping and localization. In *Proceedings of the 13th ACM conference on embedded networked sensor systems*, pages 73–84, 2015.

[44] Mortaza S Bargh and Robert de Groote. Indoor localization based on response rate of bluetooth inquiries. In *Proceedings of the first ACM international workshop on Mobile entity localization and tracking in GPS-less environments*, pages 49–54, 2008.

[45] Swarun Kumar, Ezzeldin Hamed, Dina Katabi, and Li Erran Li. Lte radio analytics made easy and accessible. *ACM SIGCOMM Computer Communication Review*, 44(4):211–222, 2014.

[46] Guolin Sun, Jie Chen, Wei Guo, and KJ Ray Liu. Signal processing techniques in network-aided positioning: a survey of state-of-the-art positioning designs. *IEEE signal processing magazine*, 22(4):12–23, 2005.

[47] Deepak Vasisht, Guo Zhang, Omid Abari, Hsiao Ming Lu, Jacob Flanz, and Dina Katabi. In-body backscatter communication and localization. In *SIGCOMM 2018 - Proceedings of the 2018 Conference of the ACM Special Interest Group on Data Communication*, pages 132–146. Association for Computing Machinery, Inc, aug 2018.

[48] Rajalakshmi Nandakumar, Vikram Iyer, and Shyamnath Gollakota. 3D localization for sub-centimeter sized devices. In *Proceedings of the 16th*

ACM Conference on Embedded Networked Sensor Systems, pages 108–119, 2018.

[49] Yunfei Ma, Nicholas Selby, and Fadel Adib. Minding the billions: Ultra-wideband localization for deployed rfid tags. In *Proceedings of the 23rd annual international conference on mobile computing and networking*, pages 248–260, 2017.

[50] Michiel Aernouts, Noori BniLam, Rafael Berkvens, and Maarten Weyn. Tdaoa: A combination of tdoa and aoa localization with lorawan. *Internet of Things*, 11:100236, 2020.

[51] Nico Podevijn, David Plets, Jens Trogh, Luc Martens, Pieter Suanet, Kim Hendrikse, and Wout Joseph. Tdoa-based outdoor positioning with tracking algorithm in a public lora network. *Wireless Communications and Mobile Computing*, 2018, 2018.

[52] Atul Bansal, Akshay Gadre, Vaibhav Singh, Anthony Rowe, Bob Iannucci, and Swarun Kumar. Owll: Accurate lora localization using the tv whitespaces. In *Proceedings of the 20th International Conference on Information Processing in Sensor Networks (co-located with CPS-IoT Week 2021)*, pages 148–162, 2021.

[53] Lili Chen, Jie Xiong, Xiaojiang Chen, Sunghoon Ivan Lee, Kai Chen, Dianhe Han, Dingyi Fang, Zhanyong Tang, and Zheng Wang. WideSee: Towards wide-area contactless wireless sensing. In *SenSys 2019 - Proceedings of the 17th Conference on Embedded Networked Sensor Systems*, pages 258–270, 2019.

[54] Hazem Sallouha, Alessandro Chiumento, and Sofie Pollin. Localization in long-range ultra narrow band iot networks using rssi. In *2017 IEEE*

International Conference on Communications (ICC), pages 1–6. IEEE, 2017.

[55] Martin Bor, Utz Roedig, Thiemo Voigt, and Juan M Alonso. Do LoRa low-power wide-area networks scale? In *MSWiM 2016 - Proceedings of the 19th ACM International Conference on Modeling, Analysis and Simulation of Wireless and Mobile Systems*, pages 59–67, 2016.

[56] Krishna Chintalapudi, Anand Padmanabha Iyer, and Venkata N Padmanabhan. Indoor localization without the pain. In *Proceedings of the Annual International Conference on Mobile Computing and Networking, MOBICOM*, pages 173–184, 2010.

[57] Liqiong Chang, Jie Xiong, Xiaojiang Chen, Ju Wang, Junhao Hu, Dingyi Fang, and Wei Wang. TafLoc: Time-adaptive and fine-grained device-free localization with little cost. In *SIGCOMM 2016 - Proceedings of the 2016 ACM Conference on Special Interest Group on Data Communication*, pages 563–564, 2016.

[58] Ju Wang, Hongbo Jiang, Jie Xiong, Kyle Jamieson, Xiaojiang Chen, Dingyi Fang, and Binbin Xie. Lifs: Low human-effort, device-free localization with fine-grained subcarrier information. In *Proceedings of the 22nd Annual International Conference on Mobile Computing and Networking*, MobiCom '16, pages 243–256, 2016.

[59] Yaxiong Xie, Mo Li, Jie Xiong, and Kyle Jamieson. MD-Track: Leveraging multi-dimensionality in passive indoor Wi-Fi tracking. In *Proceedings of the Annual International Conference on Mobile Computing and Networking, MOBICOM*, 2019.

[60] Yongsen Ma, Gang Zhou, and Shuangquan Wang. Wifi sensing with channel state information: A survey. *ACM Computing Surveys (CSUR)*, 52(3):1–36, 2019.

[61] Regina Kaune, Julian Hörst, and Wolfgang Koch. Accuracy analysis for tdoa localization in sensor networks. In *14th International Conference on Information Fusion*, pages 1–8. IEEE, 2011.

[62] Akshay Gadre, Revathy Narayanan, Anh Luong, Anthony Rowe, Bob Iannucci, and Swarun Kumar. Frequency configuration for low-power wide-area networks in a heartbeat. In *17th {USENIX} Symposium on Networked Systems Design and Implementation ({NSDI} 20)*, pages 339–352, 2020.

[63] Florian Wolf, Kévin Le Déroff, Sébastien de Rivaz, Nicolas Deparis, François Dehmas, and Jean-Pierre Cances. Benchmarking of narrowband lpwa physical layer ranging technologies. In *2019 16th Workshop on Positioning, Navigation and Communications (WPNC)*, pages 1–6. IEEE, 2019.

[64] Florian Wolf, Christophe Villien, Sébastien de Rivaz, François Dehmas, and Jean-Pierre Cances. Improved multi-channel ranging precision bound for narrowband lpwan in multipath scenarios. In *2018 IEEE Wireless Communications and Networking Conference (WCNC)*, pages 1–6. IEEE, 2018.

[65] Yue Wang and KC Ho. An asymptotically efficient estimator in closed-form for 3-d aoa localization using a sensor network. *IEEE Transactions on Wireless Communications*, 14(12):6524–6535, 2015.

[66] Ahmed Badawy, Tamer Khattab, Daniele Trinchero, Tarek El Fouly, and Amr Mohamed. A simple aoa estimation scheme. *arXiv preprint arXiv:1409.5744*, 2014.

[67] Chitra R. Karanam, Belal Korany, and Yasamin Mostofi. Magnitude-Based Angle-of-Arrival Estimation, Localization, and Target Tracking. In *Proceedings - 17th ACM/IEEE International Conference on Information Processing in Sensor Networks, IPSN 2018*, pages 254–265. Institute of Electrical and Electronics Engineers Inc., oct 2018.

[68] Jie Xiong and Kyle Jamieson. ArrayTrack: A fine-grained indoor location system. In *Proceedings of the 10th USENIX Symposium on Networked Systems Design and Implementation, NSDI 2013*, number 279976, pages 71–84, 2013.

[69] Jon Gjengset, Jie Xiong, Graeme McPhillips, and Kyle Jamieson. Phaser: Enabling phased array signal processing on commodity wi-fi access points. pages 153–164, 2014.

[70] Kiran Joshi, Steven Hong, and Sachin Katti. Pinpoint: Localizing interfering radios. In *Presented as part of the 10th {USENIX} Symposium on Networked Systems Design and Implementation ({NSDI} 13)*, pages 241–253, 2013.

[71] Kiran Joshi, Dinesh Bharadia, Manikanta Kotaru, and Sachin Katti. WiDeo: Fine-grained device-free motion tracing using RF backscatter. In *Proceedings of the 12th USENIX Symposium on Networked Systems Design and Implementation, NSDI 2015*, pages 189–204, 2015.

[72] Manikanta Kotaru and Sachin Katti. Position tracking for virtual reality using commodity WiFi. In *Proceedings of the Annual International*

Conference on Mobile Computing and Networking, MOBICOM, pages 15–17, 2018.

[73] Chitra R. Karanam, Belal Korany, and Yasamin Mostofi. Tracking from one side – Multi-person passive tracking with WiFi magnitude measurements. In *IPSN 2019 - Proceedings of the 2019 Information Processing in Sensor Networks*, pages 181–192, 2019.

[74] JE Evans. High resolution angular spectrum estimation technique for terrain scattering analysis and angle of arrival estimation. In *1st IEEE ASSP Workshop Spectral Estimat., McMaster Univ., Hamilton, Ont., Canada, 1981*, pages 134–139, 1981.

[75] S Unnikrishna Pillai and Byung Ho Kwon. Forward/backward spatial smoothing techniques for coherent signal identification. *IEEE Transactions on Acoustics, Speech, and Signal Processing*, 37(1):8–15, 1989.

[76] Jingjing Pan, Meng Sun, Yide Wang, and Xiaofei Zhang. An enhanced spatial smoothing technique with esprit algorithm for direction of arrival estimation in coherent scenarios. *IEEE Transactions on Signal Processing*, 68:3635–3643, 2020.

[77] Richard Baraniuk. Compressive Sensing [Lecture Notes]. *IEEE Signal Processing Magazine*, 24(4):118–121, jul 2007.

[78] David L. Donoho. For most large underdetermined systems of linear equations the minimal l1-norm solution is also the sparsest solution. *Communications on Pure and Applied Mathematics*, 59(6):797–829, jun 2006.

[79] Emmanuel J. Candès, Justin Romberg, and Terence Tao. Robust uncertainty principles: Exact signal reconstruction from highly incomplete frequency information. *IEEE Transactions on Information Theory*, 52(2):489–509, sep 2006.

[80] B. Logan. *Properties of high-pass signals.* PhD thesis, Columbia University, 1965.

[81] Prasant Kumar Misra, Diethelm Ostry, Navinda Kottege, and Sanjay Jha. TWEET: an envelope detection based broadband ultrasonic ranging system. In *Proceedings of the 14th ACM international conference on Modeling, analysis and simulation of wireless and mobile systems*, pages 409–416. ACM, 2011.

[82] J. Wright, A. Y. Yang, A. Ganesh, S. S. Sastry, and Y. Ma. Robust face recognition via sparse representation. *IEEE Transactions on Pattern Analysis and Machine Intelligence*, 31(2):210–227, Feb 2009.

[83] Xiongbin Rao and Vincent K.N. Lau. Distributed fronthaul compression and joint signal recovery in cloud-RAN. *IEEE Transactions on Signal Processing*, 63(4):1056–1065, feb 2015.

[84] Tuan Le Dinh, Wen Hu, Pavan Sikka, Peter Corke, Leslie Overs, and Stephen Brosnan. Design and deployment of a remote robust sensor network: Experiences from an outdoor water quality monitoring network. In *32nd IEEE Conference on Local Computer Networks (LCN 2007)*, pages 799–806. IEEE, 2007.

[85] Jie Liu, Bodhi Priyantha, Ted Hart, Heitor S. Ramos, Antonio A. F. Loureiro, and Qiang Wang. Energy efficient GPS sensing with cloud

offloading. In *Proceedings of the 10th ACM Conference on Embedded Network Sensor Systems - SenSys '12*, page 85, New York, New York, USA, 2012. ACM Press.

[86] Xiang Li, Shengjie Li, Daqing Zhang, Jie Xiong, Yasha Wang, and Hong Mei. Dynamic-music: Accurate device-free indoor localization. In *Proceedings of the 2016 ACM International Joint Conference on Pervasive and Ubiquitous Computing*, UbiComp '16, pages 196–207, 2016.

[87] Ralph Schmidt. Multiple emitter location and signal parameter estimation. *IEEE transactions on antennas and propagation*, 34(3):276–280, 1986.

[88] Xinrong Li and Kaveh Pahlavan. Super-resolution toa estimation with diversity for indoor geolocation. *IEEE transactions on wireless communications*, 3(1):224–234, 2004.

[89] Robert Roy, Arogyaswami Paulraj, and Thomas Kailath. Esprit–a subspace rotation approach to estimation of parameters of cisoids in noise. *IEEE transactions on acoustics, speech, and signal processing*, 34(5):1340–1342, 1986.

[90] Richard Roy and Thomas Kailath. Esprit-estimation of signal parameters via rotational invariance techniques. *IEEE Transactions on acoustics, speech, and signal processing*, 37(7):984–995, 1989.

[91] Roshan Ayyalasomayajula, Aditya Arun, Chenfeng Wu, Sanatan Sharma, Abhishek Rajkumar Sethi, Deepak Vasisht, and Dinesh Bharadia. Deep learning based wireless localization for indoor navigation. In *Proceedings of the Annual International Conference on Mobile Computing and Networking, MOBICOM*, pages 214–227, 2020.

[92] Anzhong Hu, Tiejun Lv, Hui Gao, Zhang Zhang, and Shaoshi Yang. An esprit-based approach for 2-d localization of incoherently distributed sources in massive mimo systems. *IEEE Journal of Selected Topics in Signal Processing*, 8(5):996–1011, 2014.

[93] Ousmane Abdoulaye Oumar, Ming Fei Siyau, and Tariq P Sattar. Comparison between music and esprit direction of arrival estimation algorithms for wireless communication systems. In *The First International Conference on Future Generation Communication Technologies*, pages 99–103. IEEE, 2012.

[94] Stuart A Golden and Steve S Bateman. Sensor measurements for wi-fi location with emphasis on time-of-arrival ranging. *IEEE Transactions on Mobile Computing*, 6(10):1185–1198, 2007.

[95] Nicolai Czink, Markus Herdin, Hüseyin Özcelik, and Ernst Bonek. Number of multipath clusters in indoor mimo propagation environments. *Electronics letters*, 40(23):1498–1499, 2004.

[96] Vinko Erceg, L Schumacher, P Kyritsi, A Molisch, DS Baum, AY Gorokhov, C Oestges, Q Li, K Yu, N Tal, et al. Ieee 802.11 tgn channel models. *document IEEE*, 802, 2004.

[97] Xian-Da Zhang and Ying-Chang Liang. Prefiltering-based esprit for estimating sinusoidal parameters in non-gaussian arma noise. *IEEE Transactions on Signal Processing*, 43(1):349–353, 1995.

[98] W. Xu, J. Zhang, J. Y. Kim, W. Huang, S. S. Kanhere, S. K. Jha, and W. Hu. The design, implementation, and deployment of a smart lighting system for smart buildings. *IEEE Internet of Things Journal*, 6(4):7266–7281, 2019.

[99] Hui Liu, Houshang Darabi, Pat Banerjee, and Jing Liu. Survey of wireless indoor positioning techniques and systems. *IEEE Transactions on Systems, Man, and Cybernetics, Part C (Applications and Reviews)*, 37(6):1067–1080, 2007.

[100] Johannes Schmid, Markus Völker, Tobias Gädeke, Pascal Weber, Wilhelm Stork, and Klaus D Müller-Glaser. An approach to infrastructure-independent person localization with an ieee 802.15. 4 wsn. In *2010 International Conference on Indoor Positioning and Indoor Navigation*, pages 1–9. IEEE, 2010.